PONTIFICIA UNIVERSIDAD CATOLICA DE CHILE

SCHOOL OF ENGINEERING

UNDERSTANDING GROUNDWATER DYNAMICS IN A CHANGING CLIMATE: NUMERICAL MODELING AND REMOTE SENSING INSIGHTS FROM THE SALAR DEL HUASCO BASIN

NICOLE DANIELLE JOSEPHINE BLIN LIZASOAIN

Thesis submitted to the Office of Graduate Studies in partial fulfillment of the requirements for the Degree of Doctor in Engineering Sciences

Advisor:

FRANCISCO SUÁREZ P.

Santiago de Chile, July 2023

PONTIFICIA UNIVERSIDAD CATOLICA DE CHILE

SCHOOL OF ENGINEERING

UNDERSTANDING GROUNDWATER DYNAMICS IN A CHANGING CLIMATE: NUMERICAL MODELING AND REMOTE SENSING INSIGHTS FROM THE SALAR DEL HUASCO BASIN

NICOLE DANIELLE JOSEPHINE BLIN LIZASOAIN

Members of the Committee:

FRANCISCO SUÁREZ

JORGE GIRONÁS

SEBASTIÁN VICUÑA

CHRISTOPHER S. LOWRY

DAVID F. BOUTT

IGNACIO LIRA

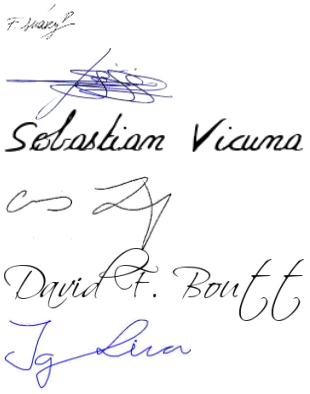

Thesis submitted to the Office of Graduate Studies in partial fulfillment of the requirements for the Degree Doctor in Engineering Sciences

Santiago de Chile, July 2023

A familia, por ser mi principal soporte y motivación.

ACKNOWLEDGEMENTS

I would like to express my profound gratitude to my advisor, Francisco Suárez, for his support and invaluable guidance. Many years ago, when he took me under his wing as his student, he saw potential in me at a time when I struggled to see it myself. His mentorship has been pivotal in my academic development.

I extend my gratitude to my Dissertation Committee. Foremost among them is Chris Lowry, whose mentorship during my internship became crucial in my growth as a professional. Also, I express my immense appreciation to Jorge Gironás, whose disposition and willing assistance in providing resources for the downscaling of climate models, further enriched my research; and to Sebastián Vicuña, Vladimir Marianov, and Ignacio Lira, whose constructive feedback provided critical insights that greatly enriched my doctoral research.

I acknowledge funding from the Agencia Nacional de Investigación y Desarrollo (ANID) through grant FONDECYT/1210221, FONDECYT/1170850 and FSEQ210018, as well as the Centro de Desarrollo Urbano Sustentable (CEDEUS, FONDAP/15110020) and the Centro de Excelencia en Geotermia de los Andes (CEGA, FONDAP/15090013).

Lastly, my deepest gratitude is extended to my family. To my parents, Maite and Felipe, and my husband, Alex, thank you for your unconditional love and your relentless support throughout this process. You were my pillars of strength when times were challenging, and your love carried me through.

TABLE OF CONTENTS

Page

OUTLINE

Chapter 1 – *Introduction*

This section introduces the pressing issue of climate change and its impacts on groundwater resources in arid regions, which is the focus of this dissertation. We outline the hypothesis formulated to address the identified research gaps, encapsulating the objectives of this study, the methodology employed, and a concise summary of the main findings.

Chapter 2 – *Potential impacts of climate change on an aquifer in the arid Altiplano, northern Chile: the case of the protected wetlands of the Salar del Huasco basin*

This chapter delved into the future conditions contributing to significant changes in groundwater discharges and water levels in natural basins (Paper 1), by employing synthetic hybrid climate scenarios to investigate potential impacts on the Salar del Huasco aquifer. Findings on the role of groundwater discharge mechanisms in balancing the future inputs are presented and discussed in this chapter.

Chapter 3 - *Evaluating the contribution of satellite-derived evapotranspiration in the calibration of numerical groundwater models in remote zones using the EEFLUX tool*

The focus of this chapter is directed to the potential of satellite products based to enhance local-scale models and better support numerical groundwater modeling (Paper 2). We present in this chapter the results on the ability of the EEFlux method in representing evaporation over the Altiplano, along with the discussion on the utility of satellite imagery as a tool for calibrating groundwater models and broaden the potential applications of EEFlux beyond agriculture.

Chapter 4 – *Groundwater response to climate change and the time of emergence of anthropogenic signals in aquifer levels: Are groundwater-fed wetlands resilient to climate change in natural basins?*

Chapter 4 examines the role of groundwater in mitigating the effects of climate change on dependent ecosystems, specifically, the Salar del Huasco wetlands (Paper 3). Results on the changes in climatic variable and how are they expected to affect the timing of groundwater recharge and discharges are presented. We evaluate the magnitude of these changes based on the natural variability of the basin as well as the time when the wetlands may be affected.

Chapter 5 – *Conclusions*

This chapter provides a comprehensive summary of the key findings derived from this study, organized according to the research questions they aimed to address and the corresponding hypotheses that were either validated or rejected. The main conclusions drawn from the research are presented, highlighting the significant outcomes of the study. Finally, the implications of the results are discussed, highlighting the potential impacts on dependent ecosystems. The significance of these findings in guiding future research endeavors related to the impact of climate change on groundwater and implications in arid ecosystems is emphasized.

TABLES

Page

FIGURES

Page

RESUMEN

El agua subterránea es la mayor fuente de agua dulce a nivel global. En regiones áridas, donde el agua superficial es limitada, el agua subterránea es la principal fuente de agua. El continuo avance del cambio climático y el crecimiento acelerado de la población generarán un aumento en la demanda de dicho recurso. Por lo tanto, es esencial comprender cómo podrían verse afectados los sistemas de agua subterránea y así gestionar sustentablemente los recursos hídricos y preservar ecosistemas.

Motivada por dichas proyecciones, esta investigación se enfoca en el estudio de la cuenca del Salar del Huasco en el árido Altiplano chileno, mediante la simulación del agua subterránea bajo diferentes escenarios de cambio climático.

La primera parte de la investigación examina la respuesta del acuífero del Salar del Huasco ante escenarios extremos de cambio climático. Los resultados indican que el acuífero se adapta a diversas condiciones externas mediante la regulación de sus descargas, con la evaporación como el principal mecanismo de descarga que mantiene estable el nivel freático alrededor de los humedales. La segunda parte evalúa la aplicabilidad de productos satelitales en la modelación del agua subterránea en áreas con monitoreo limitado. La integración de EEFlux en el modelo mejoró la representación espaciotemporal del nivel freático y la calibración de parámetros específicos, confirmando el potencial de estos productos en la modelación del agua subterránea. Finalmente, se explora el papel del agua subterránea en la mitigación de los efectos del cambio climático en ecosistemas dependientes, con enfoque en los humedales del Salar del Huasco. A pesar de los cambios climáticos proyectados, los humedales se mostraron resistentes a cambios debido a la influencia del agua subterránea. Esto sugiere que el agua subterránea podría amortiguar parte de los impactos del cambio climático en ecosistemas dependientes en regiones áridas.

Palabras Claves: Modelación de aguas subterráneas, cambio climático, ecosistemas dependientes de aguas subterráneas, altiplano chileno, regiones áridas, conjuntos de modelos climáticos.

ABSTRACT

Groundwater is the largest source of freshwater globally, sustaining a significant portion of the world's population and maintaining critical ecosystem functions. In arid regions, where surface water resources are often limited, groundwater serves as the principal water source. Given the progression of climate change and escalating global population growth in arid regions, reliance on groundwater is intensifying, understanding how climate change may impact groundwater is essential for water resources management and ecosystem preservation. Our research is centered on addressing this critical concern, focusing its study on the arid Salar del Huasco basin located in the Chilean Altiplano, led by the pivotal research question: How will climate change affect groundwater dynamics in arid regions? We explore this through simulating groundwater under various climate change scenarios.

First, we examined the response of the Salar del Huasco aquifer under extreme climate scenarios. We found that the aquifer adjusts to diverse external conditions by modulating its water discharge, with evaporation the dominant discharge mechanism that balances recharge inputs, keeping the water table around the wetlands generally stable. Subsequently, recognizing the challenging access and conditions inherent to remote arid ecosystems, we focused on assessing the potential of satellite products in supporting groundwater modeling in areas with limited monitoring. The integration of EEFlux revealed to enhance the representation of spatiotemporal water table dynamics and the calibration of specific yield parameters, highlighting the potential of remote sensing techniques in groundwater modeling. Finally, we explored the role of groundwater in mitigating the effects of climate change on dependent ecosystems, focusing on the wetlands of the Salar del Huasco. Despite anticipated shifts in climatic patterns, we found that these ecosystems exhibited substantial resilience due to the influence of groundwater, with the water table expected to remain stable in time. This implies a natural capacity of these ecosystems to buffer some climate change impacts, suggesting that groundwater plays a crucial mitigating role for dependent ecosystems in arid regions.

A unique aspect of this work is the examination of a natural system, undisturbed by human intervention. The findings can thus provide valuable insights for similar ecosystems globally, as well as inform the development of adaptive strategies for sustainable groundwater management in the face of climate change.

Keywords: groundwater modeling, climate change, groundwater-dependent ecosystems, Chilean Altiplano, arid regions, climate model ensembles.

PAPERS

Chapter 2. Blin, N., Hausner, M., Leray, S., Lowry, C., & Suárez, F. (2022). Potential impacts of climate change on an aquifer in the arid Altiplano, northern Chile: The case of the protected wetlands of the Salar del Huasco basin. Journal of Hydrology: Regional Studies, 39, 100996. https://doi.org/10.1016/j.ejrh.2022.100996.

Chapter 3. Blin, N. & Suárez, F. (2023). Evaluating the contribution of satellite-derived evapotranspiration in the calibration of numerical groundwater models in remote zones using the EEFlux tool. Science of The Total Environment, 858, 159764. https://doi.org/10.1016/j.scitotenv.2022.159764.

Chapter 4. Blin, N. & Suárez, F. [under review]. Groundwater response to climate change and the time of emergence of anthropogenic signals in aquifer levels: are groundwater-fed wetlands resilient to climate change in natural basins?

APPENDIX A. Blin, N., Soonthornrangsan, J., Lowry, C., Gironás, J., Chadwick, C., Suárez, F. [under review]. Assessing potential impacts of climate change on water resources and their interaction within the Great Lakes Region - The potential buffering capacity of groundwater on surface water processes.

1. INTRODUCTION

As the primary source of freshwater worldwide, groundwater plays a pivotal role in not only sustaining the majority of the global population, but also in supporting diverse ecosystems (Atawneh et al., 2021; Cuthbert et al., 2019; McDonough et al., 2020). As climate change continues to alter the Earth's environment, fluctuations in the amount and distribution of groundwater recharge are anticipated, impacting groundwater storage, water table levels, and, consequently, the interactions between groundwater and surface water (Amanambu et al., 2020; Condon et al., 2020; Cuthbert et al., 2019). Considering these potential consequences, it is imperative to examine the ramifications of climate change on groundwater dynamics.

These potential changes take on intensified significance in arid regions, where surface water resources are limited and groundwater serves as the primary source of water (Scanlon et al., 2006). Alarmingly, the geographic expanse of these arid regions is predicted to envelop half of the Earth's surface by the century's close, an outcome that will further exacerbate global warming due to diminished carbon sequestration (Huang et al., 2015; Koutroulis, 2019; Prăvălie et al., 2019). Furthermore, the use of groundwater in arid regions is already increasing worldwide in response to a growing global population. Thus, assessing the long-term viability of the water resource is crucial, for which accurate water budgets must be developed (Shanafield et al., 2015). This nexus of escalating demands, changing climatic conditions, and the critical reliance on groundwater in arid regions prompts the following research question: ***How will climate change affect groundwater dynamics in arid regions?***

Driven by this research question, this dissertation investigates the Salar del Huasco aquifer as a study area, located in the extremely arid Chilean Altiplano. In this basin, groundwater feeds wetlands that constitute the habitat of flora and fauna particular to the area, which is why it was declared a RAMSAR site of protected wetlands. The particularity of studying this basin resides in the natural state in which it is preserved due to its protected quality. In

their natural state prior to development, aquifers typically maintain a dynamic equilibrium, wherein the average influx of water (recharge) equals the average outflow, resulting in almost no net change in the average volume of water stored within the aquifer (Scanlon et al., 2023). Therefore, the hydrogeological response of the Salar del Huasco basin could be attributed to the system's own elements, serving as a baseline site to basins with similar characteristics and thus contribute to the global knowledge of groundwater behavior in arid zones. Considering this, a more specific question arises: ***What future conditions will contribute to significant variations in groundwater discharges and water levels in natural basins?***

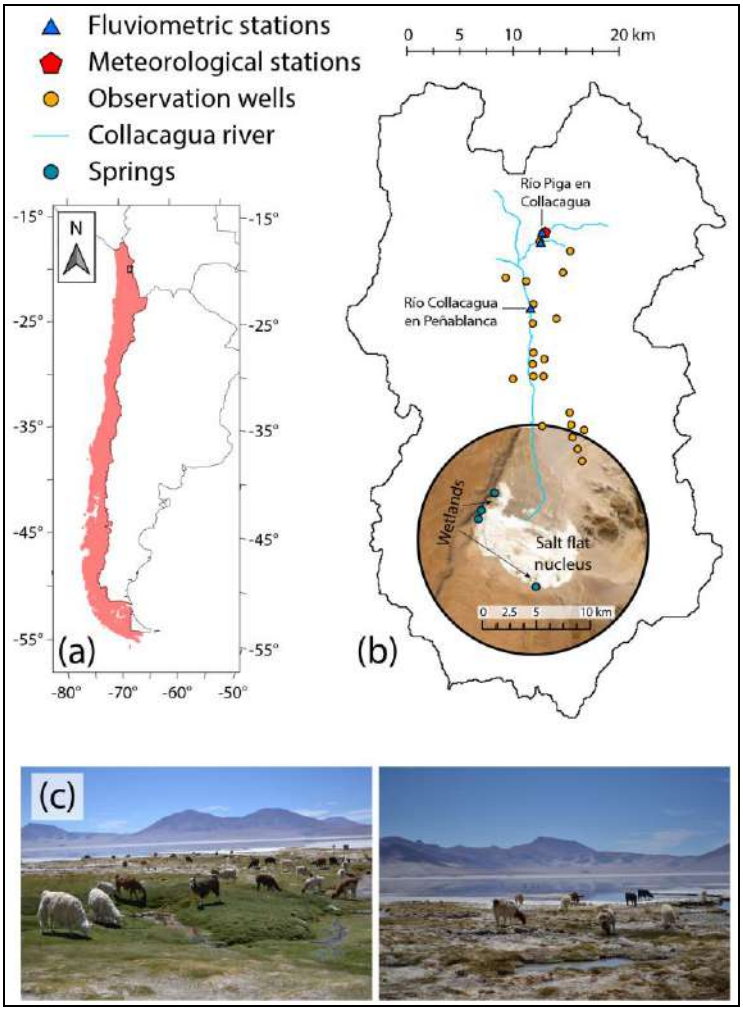

Figure 1-1: Salar del Huasco basin, used as a case study in this dissertation. Panel a) General location of the study site; b) Salar del Huasco basin, where observation wells are depicted as orange circles, Collacagua meteorological station is shown as a red pentagon and springs as blue circles near the wetlands at the salt flat nucleus; and c) shows some of the fauna and flora that inhabits the wetlands within the salt flat nucleus.

1.1 Challenges of groundwater modeling in remote locations

Numerical groundwater models provide crucial insights into hydrogeological systems, acting as an indispensable decision-support tool for local and governmental institutions striving for water security (Aghlmand & Abbasi, 2019; Post et al., 2019; Rabemaharitra et al., 2022). Developing a robust numerical groundwater model requires gathering hydrometeorological and hydrogeological data over a certain period. However, the utility of many regions' monitoring networks is often hampered by their sparsity and periods of inactivity, rendering them inadequate for real-time decision-making (Sheffield et al., 2018). Hence, remote sensing products have emerged as an increasingly popular auxiliary source, furnishing hydrological, hydrogeological, and meteorological data to support the development and calibration of hydrological and hydrogeological models, thereby offsetting the scarcity of in-situ data (Li et al., 2009; Sun et al., 2012; Sun et al., 2018).

Arid regions present a distinct context where remote sensing can compensate for the paucity of in-situ data (Adams et al., 2022; Smith et al., 2019). c. However, its measurement is challenging due to the spatiotemporal multiscale nature of the process (Lobos-Roco et al., 2022; Lobos-Roco et al., 2021). Consequently, several remote sensing tools have evolved in recent decades to estimate ET using satellite images, regardless of soil condition or crop type (Losgedaragh & Rahimzadegan, 2018).

While ET data derived from remote sensing has been used in numerous water management studies, only a handful have incorporated this information into numerical groundwater models for enhancing model calibration (Boronina & Ramillien, 2008; Carroll et al., 2015; Li et al., 2009; Sun et al., 2012; Sutanudjaja et al., 2014). Although these studies were a novel contribution towards improving groundwater model calibration, their applicability has certain limitations, such as: been oriented to regional modeling, high dependency on local vegetation (which

limits its reproducibility in heterogeneous zones); low temporal frequency of images for representing ET, and reduced capacity to calibrate multiple parameters. Given these considerations, the following research questions arise: ***Could satellite products based on energy balance models, e.g., EEFlux, contribute to improve local-scale models? How can they better support numerical modeling of hydrogeological systems?***

1.2 Groundwater response under climate change scenarios and potential consequences on groundwater-dependent ecosystems

As the slowest flowing component of the terrestrial hydrologic cycle, groundwater often acts to buffer variability in both the water and energy cycles (Condon et al., 2021). Extremes such as droughts can be buffered by groundwater-surface water exchanges that provide relatively stable flow to rivers during low flow periods and allow roots to take up water released from the groundwater storage. This potential buffering capability of groundwater has been noticed across various environmental settings, indicating a degree of potential stability in the advent of climate change (Cuthbert et al., 2019a; Erler et al., 2019; Marchionni et al., 2020; Somers et al., 2019).

In arid regions, groundwater significantly sustains ecosystems by directly providing a water source for vegetative uptake and indirectly maintaining soil moisture for ET (Yao et al., 2018). This critical link between groundwater and ecosystem health is especially vital in the context of wetlands, which provide crucial services, including climate change mitigation (Huang et al., 2021; Ma et al., 2022; Salimi et al., 2021). They regulate the atmospheric concentrations of greenhouse gases that contribute to global warming, such as methane, carbon dioxide and nitrous oxide. These ecosystems store about a third of the global soil carbon and more than half of the carbon in the atmosphere, being thus a crucial long-term carbon sink (Cuthbert et al., 2019b; Huang et al., 2021; Ma et al., 2022; Mitsch et al., 2013; Moomaw et al.,

2018). However, the response of wetlands to changing climate scenarios is not yet fully understood (Gallego-Sala et al., 2018; Ma et al., 2022; Salimi et al., 2021).

Research suggests that wetlands in arid regions would be more resilient than those in temperate or tropical climates, due to their ability to adapt to extreme climatic events and recover more effectively from disturbances (Cuthbert et al., 2019b; Cuthbert et al., 2019a; Sandi et al., 2020; Yao et al., 2018). A significant portion of this resilience might be attributed to the supporting role of groundwater. Yet, as climate change progresses, we are confronted with an impending question: will this resilience be enough to safeguard groundwater-dependent wetlands against intensifying climate change effects? This question translates into examining the impacts of climate change on groundwater levels near the wetlands. Groundwater, being the life-sustaining force of these ecosystems, any changes in its levels could potentially disrupt the delicate balance, threatening the survival and functionality of these wetland habitats.

Recent studies have drawn attention to the repercussions of shifts in groundwater levels on wetland health and functionality (Chen et al., 2021; Froend et al., 2016; House et al., 2016; Ma et al., 2022; Paquis et al., 2023; Sandi et al., 2020; Scanlon et al., 2023; Stirling et al., 2020; Zhu et al., 2020). Moreover, the timing of these shifts may critically determine the ability of these ecosystems to adapt and survive under increasing environmental pressures. Therefore, investigating the time at which significant changes in groundwater levels occur due to climate change is of paramount importance as it would allow anticipating potential challenges these ecosystems may face and to plan effective conservation strategies accordingly.

Hence, this dissertation aims to address the following pressing questions: ***What role does groundwater play in mitigating the effects of climate change on dependent ecosystems in arid regions? Are the Salar del Huasco wetlands naturally resilient***

to climate change due to groundwater's influence, and can this resilience persist through the century?

1.3 Hypotheses

This research was developed around the following hypothesis, each of them generated from a research question:

RQ1: How will climate change affect groundwater dynamics in arid regions? More specifically, what future conditions will contribute to significant variations in groundwater discharges and water levels in natural basins?

H1) Climate change will induce changes in groundwater recharge within arid regions, subsequently affecting groundwater dynamics. However, any potential impacts on the water table are expected to be moderated by the compensatory response of groundwater discharge through evaporation.

RQ2: Could satellite products based on energy balance models, e.g., EEFlux, contribute to improve local-scale models? How can they better support numerical groundwater modeling?

H2) By incorporating remotely sensed EEFlux data in local-scale groundwater models, it is possible to achieve better characterization of aquifer properties and promote sustainable groundwater management in remote regions with limited monitoring capabilities.

RQ3: What role does groundwater play in mitigating the effects of climate change on dependent ecosystems in arid regions? Particularly, are the wetlands of Salar del Huasco naturally resilient to climate change due to groundwater's influence, and can this resilience persist through the century?

H3) In arid regions, groundwater will be able to partially mitigate the impacts of climate change on dependent ecosystems, however, this buffering capacity will decline over the course of the century under extreme climate change scenarios.

1.4 Objectives

The overarching goal of this research was to evaluate the potential impacts of climate change on groundwater dynamics in an arid-zone basin, in terms of water levels and mass balance components, to enhance the existing understanding of these complex systems in arid regions. This goal will contribute to a better management of their groundwater resources, thereby supporting sustainable human use in crucial areas and preserving groundwater-dependent ecosystems.

The specific objectives (SO) defined for the completion of this work are the following:

SO1: To simulate the hydrological and groundwater processes of the Salar del Huasco basin, through the development of a hydrological model and a groundwater numerical model.

SO2: To evaluate the response of groundwater dynamics to climate change, in terms of changes in water levels and mass balance components, in the Salar del Huasco basin, under different future scenarios.

SO3: To improve the calibration of the numerical model of the Salar del Huasco aquifer using remote sensing products as ancillary data to support groundwater level records.

SO4: To explore the range of potential impacts on groundwater levels by employing two diverging future scenarios represented by SSP2 4.5 and SSP5 8.5 in the CMIP6 ensemble, while accounting for the inherent uncertainty within climate projections.

SO5: To identify the point in time at which climate change will start to affect the groundwater levels that sustain the protected wetlands of Salar del Huasco.

1.5 Methodology

To achieve the specific objectives of this dissertation, a methodological framework was designed and is presented in Figure 1-2. First, recharge processes were simulated with a rainfall-runoff hydrological model (Uribe et al., 2015) generated and calibrated for the Salar del Huasco basin. Then, groundwater processes were simulated with a MODFLOW model (Harbaugh et al., 2000) constructed as scripts with the FloPy Python library (Bakker et al., 2016). This scripting approach has the advantage of allowing multiple models to be efficiently created and modified, which is crucial for assessing diverse climate change scenarios. As part of SO3, the model was then calibrated using remotely sensed evapotranspiration (ET) data in the Salar del Huasco basin derived from the EEFlux platform.

The groundwater response to climate change in the Salar del Huasco basin was assessed by: (1) bias-adjustment of climate model projections, (2) defining the future scenarios under which the changes were to be studied, (3) simulating the recharge and groundwater processes under the previously defined scenarios, and (4) quantifying the projected changes in groundwater discharges and water table with respect to a reference period.

Finally, the time of emergence (ToE) of the climate change signal on groundwater levels was estimated in the Salar del Huasco basin using water level records.

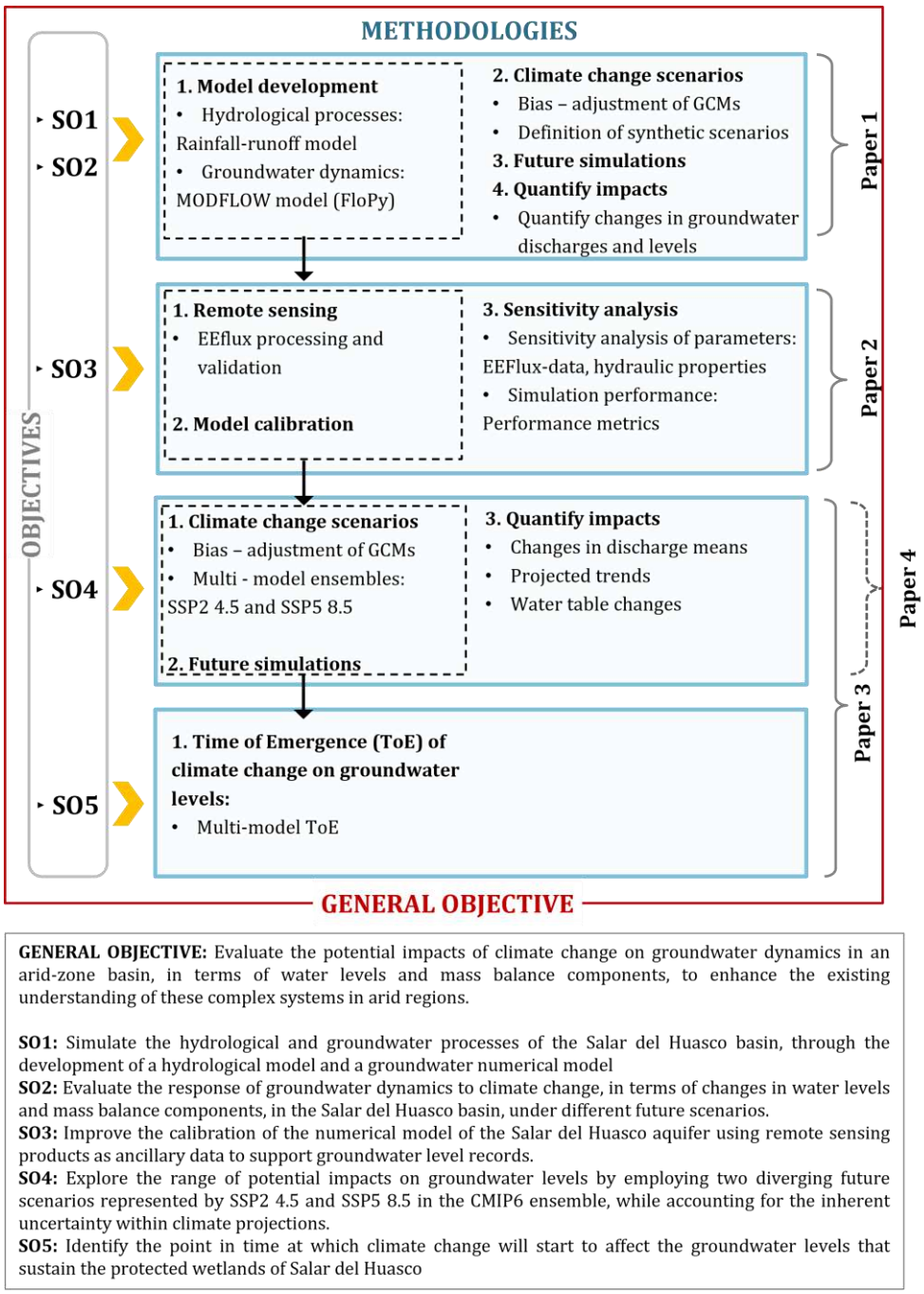

GENERAL OBJECTIVE: Evaluate the potential impacts of climate change on groundwater dynamics in an arid-zone basin, in terms of water levels and mass balance components, to enhance the existing understanding of these complex systems in arid regions.

SO1: Simulate the hydrological and groundwater processes of the Salar del Huasco basin, through the development of a hydrological model and a groundwater numerical model
SO2: Evaluate the response of groundwater dynamics to climate change, in terms of changes in water levels and mass balance components, in the Salar del Huasco basin, under different future scenarios.
SO3: Improve the calibration of the numerical model of the Salar del Huasco aquifer using remote sensing products as ancillary data to support groundwater level records.
SO4: Explore the range of potential impacts on groundwater levels by employing two diverging future scenarios represented by SSP2 4.5 and SSP5 8.5 in the CMIP6 ensemble, while accounting for the inherent uncertainty within climate projections.
SO5: Identify the point in time at which climate change will start to affect the groundwater levels that sustain the protected wetlands of Salar del Huasco

Figure 1-2: Methodological framework, presented according to the specific objectives defined in this dissertation. The dashed black rectangles indicate the methods required for achieving the subsequent objective. The dashed grey bracket points to paper 4 (APPENDIX A), which although it not comprised in the general objective, applies the methodology developed for achieving SO4.

In an endeavor to diversify the context and enhance the robustness of the methodology, this dissertation incorporates a supplementary component: the impacts of climate change on the Western New York aquifer. This additional work (conducted as part of the international internship) applies the same analytical framework used for Salar del Huasco to the Western New York aquifer. While this work is not aligned with the goals of this dissertation, the publication that resulted from it was incorporated in APPENDIX A, as it allows validating the versatility and applicability of the methodology across different settings and conditions.

1.6 Preview of results

Results derived from **SO1** and **SO2** indicate that higher precipitation would contribute to larger groundwater recharge rates (Figure 1-3a). The Salar del Huasco aquifer responds to the different external conditions by discharging and storing water accordingly, with groundwater evaporation as the main discharge mechanism that counterbalances the recharge inputs (Figure 1-3b). Low precipitation scenarios project slightly drier surface conditions in the wetlands (Figure 1-4). The analysis of the scenarios reveals that the equipotential map at 2100 m A.S.L., projected under extreme increases in temperature and precipitation, is the one that closely mirrors the 2010 map, which is depicted in the extreme-high map. Not far behind in resemblance is the cross-wet map, which shows the outcome of moderate temperature increase coupled with high precipitation surges. Therefore, the water table in the aquifer would remain stable in future scenarios that project 38% increase in precipitation, while decreases in precipitation of 15% onwards would result in lower future groundwater levels in the Salar del Huasco. Although there are changes in groundwater levels in the wetlands area, these changes are small, and the overall behavior of the spring discharge is stable over time.

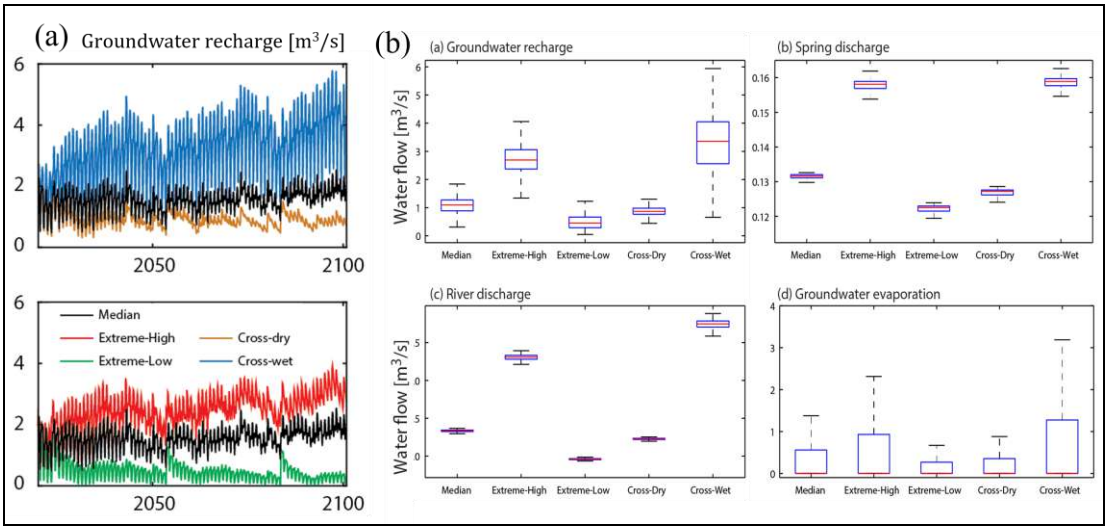

Figure 1-3: a) Future groundwater recharge estimates in the Salar del Huasco and, b) boxplot of groundwater discharge flows across hybrid scenarios. Extreme-high and Extreme-low scenarios represent extreme shifts in temperature and precipitation in the same direction, positive and negative, respectively. Cross-wet and Cross-dry scenarios project opposing trends of change in temperature and precipitation, with the former the scenario projecting increasing precipitation with slight temperature rises, and the latter projecting opposing conditions. Finally, the Median scenario projects intermediate shifts in both variables.

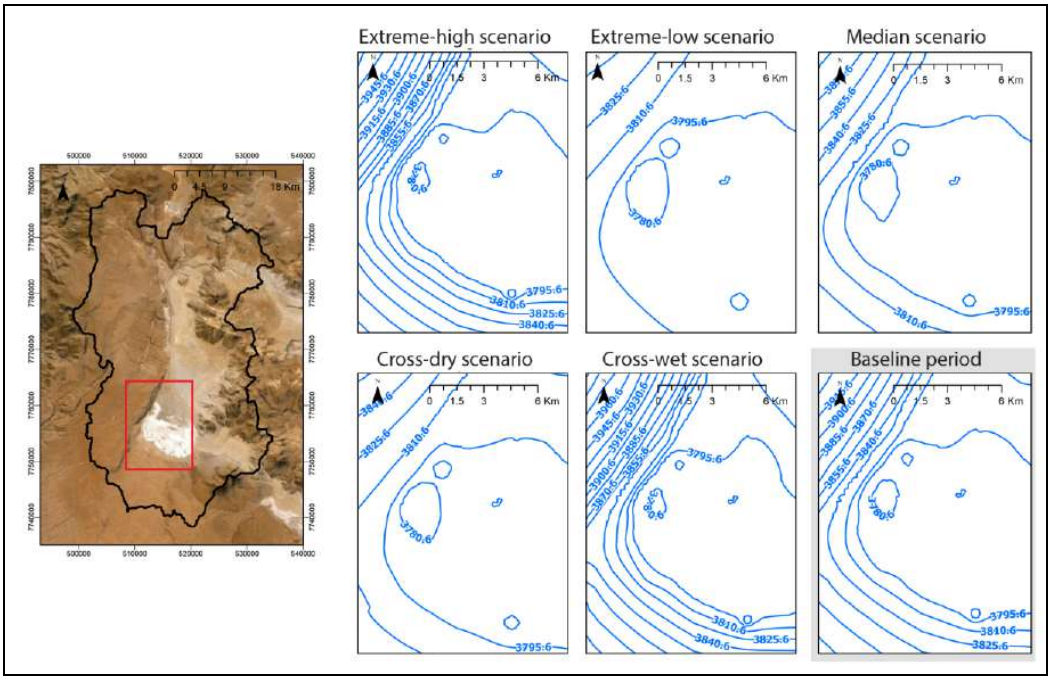

Figure 1-4: Future contour maps near the wetlands by December 2100, in comparison to baseline period (December 2010). Extreme-high and Extreme-low scenarios represent extreme shifts in temperature and precipitation in the same direction, positive and negative, respectively. Cross-wet and Cross-dry scenarios project opposing trends of change in temperature and precipitation, with the former the scenario projecting increasing precipitation with slight temperature rises, and the latter projecting opposing conditions. Finally, the Median scenario projects intermediate shifts in both variables.

The groundwater model initially developed to meet **SO1** and **SO2** was further enhanced using remotely sensed data. Specifically, ET data was derived from EEFlux (hereafter EEFlux – ET), which is a tool based on the METRIC surface energy balance model. The EEFlux – ET estimates served as ancillary data to support groundwater level records during the calibration phase, ultimately facilitating the realization of **SO3**. The results of the calibrations showed that best performance metrics were obtained when both EEFlux – ET and heads were used as observations to calibrate the hydraulic properties (normalized root mean square error = 4.1%).

Moreover, it was found that calibrating with EEFlux – ET has a direct effect on specific yield parameters, which regulate the fluctuations of the water table over time.

The groundwater model calibrated with EEFlux data was used for evaluating the impacts of climate change on groundwater levels under SSP2 4.5 and SSP5 8.5 scenarios, while accounting for the uncertainty of climate projections, according to **SO4**. It was found that warming temperatures may augment winter recharge up to three times higher than in the reference period, leading to a slight rise of the water table. Under ensemble SSP2 4.5, a basin-wide mean groundwater level change of around 5 – 9 m is projected between December 2025 (near future) and December 2100 (end of the century), while changes of ~3 – 12 m are expected under SSP5 8.5 between the same time-periods (**Figure 1-5**).

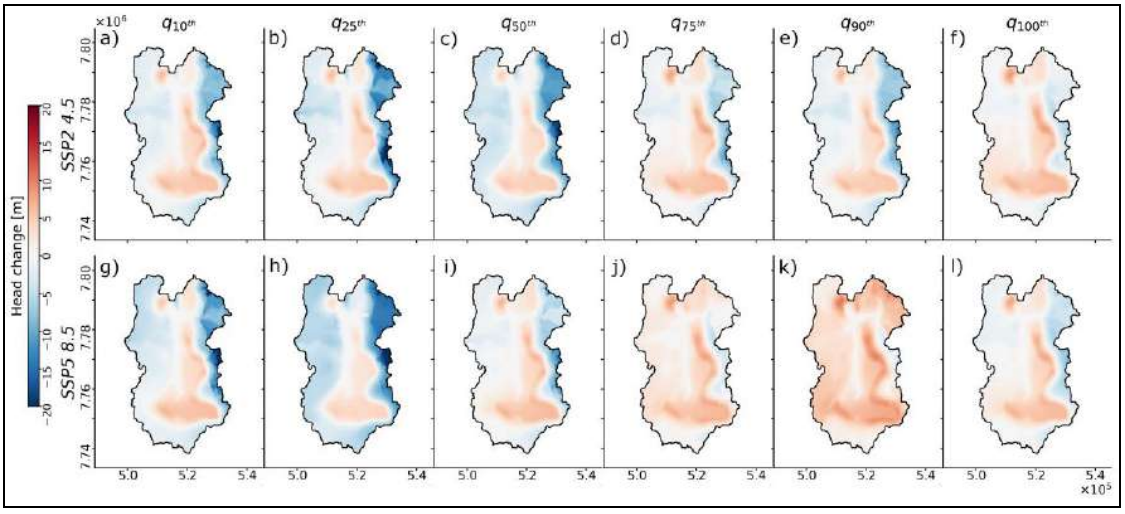

Figure 1-5: Spatial variations of the projected changes in the water table between December 2025 and December 2100 across ensemble members of scenarios SSP2 4.5 (a to f) and SSP5 8.5 (g to l). The columns separate the ensemble members representing a specific percentile of precipitation change (indicated at the top of each column).

Finally, this research revealed a 20-year difference in the ToE when different extents of natural variability were accounted for, demonstrating that accounting for both interannual and interdecadal variabilities under natural conditions leads to earlier ToEs (≥ 2080) (Figure 1-6) and achieving **SO5**. More specifically, when considering the multidecadal variability as part of the natural variability, the impacts of climate change are expected earlier on the water table, affecting thus the groundwater-dependent ecosystems from ~10 – 20 years before the end of the century.

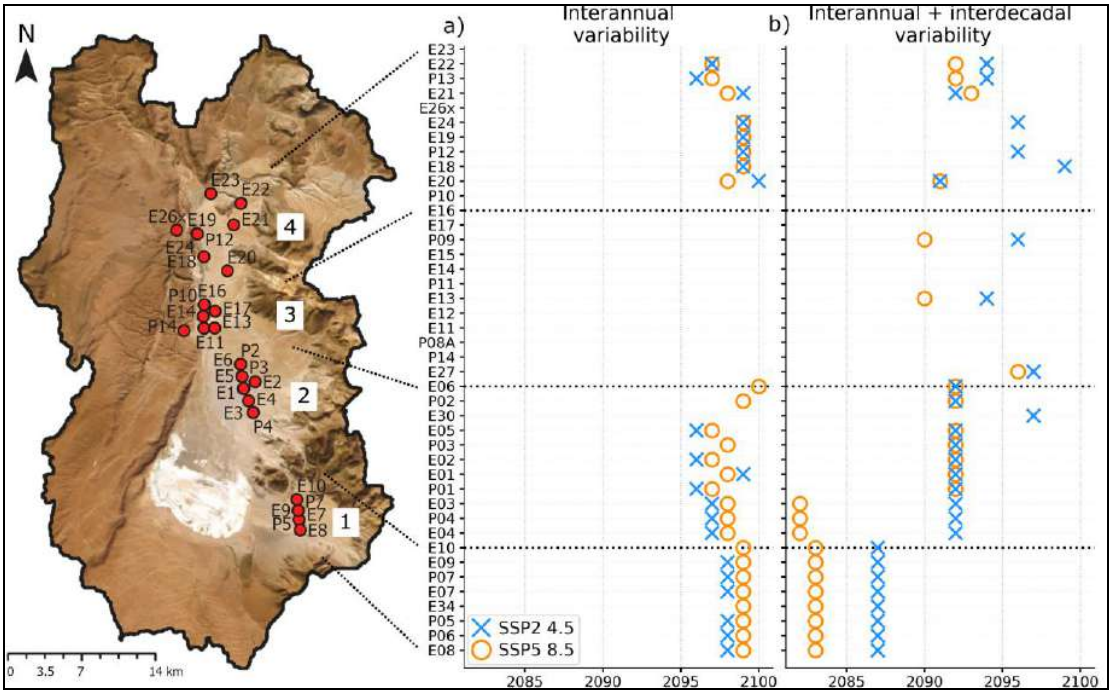

Figure 1-6: Time of emergence (ToE) of the climate change signal in monitoring wells under different approaches to account for the natural variability.

2. POTENTIAL IMPACTS OF CLIMATE CHANGE ON AN AQUIFER IN THE ARID ALTIPLANO, NORTHERN CHILE: THE CASE OF THE PROTECTED WETLANDS OF THE SALAR DEL HUASCO BASIN

2.1. Introduction

Groundwater is a vital global resource that provides one third of the planet's fresh water for domestic, agricultural and industrial uses (Bloomfield et al., 2019; Taylor et al., 2013; Velis et al., 2017). Predicted climate change poses a threat for groundwater resources, most of which are non-renewable on meaningful timescales for humans and ecosystems (Kløve et al., 2014). Future projections predict an increase in the mean global temperatures as well as an increase in the magnitude and frequency of extreme precipitation events (IPCC, 2014; Nkhonjera & Dinka, 2017). On one hand, Central Chile (latitude 30ºS) has experienced a drying trend since the mid-20th century, which is expected to continue in the future, leading to a reduction in average annual precipitation of up to 40% relative to current values (Garreaud et al., 2020). This region has experienced a significant decrease in rainfall since the late 1970s, which has been evidenced by more frequent drought events (Rivera et al., 2020). On the other hand, increasing trends have been found in average annual precipitation in the Bolivian Altiplano (Torres-Batlló & Martí-Cardona, 2020), and in annual precipitation in northern Chile (DGA, 2017; Souvignet et al., 2012). However, there is still great uncertainty concerning future precipitation changes across the Andes (Urrutia & Vuille, 2009), while there is general agreement on future increasing temperature trends in the region (DGA, 2017). Given these projections, understanding the effects of climate change on groundwater becomes of utmost importance.

Different studies have evaluated potential consequences of climate change on groundwater. Decreased snowpack, given a reduction in snow accumulation due to more precipitation in the form of rain, is likely to reduce river flow in summer months and greater evaporation rates will increase water demand of crops, thus increasing groundwater extraction and

leading to its depletion (Alam et al., 2019; Amanambu et al., 2020; Nkhonjera & Dinka, 2017; Taylor et al., 2013). Water shortage problems derived from changes in perception lead to groundwater depletion, which is particularly critical in arid and semi-arid environments where groundwater discharge dominates the water balance (Rossman et al., 2018; Velis et al., 2017), and becomes even more crucial since population and groundwater demand in arid regions are expected to increase (Huang et al., 2015; Nkhonjera & Dinka, 2017; Scanlon et al., 2006; Taylor et al., 2013). Additionally, arid zones are projected to expand to cover up to half of the terrestrial surface by the end of the century, which will diminish the natural retention (or sequestration) of carbon (Huang et al., 2015; Koutroulis, 2019; Prăvălie, 2016; Prăvălie et al., 2019).

General circulation models (GCMs) have become the primary tool for the study of projected climate change impacts on hydrological systems (Persaud et al., 2020). GCMs simulate the behavior and interaction of flow systems in the biosphere, hydrosphere, cryosphere, atmosphere and geosphere in the climate system (Green et al., 2011; Huang et al., 2015; Scanlon et al., 2006; Taylor et al., 2013). Climate change scenarios established in the fifth report of the Intergovernmental Panel on Climate Change (IPCC) are expressed in terms of Representative Concentration Pathways (RCP), which provide quantitative information of the concentration in time of contaminants associated to climate change. However, the coarse resolution of GCM outputs prevents them from being used directly with local (basin-scale) models because they do not represent processes taking place at scales finer than their own grids, which are generally of the order of ~200 km (Fowler et al., 2007; Green et al., 2011; Persaud et al., 2020; Wilby et al., 1998). Therefore, downscaling techniques are required to bring the GCM's raw data into the local scale for them to be applicable in basin scale models.

Previous studies have used GCM projections to evaluate potential effects of climate change on hydrogeological systems through different approaches. Studies by Crosbie et al. (2011, 2013), Hartmann et al., (2017), Hashemi et al. (2015), Holman (2006); McKenna & Sala (2018), Rossman et al. (2018), Tillman et al. (2016) and Zhang et al. (2019) focused

on groundwater recharge or unsaturated zone processes, but differed in the number of GCMs and scenarios considered for future projections, as well as in the methodology applied for estimating recharge. Other studies have assessed groundwater recharge uncertainty under future conditions (Goderniaux et al., 2015; Shen et al., 2018; Xie et al., 2018). Groundwater modeling has been applied to investigate future impacts of climate change on aquifers and their interaction with surface waters (Persaud et al., 2020; Scibek et al., 2007; Scibek & Allen, 2006; Taheri Tizro et al., 2019; Usman et al., 2020), and remote sensing has been used to study historical climate change impacts on groundwater resources (e.g., Usman et al., 2020; Xu & Su, 2019). Nevertheless, there will always be uncertainty associated with climate models, particularly in mountainous regions such as the Central Andes where the topography changes abruptly, hindering its correct representation in models with large grids (Vuille et al., 2008). Therefore, studies that incorporate multiple scenarios to investigate hydrological and hydrogeological systems in arid catchments with complex topography, such as the Chilean Altiplano, are still scarce.

Recent studies have investigated the hydrological processes occurring in the Andean Chilean altiplano to evaluate groundwater recharge (Herrera et al., 2016, 2021; Uribe et al., 2015; Urrutia et al., 2019), to assess evaporation (de la Fuente et al., 2021; Hernández-López et al., 2014; Mosre & Suárez, 2021; Suárez et al., 2020); water table fluctuations (Viguier et al., 2019) and wetland dynamics (de la Fuente & Meruane, 2017; de la Fuente et al., 2021). Additionally, numerical groundwater modeling has been used to study the impacts of anthropogenic exploitation (Marazuela et al., 2020; Marazuela et al., 2019b, 2019a; Samuel et al., 2020; Scheihing & Tröger, 2018; Scheihing et al., 2017). Nonetheless, to the best of the authors' knowledge, there are no studies that have used numerical groundwater modeling to study and quantify the impacts of climate change in the Chilean Altiplano, despite this being essential to manage water resources in a sustainable way and to ensure the survival of groundwater-dependent ecosystems.

The main objective of this research is to develop a methodology that allows a proper management of groundwater resources in the Chilean Altiplano by: (1) accounting for

future uncertainty of climatic variables through ensemble scenarios, and (2) assessing potential impacts of climate change on groundwater recharge, groundwater levels, and groundwater discharge fluxes. To achieve this objective, this research uses statistical downscaling techniques to process GCM outputs, from different RCPs, to the local scale in an arid region in northern Chile. The downscaled outputs are used as input to a hydrological model for groundwater recharge estimation, which is then used in a hydrogeological model to simulate the aquifer's response to future climate change scenarios defined in this study. Our analysis considers two main time spans: a reference period (1981-2010) against which a future period (2020-2100) is evaluated. Therefore, even when the incidence of climate is important in long-term aquifer recharge in the central Andes during the Holocene (Herrera et al., 2018; Sáez et al., 2016), our work focuses on time scales on the order of decades. Furthermore, the focus of this research is to evaluate potential changes particularly in groundwater resources due to climate change in terms of water table changes and flow balance of the hydrogeological system. Therefore, even though recharge is a fundamental process related to groundwater, its particular aspects, such as timing shifts and intersessional behavior of sub-processes taking place in the vadose zone, are not the main focus of this research.

The Salar del Huasco basin, located in the Chilean altiplano, was chosen as our study site. The basin lies in the presence of groundwater-fed wetlands that sustain the life of unique flora and fauna (de la Fuente et al., 2021; Johnson et al., 2010). The wetlands are located in the boundaries of the salt flat nucleus, where groundwater springs form a shallow lake of 5-15 cm deep (de la Fuente & Meruane, 2016; Lobos-Roco et al., 2021). The Salar del Huasco is ecologically important because it is the home of three out of the six species of flamingos that exist in the world (the Andean flamingo, the Chilean flamingo and the James's flamingo), which come to the salt flat to create their nests (CONAF, 2005). It also shelters unique species such as Andean foxes, lamas, vicuñas, pumas, among others. As a result of this diversity, the salt flat was declared a RAMSAR zone of protected wetlands in 1996 and a National Park by the Chilean government in 2020. Given the importance of these wetlands in the study area, the achieving of our objective is focused on the

assessment of groundwater changes that could threaten future life in these groundwater-dependent ecosystem due to climate change. Groundwater resources in the Salar del Huasco basin have had no human intervention, and therefore all results obtained in this study represent the natural response of the system to the environmental forcing. Consequently, this basin could be considered as a baseline against which to compare other basins in the area where intervention exists, and thus be able to quantify the effects of such interventions in contrast with the natural response of the Salar del Huasco. Additionally, we expect that our results could be further extended and be a helpful reference for groundwater assessment in similar areas worldwide.

2.2. Study area

The Salar del Huasco is an endorheic basin located in the Andean plateau of northern Chile (latitude 20.28°S and longitude 68.85°W) (Figure 2-1). The basin extends over an area of 1,470 km^2 and it has a mean elevation of 4,165 m ASL. Its shallow lake is at the end of a well-developed alluvial system draining from the north of the basin, and constitutes the main water source that sustains life of unique flora and fauna species under extreme arid conditions (de la Fuente et al., 2021; Suárez et al., 2020).

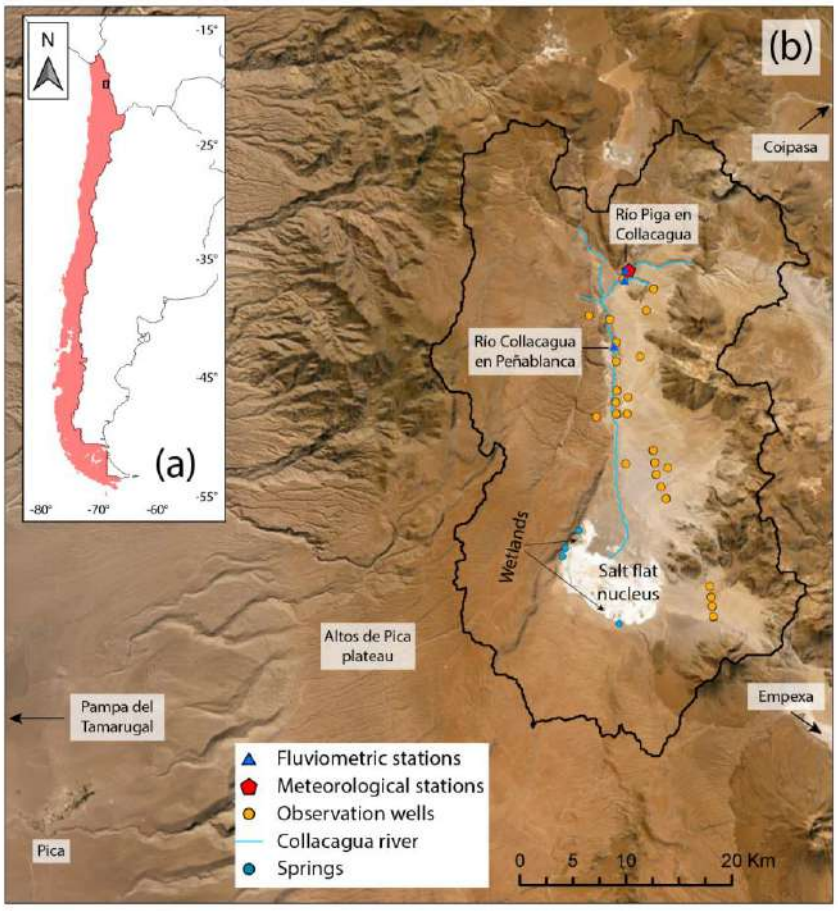

Figure 2-1: (a) General location of the study site; (b) the Salar del Huasco basin (outlined in black) with the location of fluviometric and meteorological stations, observation wells and springs. Nearby basins are also indicated in (b). (Background source: Esri, Maxar, Earthstar Geographics, CNES/Airbus DS, USDA, USGS, AeroGRID, IGN, and the GIS User Community).

2.2.1. Geological settings

The Salar del Huasco basin is bordered to the west by the Altos de Pica plateau, which represents the water divide from Pampa del Tamarugal (Viguier et al., 2019), and by the

Andes mountain range to the east that separates it from the Bolivian basins of Coipasa and Empexa. The Salar del Huasco basin was formed by volcanic activity that caused the emergence of Mesozoic and Paleozoic rocks to form the depressed basement area on which alluvial and lacustrine sedimentary materials were deposited as basin fill. Subsequently, Miocene rhyolitic tuffs with high degrees of welding originated from volcanic eruptions and deposited in the basin, being the Huasco ignimbrite the most important geological formation due to its extension and volume (Gardeweg & Sellés, 2015; Tapia et al., 2020). This volcanic activity gave rise to the Andes mountain range, closing the basin to the east, which continued to fill with volcanic debris and pyroclastic materials (DGA, 2009).

In general, the basin is considered a closed basin with little to no hydrologic connection to the neighboring basins. Previous studies, using isotope and geochemical information, have discarded a possible connection between the Salar del Huasco and the aquifer of Pica (Risacher et al., 1999; Uribe et al., 2015). However, Scheihing et al. (2017) discarded this connection arguing that water from Salar del Huasco would have to travel a long way under the mountain range, passing through geothermal deposits that would raise the temperature of water that discharge to Pica. Since that is not the case, they concluded that such connection does not exist. Consequently, in this study the Salar del Huasco is considered a hydrogeologically closed basin until there is more evidence to confirm otherwise.

2.2.2. Climate

Two types of climates can be identified in the Salar del Huasco, according to Köppen classification system: the Tundra climate due to high altitudes of the Andes and the Cold Desert climate. The former is in the northeastern part of the basin while the latter is mainly in the southwestern part. Mean daily temperatures are around 4-14ºC depending on the altitude, with great thermal oscillation between day and night. In winter months the lowest temperatures reach -20ºC (DGA, 2009). Evaporation is the main water discharge mechanism of the basin, with a mean annual potential evaporation of 1,200 mm/year (de la

Fuente & Meruane, 2016). Precipitation in this part of the Altiplano occurs in the austral summer (November through March) as heavy convective storms originated by the intense surface heating that destabilizes the local troposphere and by the establishment of upper-level easterly winds that transport moist air from the interior of the continent (Sáez et al, 2016, Garreaud, 2009; Garreaud et al., 2003). Interannual precipitation is highly variable, ranging from 11 to 400 mm/year (Garreaud et al., 2003; Hernández-López et al., 2014). Although marked wet and dry periods can be identified on the millennial time-scales (Sáez et al., 2016), the El Niño-Southern Oscillation (ENSO) phenomenon is the major source of the interannual variability in the Altiplano (Garreaud, 2009). It directly affects the coasts of Ecuador, Perú and northern Chile, causing indirect effects on most of subtropical South America and higher latitudes (Garreaud et al., 2009). Given the large-scale nature of this phenomenon in terms of its spatial and temporal extents, its assessment is beyond the scope of this study. However, note that GCMs used to study climate change do include these large-scale phenomena in their formulation (Stocker, 2014).

2.2.3. Hydrology

The Collacagua river is the main surface watercourse in the basin (Figure 2-1). It runs from north to south with daily flow rates that vary throughout the year in response to precipitation. Despite this, the average monthly flow rates do not vary significantly throughout the year. The upper section of the river, at the *Río Piga en Collacagua* fluviometric station, has a daily average flow rate of 0.13 m^3/s while the downstream section, at the *Río Collacagua en Peñablanca* fluviometric station, has an average of 0.15 m^3/s. The river between these two fluviometric stations gains water during most of the year. However, downstream *Río Collacagua en Peñablanca*, the water from the river infiltrates as it gets near the salt flat nucleus. The seasonal river flow dynamics are shown in the supplementary material.

In the topographic lowest point of the basin, a salt flat nucleus that originated due to long-term phreatic evaporation extends over 50-60 km^2, the flow paths of mineral-enriched

groundwater converge and are discharged to the atmosphere through evaporation (Corenthal et al., 2016). The Salar del Huasco aquifer discharges mainly into four springs that feed the wetlands located in the borders of the salt flat nucleus (Figure 2-1). Records at gauging stations at these four springs provided by the Chilean National Water Division (Dirección General de Aguas, DGA) show relatively stable discharges throughout the year, with annual averages ranging from 0.008 to 0.0023 m^3/s for the lowest and highest discharges, respectively (DGA, 2009)

2.3. Methods

The general methodology followed in this study is based on three major steps. The first step is to downscale temperature and precipitation outputs from multiple GCMs so they can be used at the basin scale. The projected scenarios used for climate change impacts assessment are also established in this step to represent different future conditions up to the end of the century. The second step is to calculate groundwater recharge using the downscaled meteorological data for each projected climate scenario and the hydrologic model developed by Uribe et al. (2015). In the third step, the groundwater recharge rates are used as inputs in the hydrogeological model of the Salar del Huasco aquifer. The model then simulates the behavior of groundwater over time under each projected scenario.

2.3.1. Climate projections

Simulations of projected climate scenarios were carried out using the hybrid delta (HD) approach with precipitation and temperature offsets based on the Coupled Model Intercomparison Project Phase 5 (CMIP5) (Taylor et al., 2012), multi model ensemble output. Ensemble models include all four RCPs scenarios. The HD method combines two well-established downscaling techniques: bias correction and spatial downscaling (BCSD) (Reclamation, 2014) and the delta method (DM) approach (Tohver & Hamlet, 2014). Here, we briefly describe both techniques and how they are applied in the HD statistical downscaling.

As a first step of the HD approach, the BCSD method is applied. In the BCSD technique, statistical properties of the cumulative distribution function (CDF) of climatic simulations from the GCMs are adjusted according to the statistical properties of the observed CDF in a baseline period. Thus, systematic bias of the GCM relative to the observed probability distribution is removed (Tohver & Hamlet, 2014; Wood et al., 2002).

The second step consists of applying the DM. In the DM, monthly changes of variables projected by the GCMs are determined and applied to monthly means of observations. To do this, the future is divided into time windows of equal length as the baseline observational period. For that purpose, the Collacagua station was chosen given it was the only one with enough precipitation and temperature records, in fact, from 1980 to 2010 there is a complete temperature record, and only one month (February 1992) with no precipitation records. In this case, 30-year windows were defined according to the available data in the station: 1981-2010 (baseline period), 2011-2040 (near future), 2041-2070 (mid-future) and 2071-2100 (far future). These windows were defined so there are no time gaps between the baseline and the distant future. Therefore, the downscaling results are continuously applied in the hydrological processes. The changes or deltas are calculated for temperature and precipitation, according to the following equations (Camici et al., 2014; Hamlet et al., 2010; Tohver & Hamlet, 2014):

$$T_{DM\,fut} = \overline{T_{obs}} + \left(\overline{T_{GCM\,fut}} - \overline{T_{GCM\,base}}\right) \tag{2-1}$$

$$P_{DM\,fut} = \overline{P_{obs}} \cdot \left(\frac{\overline{P_{GCM\,fut}}}{\overline{P_{GCM\,base}}}\right) \tag{2-2}$$

where *T* is temperature and *P* is precipitation. The subindices in equations (2-1)(2-2) are as follows: *obs* corresponds to the observed variables, *DM* is related to the variables corrected by that method, and *GCM base* and *GCM fut* refer to the variables simulated by the climate models in the baseline period and in the future, respectively. The overbar

reflects that the variables are monthly means. For a step-by-step description of the HD method see Hamlet et al. (2010) and Tohver & Hamlet (2014).

The final step in the HD approach is the temporal disaggregation, from which future daily series of the downscaled variables are obtained. Daily time series are then used as input to the hydrological model. This temporal disaggregation was performed according to Tohver et al. (2014) and Vormoor & Skaugen (2013):

$$T_{fut\ daily} = T_{obs\ daily} + \left(T_{fut\ monthly} - T_{obs\ monthly}\right) \quad (2\text{-}3)$$

$$P_{fut\ daily} = P_{obs\ daily} \cdot \left(\frac{P_{fut\ monthly}}{P_{obs\ monthly}}\right) \quad (2\text{-}4)$$

where $T_{fut\ daily}$ and $P_{fut\ daily}$ are the daily future variables; $T_{obs\ daily}$ and $P_{obs\ daily}$ are the observed daily temperature and precipitation data; $T_{fut\ monthly}$ and $P_{fut\ monthly}$ are the future monthly values obtained by the HD method; and $T_{obs\ monthly}$ and $P_{obs\ monthly}$ are the observed monthly temperature and precipitation data.

Consequently, the HD method perturbs the entire CDF, as opposed to the traditional use of the DM that only perturbs the monthly means of the observed variable (Tohver & Hamlet, 2014). Thereby, future time series of temperature and precipitation represent the changes projected by the GCM while preserving at the same time its characteristics and behavior (e.g. duration, location, interarrival time of storms) given by the observed data at a local scale (Hamlet et al., 2010).

In this study, the HD approach was applied to 219 climate models that include emission scenarios RCP2.6, RCP4.5, RCP6.0 and RCP8.5, to cover a larger range of climate projections and in the absence of a justification for choosing a particular RCP scenario (Hausner et al., 2014). Subsequently, the 10th, 50th and 90th percentiles of the downscaled variables were calculated to generate hybrid scenarios of temperature and precipitation that

are not subjected to a particular radiative forcing but instead are a compound of different emission scenarios simulated by different models (Hausner et al., 2016).

Table 2-1: Future scenarios configuration.

Temperature percentile	Precipitation (P) percentile	Scenario
T_{min}	P_{min}	Extreme-low
T_{max}	P_{max}	Extreme-high
T_{med}	P_{med}	Median
T_{min}	P_{max}	Cross-wet
T_{max}	P_{min}	Cross-dry

To have a broader spectrum of possible future scenarios, all precipitation and temperature percentiles were combined in the scenario definition, as shown in Table 2-1, where the 10^{th} percentile sub index was replaced by "min", 50^{th} by "med" and 90^{th} by "max", for simplicity.

In doing so, the hybrid scenarios take into consideration the large uncertainty that comes along with projected precipitation in the Altiplano due to the coarse resolution of GCMs that hinders an adequate representation of climatic gradients given by complex topographies (Urrutia & Vuille, 2009).

2.3.2. Groundwater recharge estimations

The semi-distributed hydrological model developed by Uribe et al. (2015) for the Salar del Huasco catchment was used to predict groundwater recharge under the climate change scenarios previously defined. The model uses as inputs the downscaled mean temperature

and precipitation. Estimates of reference evaporation (ET_o) at a daily basis are also used to obtain groundwater recharge. ET_o (mm/day) was calculated using the FAO-modified Blaney-Criddle (1950) equation (Doorenbos & Pruitt, 1977).

$$ET_o = a + b[c(0.46T_{mean} + 8.13)] \quad (2\text{-}5)$$

where a and b are fitting parameters, c is the mean annual percentage of daylight hours, and T_{mean} is the monthly mean temperature. The fitting parameters (a and b) were estimated using observed monthly pan evaporation data at Collacagua station in the period between January 1981 and December 2010, corrected by a pan factor of 0.7 as suggested by DGA (2009). Equation (2-5) was selected to estimate future projections of ET_o since it is a simple approach that uses T_{mean} as an input variable. In climate ensembles, T_{mean} is more reliable than other variables that are required for estimating ET_o with more sophisticated models, e.g., the Penman-Monteith, Thornwaite or Hargreaves equations (Allen et al., 2011).

The rainfall-runoff model used in this study was previously developed and validated by Uribe et al. (2015) for the Salar del Huasco basin and it is based on the Soil Moisture Accounting routine (SMA) of the HEC-HMS model (Feldman, 2000; Hydrologic Engineering Center (US), 2001). For its development, they defined five hydrologic response units (HRU) (Figure 2-2b) according to the hydrogeological characteristics of the basin, whose connectivity was set using a 90 m resolution digital model elevation (DEM) from the Shuttle Radar Topography Mission (SRTM). HRU R1 was defined as rocks with very low effective porosity and without fractures, R2 represents fractured rocks with significant effective porosity; S1 represents lacustrine and evaporite deposits, S2 corresponds to alluvial and colluvial deposits, and S3 represents fluvial deposits. A set of 15 parameters were defined for representing the hydrological processes at each HRU, which were calibrated and validated using stream flow records between 1978 and 2010 at

station *Río Piga en Collacagua*. Here, we provide a brief description of this model. For a detailed description of the model structure the reader is referred to section B of the supplementary material, and to Uribe et al. (2015) for details on the model configuration (such as HRU definition), the parameters involved and their calibration, long-term recharge characterization and model performance.

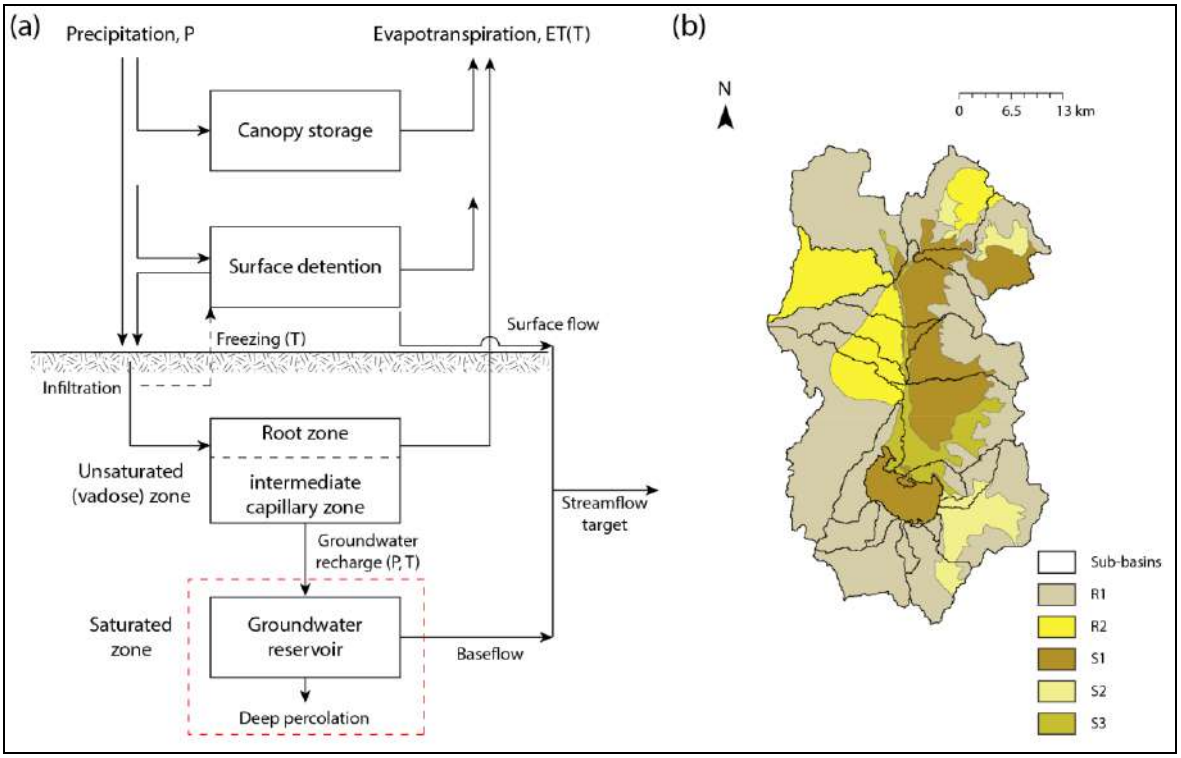

Figure 2-2: a) Diagram of the rainfall-runoff model structure that shows a conceptual description of the hydrological processes considered in each hydrologic response unit (HRU) in the Salar del Huasco basin. In the current work, the groundwater reservoir is represented by the groundwater model. The variables that are inside the parenthesis indicate that the hydrological process is dependent on these variables, e.g., evapotranspiration depends on temperature: ET(T). b) Map of the model configuration that shows the five HRUs defined by Uribe et al. (2015) and the 21 subbasins that contribute to the main drainage network of the basin.

The rainfall-runoff model simulates the hydraulic processes occurring at the surface and soil in HRUs through mass balance relationships in four reservoirs that represent the different levels of the system at daily time steps (Figure 2-2a). The reservoirs simulate: (1) canopy storage, (2) surface detention, (3) unsaturated soil processes and (4) the saturated

zone. The basic mechanism behind the balance in each reservoir is that the incoming water can change its storage, evaporate, become runoff, or percolate into the next reservoir (Uribe et al., 2015). In the canopy storage reservoir, precipitation intercepted by vegetation's foliage evaporates while the remaining precipitation that was not captured passes as input to the next reservoir. Since vegetation species that develop in this arid zone have little or no foliage, canopy storage is almost negligible. Modifications made by Uribe et al. (2015) to adjust the model to the climatic conditions of the Salar del Huasco consisted in the simulation of freezing at the unsaturated zone by introducing a temporal lag if the daily mean temperature is below 0 ºC, and the simulation of groundwater routing using a series of linear reservoirs to better represent the generated hydrograph. The former modification was meant to represent the general behavior of the basin at low temperatures. Sublimation or a more detailed representation of snow melting are not included in this model. To justify the use of a simplified mechanism instead of a more complex representation of snow-related processes, we used Landsat images, acquired from USGS's Earth Explorer (earthexplorer.usgs.gov/), to estimate the number of pixels with snow in the months in which it occurs in the baseline period. To do this, we calculated the Normalized Difference Snow Index (NDSI) and estimated the percentage of area that the pixels with snow represent of the total basin. We found that the average snow coverage between 1986 and 2010 is of 1.52% of the total basin and the median value is of 0.46%, which supports the simplification of Uribe et al. (2015) already validated model.

The mass balance in the vadose zone reservoir depends on the soil's storage capacity, the percolation rate to the next reservoir, and the meteorological conditions of the day being analyzed. Additionally, a temporal lag in evaporation and infiltration processes is represented when temperatures are too low. The outputs of the balance in the saturated zone are the deep percolation and the baseflow, the latter calculated as a series of linear reservoirs to simulate the routing hydrograph through the basin. Groundwater recharge is defined as the total amount of water entering the saturated zone, which can become deep percolation or baseflow (Uribe et al., 2015). The usefulness of the saturated zone reservoir

is that it allows simulating the processes of deep percolation and baseflow separately, allowing the latter to be used to calibrate the parameters of the hydrological model.

In the SMA routine of the HEC-HMS model (Hydrologic Engineering Center (US), 2001), the rate of percolation between the soil-profile storage and the saturated zone (i.e., groundwater recharge), depends on the volume in the source and receiving reservoirs. It is calculated as a function of a maximum percolation rate and the contents of the storage from which percolation is occurring (Bennett & Peters, 2004). The maximum percolation rate and maximum storage capacity of each reservoir are parameters that are different for each HRU of the model. Their values are determined after calibrating the model, and future simulations of groundwater recharge are performed under the assumption that they remain constant in time. Since changes in vegetation would impact soil parameters (due to root uptake and transpiration), it is assumed that variations in vegetation patches in the basin does not change dramatically in the future.

Actual evaporation from the subsurface (E_a) is among the calculations performed by the hydrological model to obtain groundwater recharge. This value is further used to calculate how much water remains from ET_o that is still available to be evaporated in the aquifer, which we define as remnant evaporation (E_{rem}).

Note that recharge resulting from the hydrological model is used as input to the groundwater flow model and is therefore considered as actual recharge as it reaches the water table (de Silva & Rushton, 2007; Scanlon et al., 2002).

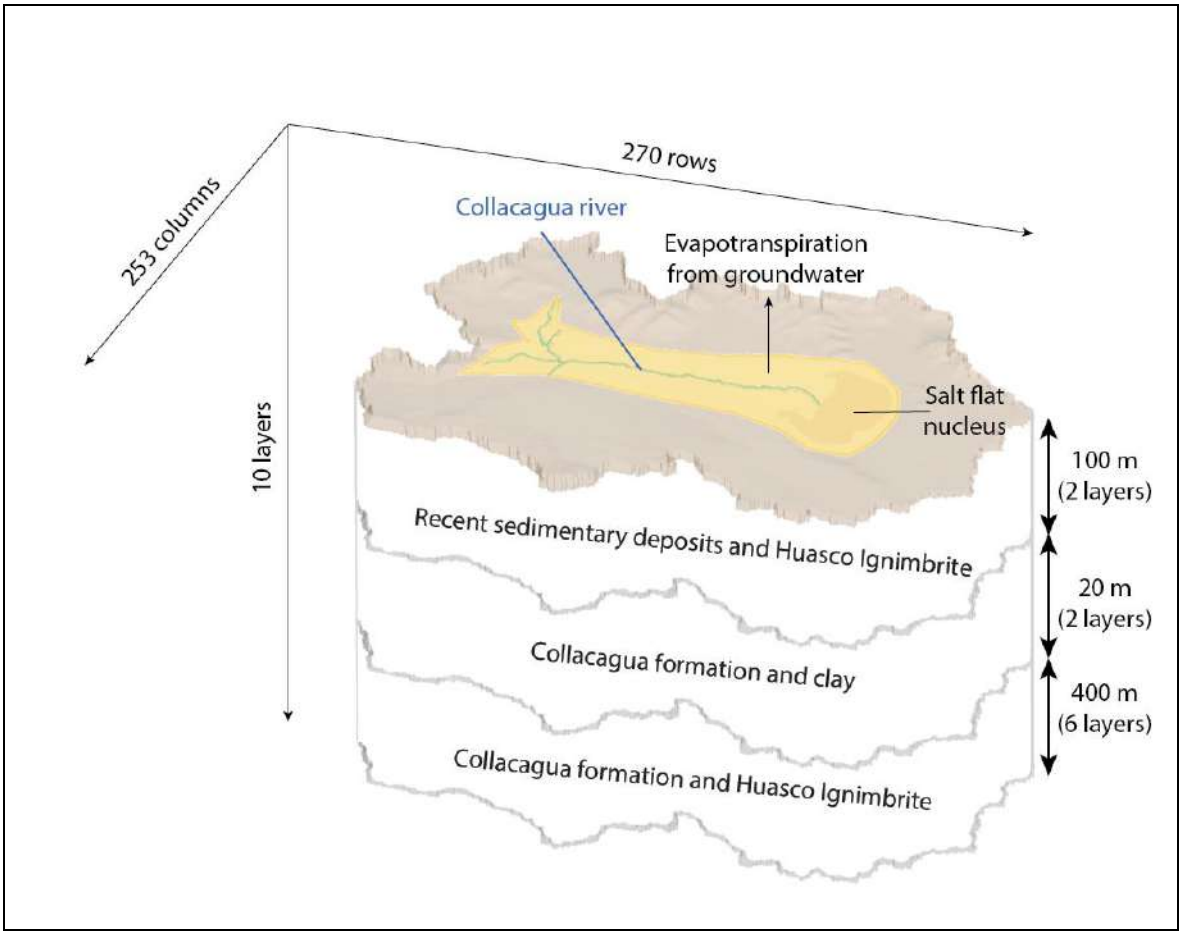

Figure 2-3: Configuration of the hydrogeological model developed in Modflow using ModelMuse. The "z" axis shows discretization into layers of three main aquifers: an upper aquifer made of recent sedimentary deposits and Huasco Ignimbrite, a middle aquifer of clay and Collacagua formation (sequence of gravel lacustrine deposits, silt, clay and sand (Acosta, 2004)) and a lower aquifer of Collacagua formation and Huasco Ignimbrite. A geologic fault develops at the bottom of the lower aquifer, represented in the model as a zone of higher hydraulic conductivity.

2.3.3. Groundwater flow model development

The groundwater flow model used to simulate the behavior of the aquifer under each scenario was developed in MODFLOW (Harbaugh et al., 2000), which is a widely used numerical model that solves the groundwater flow equation through a porous media in three dimensions, and can represent groundwater and surface water interactions. The main focus of our research is to assess the effects of climate change by analyzing changes in future simulations with respect a baseline period rather than analyzing absolute values of potentiometric surfaces, and therefore, effects of variable density were not considered since they are not expected to affect such changes. Furthermore, given the ecological importance that exists in the surroundings of the wetlands, we gave especial attention to this area.

The model was built using the open-source interface ModelMuse (Winston, 2009). The geometry of the model consists of 270 rows, 253 columns and 10 layers (Figure 2-3) that discretize three main aquifers. The vertical discretization of the three aquifers into 10 layers was defined to avoid convergence problems associated with cell dimensions, which was done using the uniform spacing option in ModelMuse (Winston, 2009). No-flow boundary condition were set at the edges of the model according to previous hydrogeological and geochemical studies (Risacher et al., 1999; Scheihing et al., 2017). The model was run under steady state conditions for the baseline period and under transient conditions for the future projections. In the latter, monthly stress periods were used from 2020 to 2100. The spatially distributed monthly groundwater recharge projections, obtained from the hydrological model, were incorporated in the groundwater flow model using MODFLOW's Recharge package (RCH) (Harbaugh et al., 2000). More specifically, monthly recharge rates calculated with the rainfall-runoff model (described in section 3.2) were imported to ModelMuse using a shapefile to distribute them throughout the model domain, according to the sub-basin spatial distribution Figure 2-2b. The Collacagua river was represented in the groundwater model using the River package (RIV) (Harbaugh et al., 2000). An average river depth of 10 cm and conductance of 0.06 - 0.12

m^2/s were assigned along the course of the Collacagua river. These values were defined after the steady state calibration to represent the flux interacting with the aquifer (Acosta, 2004).

The four springs located near the wetlands were represented in the model using the Drain package (DRN) (Harbaugh et al., 2000). The stage and conductance of each drain were defined and calibrated using DGA's records of fluviometric stations at the springs, which are available at www.dga.cl. Groundwater evaporation was modeled with the Evapotranspiration package (EVT) (Harbaugh et al., 2000), and was defined near the wetlands and streambed of the Collacagua river, where the water table is shallow enough to allow groundwater evaporation. A potential evaporation of 6.3 mm/day was defined in the steady state simulation, according to pan evaporation records in Collacagua meteorological station, between April 1994 and May 2007 (Acosta & Custodio, 2008; Uribe, 2012). In the transient simulations, monthly evaporation rates were introduced, corresponding to the simulated E_{rem}, which represents the water available for evaporation in the aquifer. The extinction depth was set to 3 m beneath the surface, typical for arid saline soils (Shanafield et al., 2015), and in agreement with ET measurements performed in the basin with the portable chamber method (DGA, 2009; Johnson et al., 2010). To avoid confusion, in the rest of the document we use the term "groundwater evaporation" to refer to this discharge, while the term "groundwater recharge" refers to the output of the hydrological model, which includes the evaporation at the subsurface (*i.e.*, E_a).

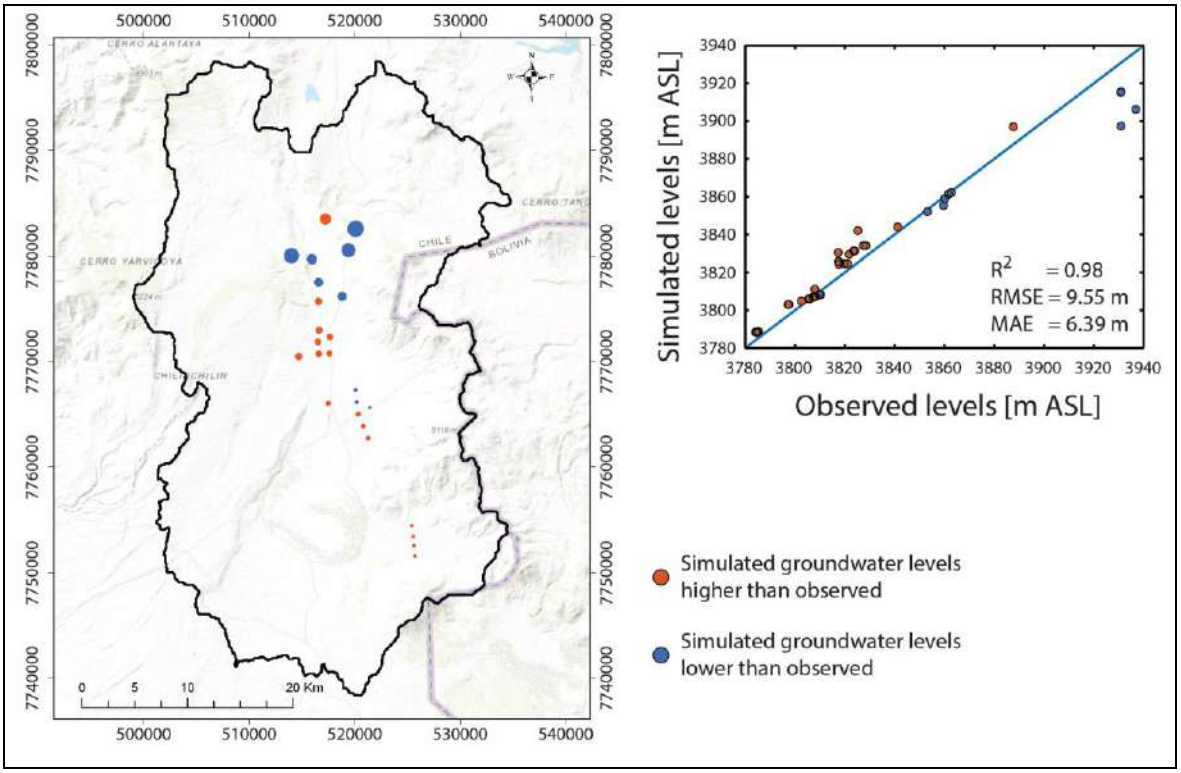

Figure 2-4: Observed and simulated groundwater levels obtained in the steady state calibration. The map on the left shows the level of adjustment of the simulated heads in wells distributed throughout the basin, where blue circles denote simulated levels lower than observed and red circles denote simulated levels higher than observed. The size of the circles is proportional to the difference between the observed and simulated level. The chart on the right shows the adjustment of simulated levels to observations, where the same color notation as in the left map is used, with red and blue markers that represent simulated levels higher and lower than observed, respectively.

2.3.4. Groundwater flow model calibration and simulations

A steady state simulation was performed to represent the long-term historical (last 40 years) behavior of the aquifer. To ensure the adequate representation of conceptual model

inflows and outflows of the groundwater system according to previous studies (Acosta & Custodio, 2008; DGA, 2009; Johnson et al., 2010; Uribe et al., 2015), a manual calibration of hydraulic conductivity was performed using observed levels at 44 monitoring wells (Figure 2-4), using the minimum of the mean absolute error (MAE) as objective function (Bennett et al., 2013). An ideal model would achieve a MAE of 0, nevertheless, the model is considered accurate if the MAE is less than 5% of the largest difference of observed data (SEA, 2012). The performance of the model was then evaluated with the root mean square error (RMSE) and the coefficient of determination (R^2) indicators (Bennett et al., 2013).

Due to the state of conservation that protects the Salar del Huasco basin from human intervention, there is little data on aquifer levels over the baseline period, which are required to perform a transient calibration. Thus, hydraulic conductivities were calibrated through a steady state calibration and storage values in the aquifer were assigned based on previous studies (Acosta & Custodio, 2008; DGA, 2009). Despite not having long time series of groundwater level information over the baseline period, records from 2005 and 2014 (SEA, 2019), along with isolated records from November 2018 (Suárez et al., 2020) were used to validate the model. The available groundwater levels are presented in section A of the supplementary material.

The groundwater model was used to simulate the aquifer's behavior in the baseline period: January 1981- December 2010; and in different future scenarios starting in the near future until the end of the century: January 2020 – December 2100. The results of this simulation characterized the aquifer behavior in a reference period against which future climate change simulations were compared.

2.4. Results

2.4.1. Climate projections

Future precipitation and temperature scenarios (10th percentile: denoted by subscript *min*, 50th percentile: *med*, and 90th percentile: *max*) projected with the HD approach are compared at a daily basis with observations in the baseline period (Table 2-2). Scenarios percentile from *min* to *max* are chosen to set guidelines for determining the system sensitivity to climate change. Future temperature scenarios, in all three-time windows, project a daily increasing trend in maximum, mean and median temperatures in comparison with the baseline period. Differences can be noted between scenarios though, where projected values increase from T_{min} to T_{max}.

Table 2-2: Comparison of projected future variables in the Near, Mid- and Far future periods with observations in the baseline period at a daily basis.

	Baseline	Near future			Mid-future			Far future		
	1981-2010	2011-2040			2041-2070			2071-2100		
T (°C)	Obs	T_{min}	T_{med}	T_{max}	T_{min}	T_{med}	T_{max}	T_{min}	T_{med}	T_{max}
minimum	-8	-5.50	-5.07	-4.57	-4.90	-4.01	-2.85	-4.61	-3.04	-0.60
maximum	14.1	14.66	15.13	15.90	15.18	16.28	17.70	15.43	17.09	20.09
mean	4.46	5.04	5.44	5.96	5.61	6.44	7.68	5.78	7.16	9.88
median	4.4	4.91	5.31	5.84	5.48	6.32	7.55	5.66	7.01	9.77
standard deviation	3.56	3.35	3.32	3.27	3.34	3.26	3.25	3.30	3.20	3.19
P (mm)	Obs	P_{min}	P_{med}	P_{max}	P_{min}	P_{med}	P_{max}	P_{min}	P_{med}	P_{max}
minimum	0	0	0	0	0	0	0	0	0	0
maximum	31	28.5	34.87	65.94	28.5	41.35	81.68	28.5	39.69	87.82
mean	0.36	0.17	0.30	0.53	0.16	0.29	0.58	0.13	0.32	0.64
median	0	0	0	0	0	0	0	0	0	0
standard deviation	1.82	0.96	1.63	3.03	0.92	1.64	3.43	0.78	1.77	3.75

Unlike temperatures, projected precipitation behaves differently in each scenario. Substantial differences are observed in the mean and maximum statistics, where in all three future windows, P_{max}'s mean and maximum exceed those in the baseline period, while in P_{min} the opposite occurs. Increasing and decreasing trends can also be easily distinguished between scenarios at monthly basis (Figure 2-5), where all temperature scenarios project a total increase, while precipitation varies throughout the scenarios defined in Table 2-1.

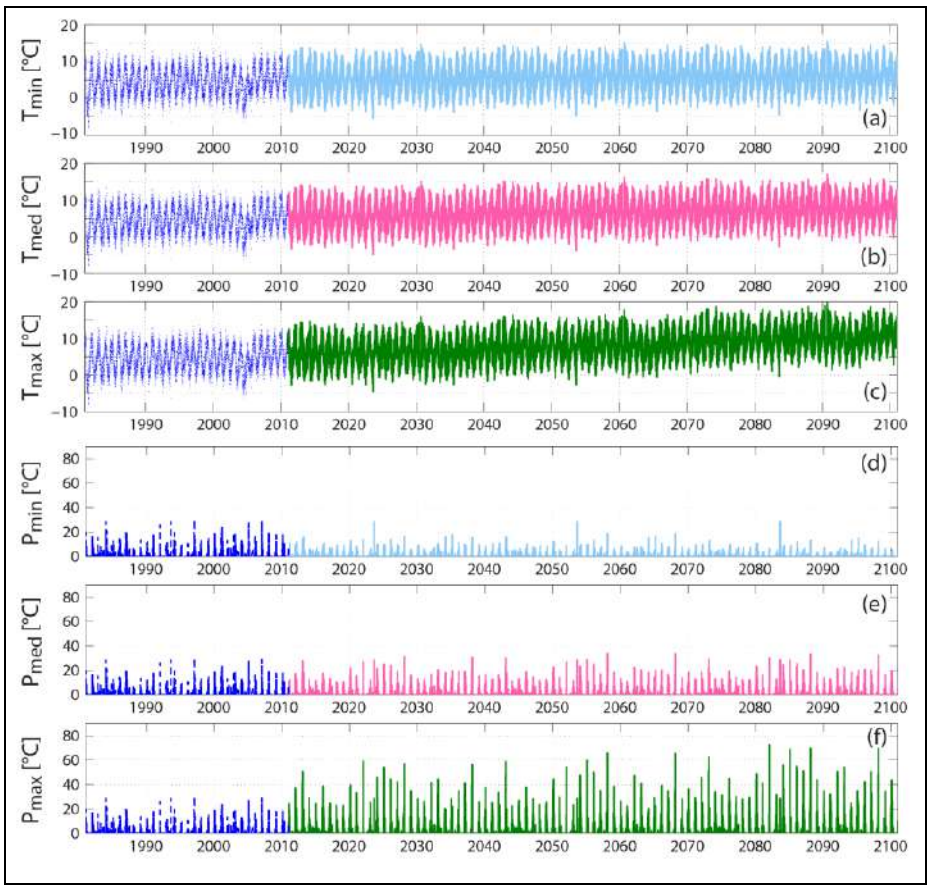

Figure 2-5 Temporal evolution of temperature, T, (top three charts) and precipitation, P, (bottom three charts) for the minimum, median and maximum scenario at monthly basis. In all charts, the dashed dark blue line represents the observations between 1981 and 2010 registered in Collacagua meteorological station.

2.4.2. Groundwater recharge

2.4.2.1. Baseline period

The hydrological model was run first for the baseline period to simulate historical groundwater recharge. The model took approximately seven years to stabilize, and after this spin-up period groundwater recharge is relatively stable in time, with an estimated value of 42.9 ± 27.9 mm/yr (mean ± standard deviation) (Figure 2-6) over the model domain. Groundwater recharge varies with seasons with peaks occurring mostly during summer months, which means that summer precipitation is transformed almost immediately into groundwater recharge.

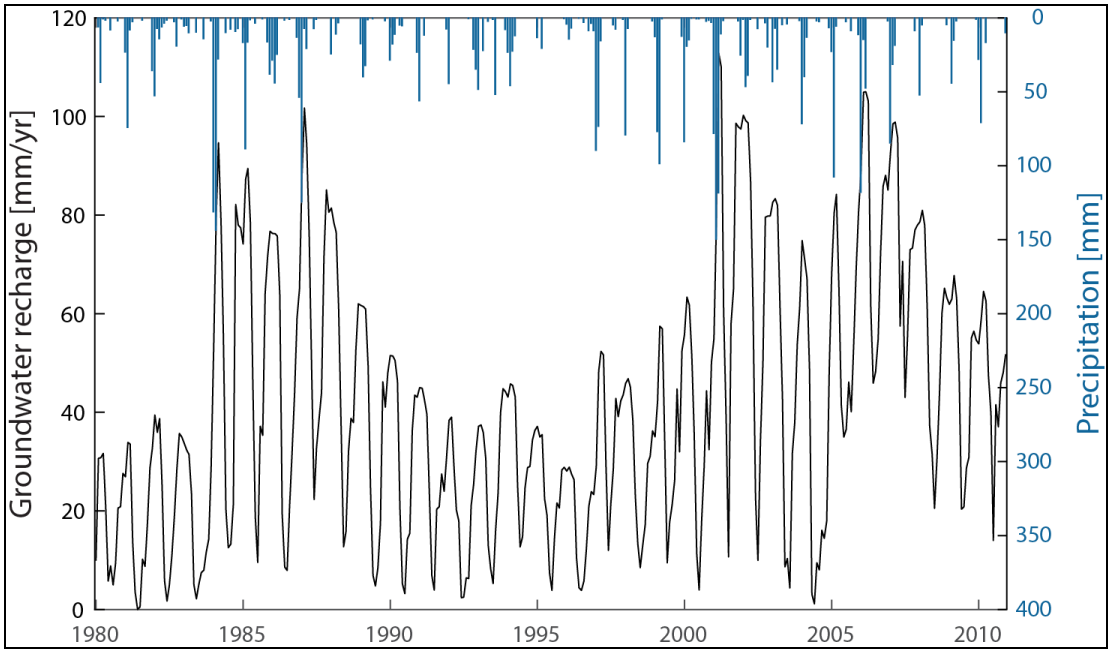

Figure 2-6: Groundwater recharge estimated for the baseline period presented as monthly averages. Monthly observed precipitation data are also presented in right axis.

2.4.2.2. Future projections

Scenarios that project an increase in recharge represent those with the highest precipitation input (P_{max}), corresponding to the cross-wet and extreme-high scenarios (Figure 2-7). Both scenarios differ in their temperature inputs, which greatly affects seasonal variability of recharge. Higher temperatures in the extreme-high scenario allow for higher percolation in winter months in comparison with the cross-wet scenario, reducing the differences between summer and winter recharge as opposed to what occurs in the cross-wet scenario. However, an overall greater recharge is generated in the cross-wet since the higher temperatures of the extreme-high scenario produce higher evaporation rates in the surface, reducing the amount of water that infiltrates and transforms into recharge.

Temperature effects can also be observed in scenarios with the lowest precipitation input (P_{min}). As mentioned before, higher temperatures mean that groundwater recharge does not decrease as much in winter months due to the relatively warmer temperatures. As a result, the cross-dry scenario has an overall greater recharge in comparison with extreme-low, which is the scenario that projects the lowest recharge rates.

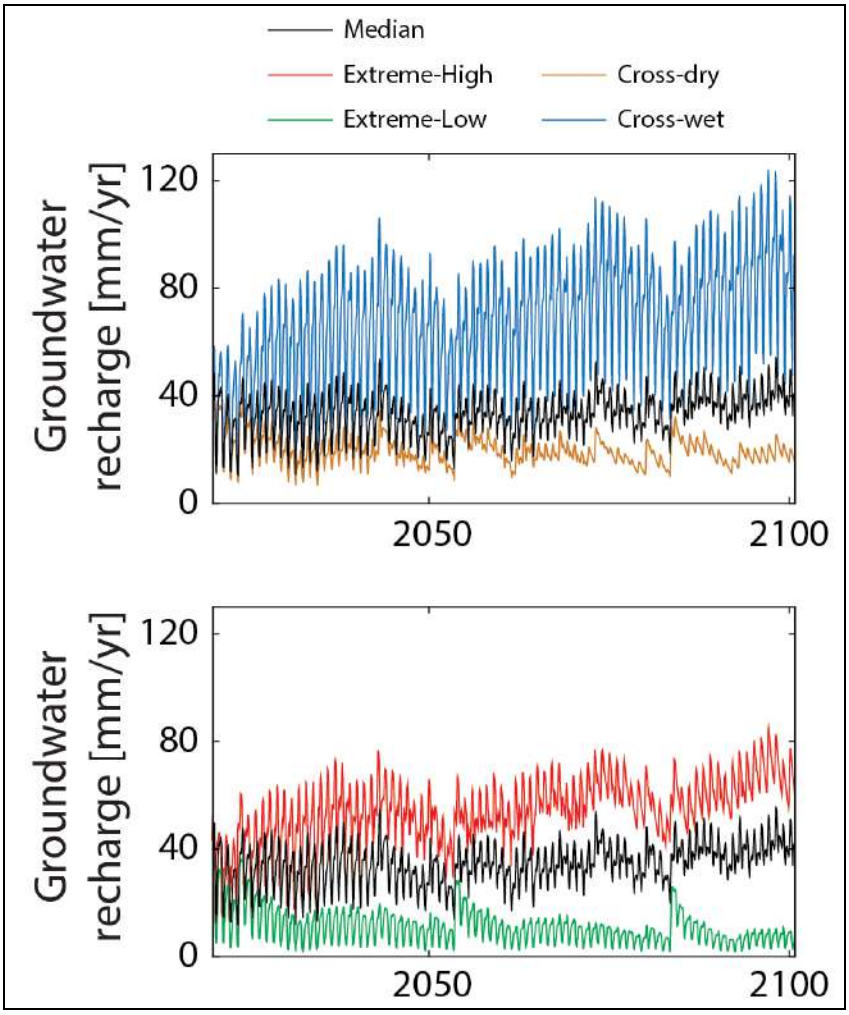

Figure 2-7: Groundwater recharge estimated for the different scenarios evaluated in this study. The Median scenario (black line) is plotted in both charts in order to compare median conditions with both cross and extreme scenarios.

Table 2-3 shows projected changes in groundwater recharge for the mid- and far-future periods with respect to the baseline period (the near-future period was not included in the table since future simulations start in 2020). Positive changes are projected in both periods in scenarios with increasing recharge, while negative changes are projected otherwise.

Table 2-3: Comparison of groundwater balance components for the mid-future (2041–2070) and far-future (2071–2100) periods with respect to the baseline (1981–2010) as fluxes percentiles. Baseline shows absolute values, while future periods show the projected changes (future values minus baseline value). The percentages of change that each delta represents are in parenthesis.

			Baseline	Median	Extreme-High	Extreme-Low	Cross-Dry	Cross-Wet
Recharge (mm/yr)	*25th*	Mid-future	15.3	-4.02 (-26.3%)	16.2 (105.9%)	-9.95 (-65%)	-3.70 (-24.2%)	23.5 (153.7%)
		Far-future		-2.10 (-13.7%)	20.27 (132.5%)	-11.86 (-77.5%)	-4.40 (-28.7%)	29.30 (191.6%)
	50th	Mid-future	22.61	-10.33 (-45.7%)	10.29 (45.5%)	-16.81 (-74.4%)	-10.41 (-46.1%)	18.69 (82.6%)
		Far-future		-8.98 (-39.7%)	15.34 (67.8%)	-18.61 (-82.3%)	-10.91 (-48.3%)	26.59 (117.6%)
	75th	Mid-future	34.19	-21.53	0.17 (0.5%)	-27.19 (-79.5%)	-20.19 (-59%)	9.31 (27.2%)
		Far-future		-19.91	5.71 (16.7%)	-29.37 (-85.9%)	-20.69 (-60.5%)	16.91 (49.5%)
Groundwater evaporation (mm/yr)	*25th*	Mid-future	0	0	0	0	0	0
		Far-future		0	0	0	0	0
	50th	Mid-future	0	0	0	0	0	0
		Far-future		0	0	0	0	0
	75th	Mid-future	14.5	-2.49	7.59 (52.3%)	-7.64 (-52.7%)	-4.85 (-33.5%)	14.45 (99.6%)
		Far-future		-1.85	5.87 (40.5%)	-8.93 (-61.6%)	-5.71 (-39.4%)	17
River discharge (mm/yr)	*25th*	Mid-future	20.3	-13.3 (-65.4%)	7.4 (36.2%)	-21.3 (-105%)	-15.6 (-76.8%)	16.6 (81.6%)
		Far-future		-13.2 (-65.1%)	8.0 (39.4%)	-21.2 (-104.4%)	-15.4 (-75.7%)	17.9 (88%)
	50th	Mid-future	20.7	-13.5 (-65.1%)	7.2 (35%)	-21.5 (-104.2%)	-15.7 (-76.1%)	16.5 (79.6%)
		Far-future		-13.4 (-64.7%)	7.9 (38.1%)	-21.4 (-103.7%)	-15.7 (-76.1%)	17.7 (85.9%)
	75th	Mid-future	21.8	-14.3 (-65.6%)	6.5 (29.8%)	-22.6 (-103.4%)	-16.7 (-76.8%)	15.7 (72.1%)
		Far-future		-14.3 (-65.6%)	7.2 (32.8%)	-22.5 (-103%)	-16.7 (-76.4%)	17.0 (78%)
Spring discharge (mm/yr)	*25th*	Mid-future	3	-0.2 (-7.1%)	0.4 (12.9%)	-0.4 (-12.9%)	-0.3 (-9.3%)	0.4 (12.9%)
		Far-future		-0.3 (-9.2%)	0.3 (9.8%)	-0.5 (-15.1%)	-0.4 (-12%)	0.3 (10.2%)
	50th	Mid-future	3.1	-0.3 (-8.5%)	0.3 (9.6%)	-0.5 (-15.4%)	-0.4 (-11.9%)	0.3 (10.3%)
		Far-future		-0.3 (-9.2%)	0.3 (9.8%)	-0.5 (-15.1%)	-0.4 (-12%)	0.3 (10.2%)
	75th	Mid-future	3.1	-0.3 (-9.2%)	0.3 (9.4%)	-0.5 (-15.4%)	-0.4 (-12%)	0.3 (9.4%)
		Far-future		-0.3 (-9.2%)	0.3 (9.8%)	-0.5 (-15.1%)	-0.4 (-12.0%)	0.3 (10.2%)

Finally, Figure 2-8 shows seasonal changes projected per each scenario by the end of the century in terms of monthly mean recharge throughout the year over the far-future period (2071 – 2100) in comparison with the baseline simulation (blue dashed line). Figure 2-8 allows assessing groundwater recharge changes not only in magnitude, but also in terms of its behavior between seasons. Taking that into account, the groundwater recharge behavior in the cross-wet scenario is the one that most closely resembles that of the baseline, but with higher magnitudes. Regarding magnitudes, recharge in the median and cross-dry scenario are closest to the baseline in winter months (May through August), while in summer recharge in the extreme-high scenario is the closest. Also, the effect of temperature in recharge in winter in scenarios with higher temperatures (cross-dry and extreme-high) mentioned above can also be observed in Figure 2-8, where less variations between winter and summer can be observed.

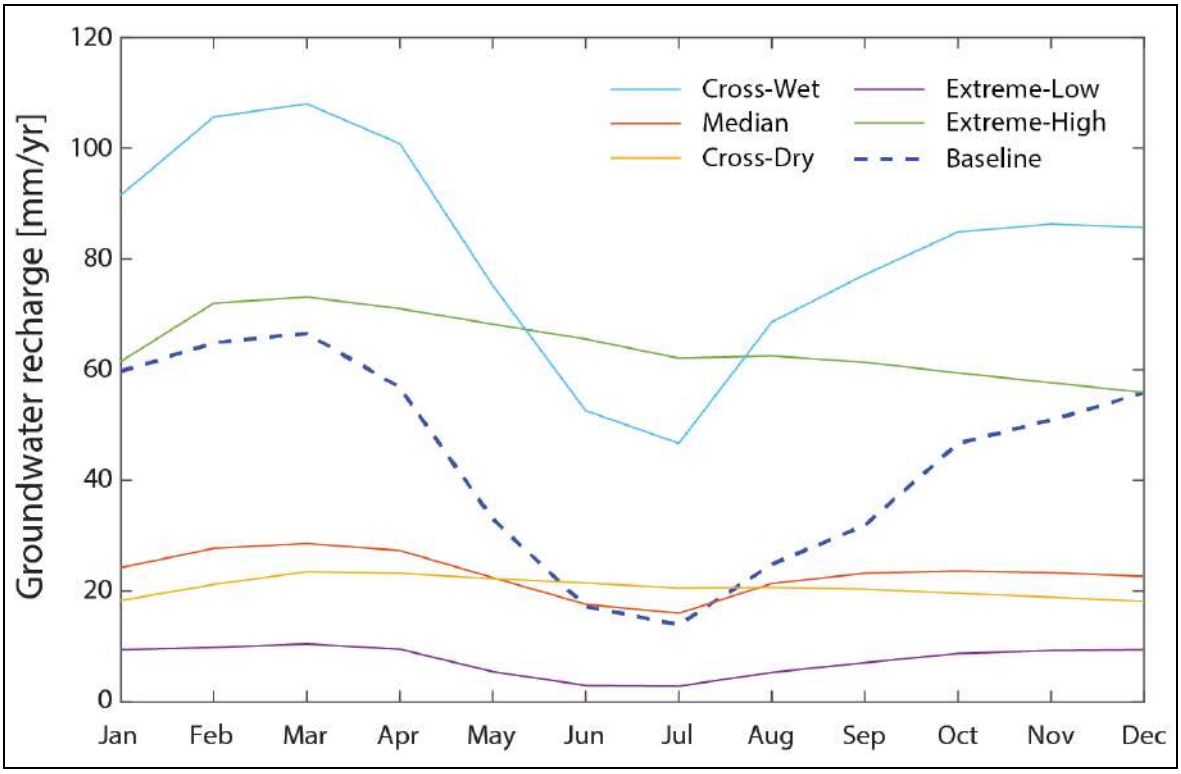

Figure 2-8: Mean monthly recharge over the far-future period (2071 – 2100). The blue dashed line shows the recharge rate simulated in the baseline period (1981 – 2010).

2.4.3. Groundwater model simulation

2.4.3.1. Steady state simulation

The MAE in the steady state simulation was of 6.4 m, which corresponds to 4.2% of the largest observed difference. RMSE and R^2 values, of 9.55 m and 0.98 m, respectively, indicate a good model performance, with an overall good fit (simulated levels close to the 1:1 line). The map in Figure 2-4 shows the spatial distribution of the calibration performance at each well given by the size of the circular marker, that increases along with

the difference between observations and simulations. It can be thus noted that groundwater levels are being better represented at lower altitudes in the basin, which includes the area of the wetlands and their surroundings. Using the groundwater levels registered in nine observation wells in the November 2018 field campaign, a MAE of 9 m (which corresponds to 5.8% of the largest observed difference) and a R^2 of 0.90 were obtained.

2.4.3.2. Baseline period

Water discharge from the springs and the river are the fluxes that remain most stable in time, while evaporation is the discharge with the largest variation (Figure 2-9). The median evaporation rate is null, signifying half of the time water is not being discharged through this process, but when evaporation occurs its magnitude varies greatly, reaching up to 1.8 m^3/s (38.6 mm/yr). Zero groundwater evaporation means that the water table is below the extinction depth of evaporation and consequently the aquifer is not discharging by evaporation in the stress periods when that occurs. Thus, despite the high magnitudes that can be reached by evaporation, its average is below that of groundwater recharge.

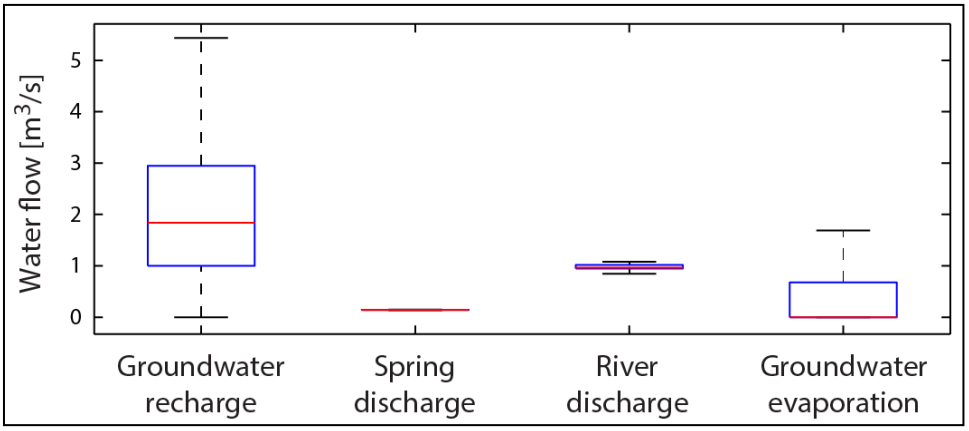

Figure 2-9 Boxplot of mass balance components of the baseline period simulation (1981-2010). Medians correspond to the red lines. Groundwater recharge component corresponds to an input of the MODFLOW model estimated with the rainfall-runoff model.

2.4.3.3. Future projections

The groundwater model was used to simulate future behavior of the system using the projected recharge for each scenario. The obtained results are analyzed in terms of mass balance components and equipotential contours.

Groundwater recharge corresponds to the only (external) source of water entering the aquifer. Groundwater-surface water interactions vary along the river course, starting from the northern-most elevated alluvial parts of the basin, where the river has a gaining reach, until the river reaches the lowest elevations near the salt flat nucleus, where it becomes a losing river. However, the net interaction between the river and the aquifer results in a groundwater discharge towards the river (referred to from here on as river discharge) in most scenarios.

Changes projected in mass balance components with respect to the baseline period in the mid- and far-future periods are presented in Table 2-3, which shows 25^{th}, 50^{th} and 75^{th} percentiles of flow changes. Note that the 25^{th} and 50^{th} percentiles of groundwater evaporation are zero, which means that most of the time evaporation is not from the aquifer, but it is only occurring at ground surface both in the baseline and future scenarios. Positive changes in the 75^{th} percentile result from the scenarios that project an increase in recharge, while negative changes are observed in the ones where recharge decreases (see section C of the supplementary material). Additionally, despite the slight projected changes reported in Table 2-3, spring discharge is the most stable flux in both future periods, with the lowest percentage of change with respect the baseline period. Scenarios with increasing recharge are the ones that project greater changes in all discharge fluxes, showing the buffering behavior of the basin (Table 2-3).

Figure 2-11 shows the simulated equipotential contours of climate change scenarios by the end of the year 2100, as well as the contours resulting from the baseline simulation by the end of 2010, in the sector of the wetlands. Looking at the shape of this equipotential line, it

is possible to observe that the 2100 equipotential map of the extreme-high scenario is the one that most closely resembles that of 2010 in the baseline simulation, while the rest of the future maps show changes in the shape of this contour.

2.4.4. Discussion

2.4.5. Groundwater recharge: future projections

Precipitation occurs mainly at higher altitudes and thus infiltration is greater in higher areas (higher subbasins), contributing thus to the overall increase in the total groundwater recharge. Temperature also plays a role, although minor, on groundwater recharge since the process of evaporation from the soil depends on it. When higher temperatures are projected at higher elevations (where temperatures are lowest within the basin) more water is evaporated in the root zone, increasing the space available in the soil reservoir for the incoming infiltration. This increases the potential infiltration rate, enhancing infiltration in areas where low temperatures normally limit the process. Nevertheless, the effect of temperature on groundwater recharge is smaller than that of precipitation. More details on the groundwater recharge produced in higher and lower subbasins and their contribution to the total recharge can be found in section D of the supplementary material. Other studies have also concluded that warmer temperatures reduce the amount of ground frost, allowing more water infiltration that leads to increased groundwater recharge in cold regions (Jyrkama & Sykes, 2007; Kovalevskii, 2007).

Evaporation depends on two aspects: the amount of precipitation entering the system and the ET_0 defined for each scenario (calculated with Equation (2-5) for the three temperature percentiles). As expected, scenarios with higher precipitation, i.e., cross-wet and extreme-high, produced the largest E_a rates, since not all precipitation can be transformed into groundwater recharge in the same time step.

2.4.6. Groundwater model: steady state simulation

Elevated parts of the basin, as shown in Figure 2-4, is where the greatest differences between observed and simulated heads occur. The steady state simulation underestimates the observed head in these elevated areas. Consequently, river discharge is likely to be underestimated in elevated areas.

2.4.7. Groundwater model: future projections

Groundwater evaporation is the main discharge mechanism that balances recharge inputs, being thus a major contributor in the equilibrium of the basin. Consequently, when recharge increases, groundwater evaporation increases due to a higher water table, eliminating the excess of water entering to the system. However, as shown in Figure 2-10d, across all model runs the median evaporation rate was zero, signifying that during half the simulation period no groundwater evaporation was occurring, but during the other half of the period groundwater evaporation is occurring with greater variability than the other mass balance discharge components. Therefore, although groundwater evaporation reaches the highest discharge, half of the time it has a null value. When evaporation is zero, river discharge is the main mechanism with which the basin stabilizes the recharge input.

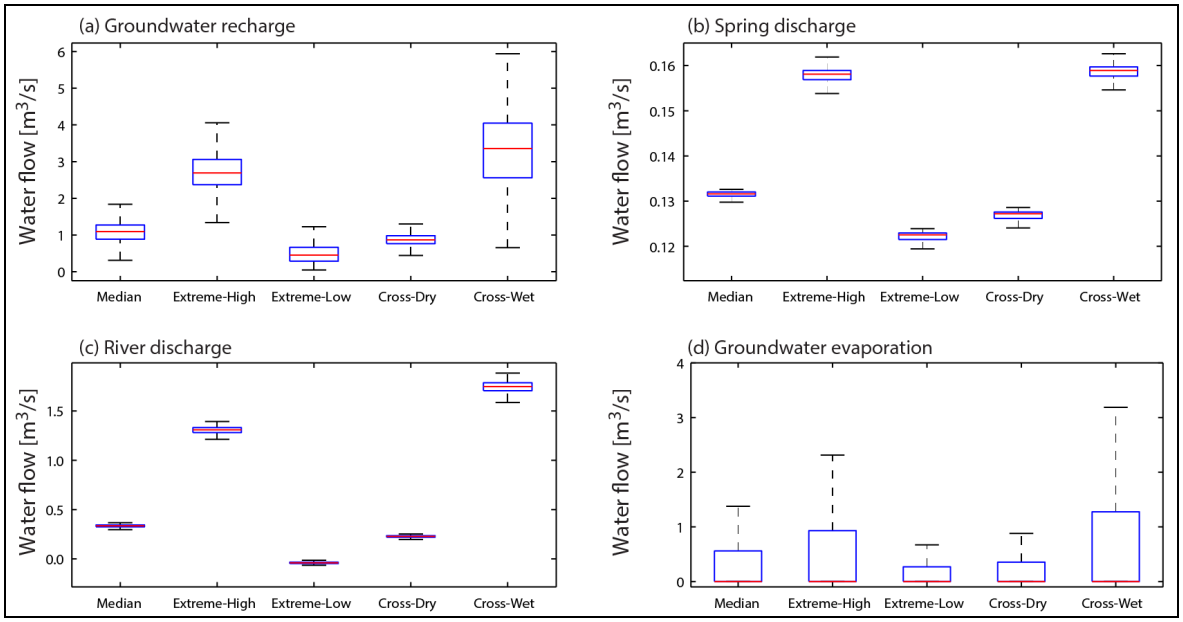

Figure 2-10: Box plot of mass balance components of (a) groundwater recharge (estimated with the rainfall-runoff model), (b) spring discharge; (c) river discharge and (d) groundwater evaporation, for the entire simulated period for each future scenario. The blue box indicates where the 50% of the results are concentrated, the red line is the median, whiskers extend to minimum and maximum values.

Results show that river and spring discharge are strongly related to the amount of recharge entering the system in each scenario (Figure 2-10). Groundwater recharge is higher in the most elevated parts of the basin, where river discharge occurs. Therefore, when groundwater recharge increases, the aquifer discharges more water into the river to maintain its balance. Consequently, scenarios with higher groundwater recharge project an increase in the median of this flux in comparison with the baseline period, whereas river discharge decreases as a result of a reduction in groundwater recharge. However, only in the extreme-low scenario does the river becomes a water source for groundwater, thus maintaining the balance in the system. Spring discharge shows a similar behavior, but with

much less variation between scenarios. This result implies that groundwater evaporation and river discharge balance groundwater recharge without significant changes in springs discharge, thus protecting this area from potentially big impacts. Table 2-3 shows that scenarios projecting greater changes in recharge are the ones that also project greater changes in all discharge fluxes, evidencing thus the buffering capacity of the groundwater system.

Future changes in the water table at the wetlands are analyzed in detail given the ecological interest of this area (de la Fuente et al., 2021; Suárez et al., 2020). By analyzing how the shape of the 3,780.6 m ASL equipotential line changes between scenarios (Figure 2-11), direct comparisons can be made of their forecasts in terms of wetter or drier conditions in the wetlands. This equipotential line represents the minimum value of the water table simulated in all scenarios and in the baseline period. Note the surface enclosed by this equipotential line (referred to herein as water table surface of lowest level) is not necessarily the lake surface since topography might be higher. In fact, a larger surface enclosed by this contour represents a lowering of the water table across the wetlands leading to a drier surface condition across the study site. On the contrary, when the surface enclosed by this contour is smaller, the water table is on average higher across the wetlands leading to wetter surface conditions and an increase in lake levels. The changes in the extension of this surface will surely affect the size of the wetlands and therefore the fauna and plant communities that depend on groundwater. As our focus is related to potential impacts of climate change on aquifer dynamics (i.e., impacts on potentiometric surface and water balance), it is critical to monitor how ecosystems can be impacted as the wetlands size changes, we refer the reader to the work of others (Fu et al., 2020; Mao et al., 2020; Mu et al., 2020; Peng et al., 2020; Shen et al., 2019; Weise et al., 2020; Wu & Zheng, 2020).

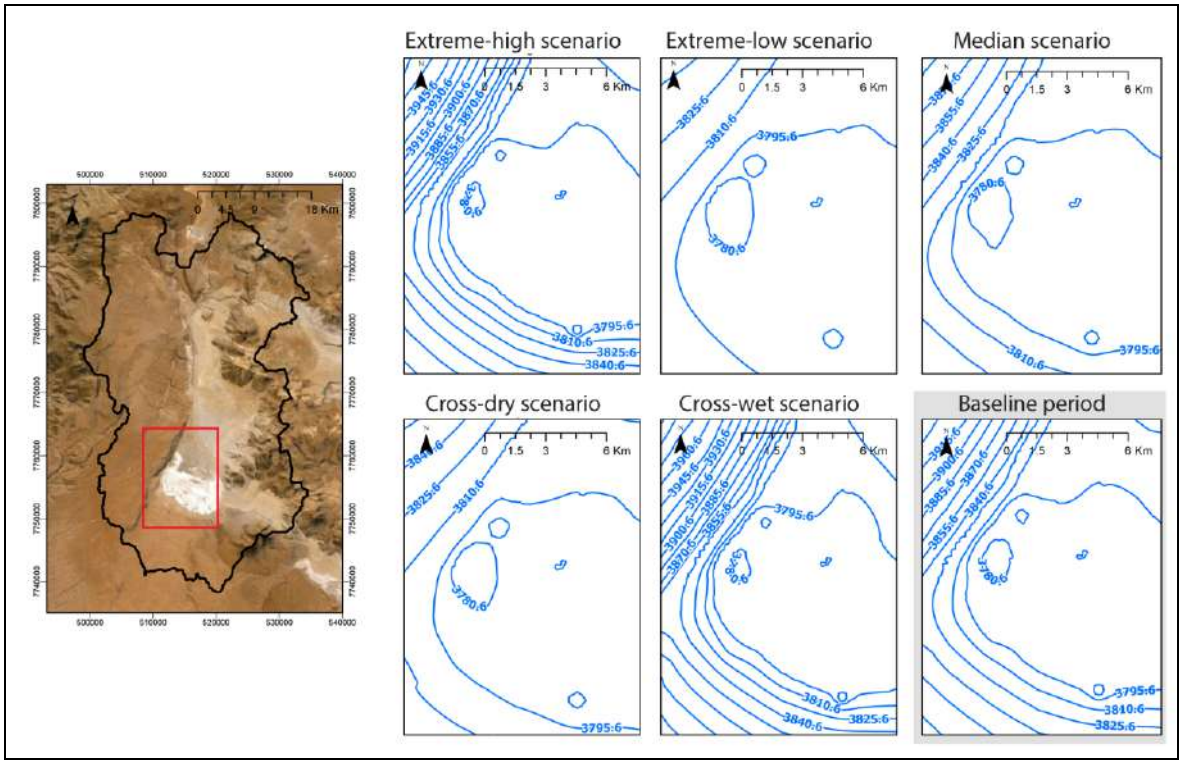

Figure 2-11 Simulated equipotential contours, i.e., contour maps, near the wetlands for the last stress period in the future projections (i.e., December 2100) and the baseline period (i.e., December 2010).

Low precipitation scenarios (P_{min} and P_{med}) project an increase in the water table surface of lowest level, i.e., deeper water table, forecasting slightly drier surface conditions in the wetlands. In comparing these scenarios, the 2100 equipotential map that most closely resembles that of 2010 is the extreme-high map, followed closely by the cross-wet map. This means the water table in the aquifer would remain stable (with slight increases) in future scenarios that project 38% increase in precipitation, while decreases in precipitation of 15% onwards would result in lower future groundwater levels in the Salar del Huasco.

Although there are changes in groundwater levels in the wetlands area, these changes are slight, and the overall behavior of the spring discharge is stable over time (Figure 2-10). These projections are in accordance with the stable behavior of the water levels observed in the basin between 2000 and 2016 (Figure A1 in Supplementary material), from which the buffering capacity maintained its balance despite the climatic changes (i.e., increasing temperature trends mostly). This is consistent with other studies such as that of Cuthbert et al. (2019), who found that groundwater fluxes in arid regions, and particularly groundwater discharge to wetlands in dry landscapes, are unaffected by climate change, showing lower response to climate variability than humid regions.

Regarding the groundwater modeling approach, our model does not consider variable density flow. Therefore, in reality, the absolute value of the potentiometric surface is likely to be affected in the salt flat margin, where a fresh-salt water interface develops (Marazuela et al., 2019c). However, as this occurs in a system with no anthropogenic perturbation, for the timescales investigated in this research the projected changes between the baseline and future simulations, which are the focus of assessment in our research, should not be affected.

As a final remark, model results are subject to the imposed boundary conditions, as well as to the mechanisms defined to represent the system's sinks and sources through which water exchange between the aquifer and its surroundings takes place. The quality of the representation of sinks and sources will depend on the available information in the study area and the objective of the modeling. In this case the main purpose of the model was to quantify the behavior of the groundwater system in the basin and its potential future changes. Therefore, further improvements may consider using additional remote sensing resources to fill the scarce available in-situ information in the study site to better represent such elements that simulate important water balance components such as evaporation, river infiltration and river discharge.

2.4.8. Future work

As part of future work regarding future groundwater recharge, it would be valuable to assess not only changes in its magnitude but also in its interannual variability and potential timing shifts. Additionally, it would be interesting to assess potential impacts of climate change using the new future scenarios of CMIP6.

2.5. Conclusions

This study investigated potential impacts of climate change by the end of the century in the aquifer of the Salar del Huasco basin, located in the high mountains of the Chilean Altiplano, characterized by its arid climatic conditions. The main conclusions of this work are:

- Future climate scenarios in the Salar del Huasco basin project an increasing trend in mean temperature, while precipitation shows varying trends between scenarios. However, all scenarios agree that there will be an increase in the magnitude of extreme events.

- Precipitation is the main driver of larger groundwater recharges resulting in higher groundwater evaporation rates. Additionally, the expected increase in future temperatures would likely lead to recharge with less seasonal variability.

- Groundwater evaporation is the main discharge mechanism that counterbalances the recharge inputs, being thus a key element in the system's balance.

- The aquifer responded to the different external conditions represented in each scenario by discharging and storing water accordingly, which results in different potentiometric levels. In scenarios where a lower groundwater

recharge is projected, results in lower groundwater levels and drier surface conditions near the wetlands; wetter surface conditions are expected when larger groundwater recharge is projected. However, these changes in the potentiometric surface are almost negligible in the area of the wetlands, where the groundwater-dependent systems are located, as a result of the balance between recharge and discharge fluxes, which manages to keep the water table generally stable in this area.

Results from this research demonstrate the Salar del Huasco aquifer would be able to buffer the impacts of climate change by balancing the inputs with outputs, maintaining the levels in the lake and wetlands, thus ensuring the conservation of unique ecosystems in the Chilean Altiplano. It is important to note, however, that the resilient capacity of the aquifer may be due to its protected status, and different results could be obtained if anthropogenic factors were interfering with the response of the system. Therefore, the advantages of being able to carry out this type of study in a protected area of the arid Altiplano are that (1) it could contribute to better manage the exploitation of other Altiplano groundwater-dependent ecosystems and even to define if any protection measures are necessary; (2) it could serve as a baseline of systems without anthropogenic action, allowing it to be compared with developed basins such as those used in the mining industry to distinguish the effects purely associated with climate change and those intensified by anthropogenic effects; and finally, (3) the results obtained could be generalized to regions of similar characteristics, which would contribute to a wider knowledge of what will happen in these areas and thus be able to manage groundwater resources more efficiently.

2.6. Acknowledgments

We acknowledge funding from the Agencia Nacional de Investigación y Desarrollo (ANID) through grant ANID/FONDECYT/1210221, as well as the Centro de Desarrollo Urbano Sustentable (CEDEUS – ANID/FONDAP/15110020) and the Centro de Excelencia en Geotermia de los Andes (CEGA – ANID/FONDAP/15090013). We also

thank the contribution of the reviewers (Dr. Alberto Sáez and an anonymous reviewer) and editors, which greatly improved the presentation of our results.

3. EVALUATING THE CONTRIBUTION OF SATELLITE-DERIVED EVAPOTRANSPIRATION IN THE CALIBRATION OF NUMERICAL GROUNDWATER MODELS IN REMOTE ZONES USING THE EEFLUX TOOL

3.1. Introduction

Numerical groundwater models are useful tools for representing aquifer dynamics at different spatiotemporal scales. They allow understanding of hydrogeological systems, making them a critical decision-making support tool for local and governmental institutions to achieve water security (Aghlmand & Abbasi, 2019; Post et al., 2019; Rabemaharitra et al., 2022). In a changing climate, it becomes even more pressing to understand the processes that govern aquifer dynamics to improve their management and mitigation of adverse consequences of overexploitation, for which groundwater modeling is key (Ezquerro et al., 2020).

To develop a robust numerical groundwater model that represents well the hydrogeological system, it is relevant to gather hydrometeorological and hydrogeological data over a certain period. However, in many regions monitoring networks are often sparse and have large inactivity, which makes them impractical for real-time decision-making (Sheffield et al., 2018). This issue is particularly true in developing regions, where the need for information is possibly greatest, and the lack of investment on infrastructure and human training has declined the number of monitoring networks (Fay et al., 2017; Lorenz & Kunstmann, 2012; Sheffield et al., 2018).

Remote sensing products are increasingly being used as a complementary source to provide hydrological, hydrogeological and meteorological information at multiple spatiotemporal scales, regardless of geopolitical boundaries (Karthikeyan et al., 2020).

Therefore, remote sensing products have increasingly been used in the construction and calibration of hydrological and hydrogeological models to balance the lack of in-situ information (Li et al., 2009; Sun et al., 2012; Sun et al., 2018). Different approaches have been followed to incorporate satellite images into hydrological/hydrogeological numerical models, such as incorporating land use and land cover images for investigating groundwater resources variability (Usman et al., 2020); using vegetation indexes for identifying groundwater areas of interest (Crossman et al., 2012; White et al., 2016; Xu & Su, 2019); calibrating or improving hydrological and hydrogeological models (Boronina & Ramillien, 2008; Ezquerro et al., 2020; Li, Brunner et al., 2009; Sun et al., 2018); and assessing groundwater recharge (Fallatah et al., 2019; Gemitzi et al. , 2017), among other applications.

Arid regions are particular locations in which remote sensing can contribute to filling the lack of in-situ data, where new and emerging advances in remote sensing hold significant promise for overcoming past challenges of dryland remote sensing, improving our ability to monitor these ecosystems across spatiotemporal scales (Smith et al., 2019). The use of groundwater in arid regions is increasing worldwide in response to a growing global population. Thus, assessing the long-term viability of the water resource is crucial, for which accurate water budgets must be developed (Shanafield et al., 2015). Evapotranspiration (ET) is a fundamental component in the water cycle in these regions, and in endoreic basins it is the basin's main outflow (de la Fuente et al., 2021; Hernández-López et al., 2014; Lobos-Roco et al., 2022; Su et al., 2022; Suárez et al., 2020; Zhang & Wang, 2021). Therefore, being able to quantify it is essential for assessing groundwater resources in these areas. However, quantifying ET is difficult since it is a spatiotemporal multiscale process (Lobos-Roco et al., 2022; Lobos-Roco et al., 2021), whose relationship with meteorological parameters, soil and vegetation properties, and the available water for ET is complex (Boronina & Ramillien, 2008). To overcome these difficulties, several remote sensing tools have evolved in recent decades to estimate ET

using satellite images, regardless of soil condition or crop types (Losgedaragh & Rahimzadegan, 2018).

The ET information derived from remote sensing has been used in numerous water management studies. However, only few investigations have incorporated this information into numerical groundwater models to improve model calibration (Boronina & Ramillien, 2008; Carroll et al., 2015; Li et al., 2009; Sun et al., 2012; Sutanudjaja et al., 2014). For example, Li et al. (2009) used head data and evaporation patterns calculated from remote sensing-derived ET from the Advanced Very High-Resolution Radiometer (NOAA-AVHRR) to calibrate five parameters of a groundwater model. Sun et al. (2012) used Gravity Recovery and Climate Experiment (GRACE) data to calibrate a regional groundwater model through constraining model-predicted groundwater storage changes. Carroll et al. (2015) calibrated a groundwater model to groundwater ET derived from Landsat estimates of the Enhanced Vegetation Index (EVI). Although these studies were a novel contribution towards improving groundwater model calibration, their applicability have certain limitations, such as: been oriented to regional modeling, high dependency on local vegetation (which limits its reproducibility in heterogeneous zones); low temporal frequency of images for representing ET, and reduced capacity to calibrate multiple parameters.

The Earth Engine Evapotranspiration Flux (EEFlux) is one of the available remote sensing tools for estimating ET that has gained attention. EEFlux applies the Mapping EvapoTranspiration at high Resolution with Internalized Calibration (METRIC) model to Landsat images to estimate ET using the Google Earth Engine (GEE) cloud-based platform (Allen et al., 2011; Gorelick et al., 2017; Irmak et al., 2012). The GEE platform offers access to high-performance computing resources, as well as a large and growing curated repository of publicly available geospatial datasets (Gorelick et al., 2017). Hence, GEE has assumed a leadership role in the geospatial and remote sensing community (Smith et al.,

2019). Many studies have used EEFlux (Carrasco-Benavides et al., 2022; de Oliveira Costa et al., 2020; Fadel et al., 2020; Salgado & Mateos, 2021). Fadel et al. (2020) estimated evaporation with EEFlux over a Mediterranean lake and assessed its correlation to other lake variables such as thermal stratification and turbidity; Salgado & Mateos (2021) estimated crop coefficients to assess irrigation schemes over fields in Argentina using EEFlux and other remote sensing techniques; and Carrasco-Benavides et al. (2022) evaluated the potential application of actual evapotranspiration (ET_a) derived from EEFlux and ancillary field data to obtain the water footprint in commercial vineyards in the central Chile. However, EEFlux has not been applied for improving or supporting groundwater model calibration yet.

The aim of this investigation is to develop a methodology that uses ET information derived from EEFlux to support groundwater model calibration in regions with limited in-situ information. For this purpose, this work estimates monthly evapotranspiration using EEFlux in the Salar del Huasco basin, which is located in the arid Chilean Altiplano. The Salar del Huasco is a RAMSAR protected zone due to its wetlands that sustain groundwater-dependent ecosystems (Blin et al., 2022). Due to its protected quality and remote location, there is limited in-situ ET information, which is still incomplete and concentrated only in some specific locations within the basin (de la Fuente et al., 2021; Johnson et al., 2010; Lobos-Roco et al., 2021; Suárez et al., 2020)..

3.2. Methods

3.2.1. Study site and its groundwater flow model

The Salar del Huasco basin is located in the extremely arid Chilean Altiplano between 19.98 ºS and 20.43ºS of latitude and between 68.94°W and 68.7°W of longitude (Figure 3-1). Previous studies have discarded a hydrogeological connection of the basin with its

neighbors (Risacher et al., 1999; Scheihing et al., 2017; Uribe et al., 2015) and it is thus considered an endorheic basin where the main groundwater discharge mechanism is ET (Blin et al., 2022). The high ET rates cause salt accumulation in the topographic lower part of the basin, generating a salt flat (Duffy & Al-Hassan, 1988). In this basin, the shallow water table feeds wetlands that support the habitat of a varied flora and fauna (Muñoz-Pardo et al., 2004; Suárez et al., 2020). For this reason, wetlands of the Salar del Huasco were protected by the RAMSAR convention (CONAF, 2005), and the site was recently declared National Park. In this basin there is few in-situ instrumentation to monitor hydrological variables. Therefore, it is important to investigate the use of satellite images to fill the lack of hydro(geo)logical information.

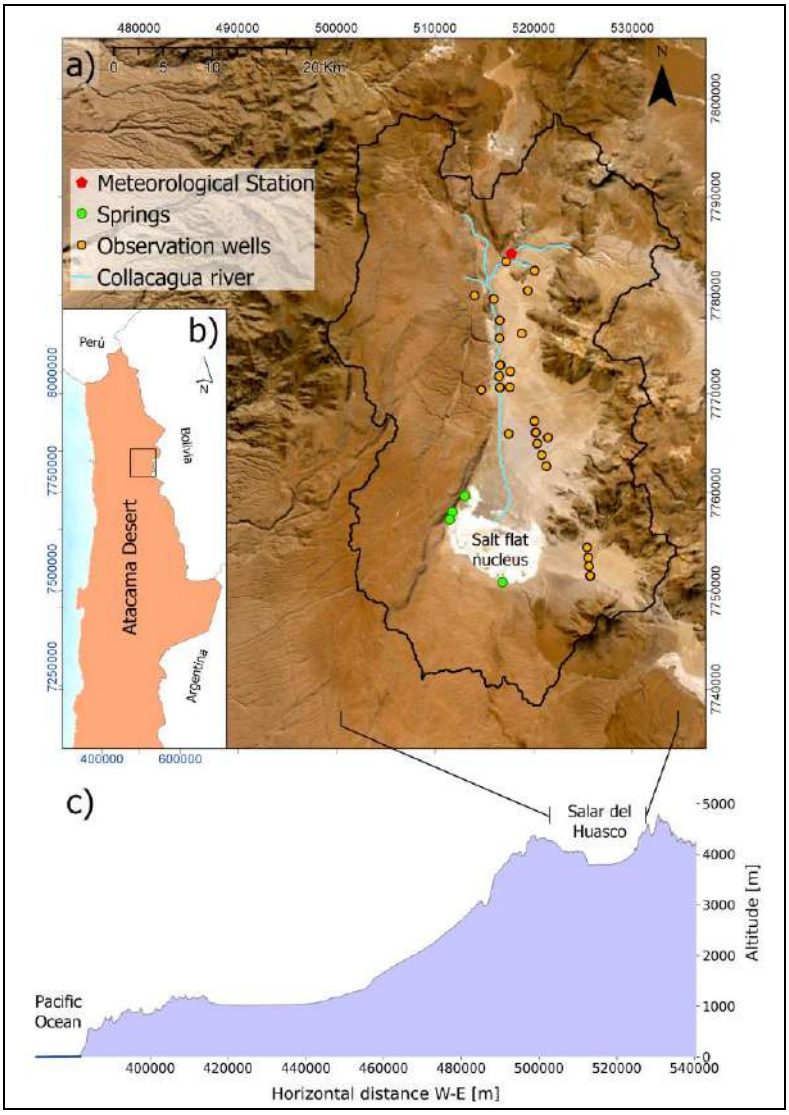

Figure 3-1: Study site. Panel a) Salar del Huasco basin, where observation wells are depicted as orange circles, Collacagua meteorological station is shown as a red pentagon and springs as bright green circles near the wetlands at the salt flat nucleus. b) Location of the Salar del Huasco basin (enclosed by a rectangle) in the Atacama Desert, northern Chile, which is colored in light orange to show its location within South America. c) Elevation profile from the Pacific Ocean (left) to the Salar del Huasco basin (right) in the Altiplano. It can be observed from c) that the basin is located in a remote area, where access is difficult due to its complex topography. X-axis is presented in UTM coordinates.

The groundwater flow dynamics of the aquifer were previously studied through numerical models (Acosta, 2004; Blin et al., 2022) using the software MODFLOW (Harbaugh et al., 2000), which simulates flow through saturated porous media:

$$S\frac{\partial h}{\partial t} = \frac{\partial}{\partial x}\left(K_x\frac{\partial h}{\partial x}\right) + \frac{\partial}{\partial y}\left(K_y\frac{\partial h}{\partial y}\right) + \frac{\partial}{\partial z}\left(K_z\frac{\partial h}{\partial z}\right) \quad (3\text{-}1)$$

where S is the storage term (-), K_x, K_y and K_z are the hydraulic conductivities along the x, y and z coordinate axes (L/T), and h is the hydraulic head (L). The S term varies depending on the type of aquifer layer, where specific storage (S_s) is used when the layer is confined throughout the simulation, while specific yield (S_y) is used for unconfined layers under water table conditions (heads below the top of a cell).

The present research develops a methodology to support the calibration of groundwater models using remote sensing products, for which it uses a previously constructed model (Blin et al., 2022). Nonetheless, the proposed methodology can be applied to any groundwater model. Therefore, here we only provide a brief description of the model, and we refer the reader to the work of Blin et al. (2022) for further details. The geometry of the model consists of 270 rows, 253 columns and 10 layers that discretize three main aquifers. No-flow boundary conditions were set along the edges of the model according to previous hydrogeological and geochemical studies (Risacher et al., 1999; Scheihing et al., 2017). Recharge is incorporated in the model using the Recharge package (abbreviated as RCH in MODFLOW) (Harbaugh et al., 2000), which applies recharge rates calculated with a rainfall-runoff model which was specifically developed, calibrated and validated for the Salar del Huasco basin (Uribe et al., 2015). Additionally, the groundwater model accounts for evaporation from the water table that is not represented in the rainfall-runoff model. Groundwater evaporation is simulated with the Evapotranspiration package (abbreviated as

EVT in MODFLOW) (Harbaugh et al., 2000), which establishes a linear relation between the surface of the model and the extinction depth (EXDP). In the EVT package, the maximum potential rate evaporates if the head at a cell is equal to or greater than the surface, whereas no ET occurs if the head is below EXDP. ET at cells in between these extremes varies linearly with depth. The EVT region defined by Blin et al. (2022) as the area where the water table is shallow enough to evaporate, was modified in this research to account for two ET zones. These zones represent different conditions of water table depth according to their EXDP. Thus, the EVT was defined inside a region of 375 km^2 (Figure 3-2) that corresponds to the surroundings of surface water bodies that interacts with groundwater, such as springs and lagoons in the salt flat nucleus (Zone 1) and the riverbed (Zone 2). EXDP was set to 3 and 4 m in Zones 1 and 2, respectively, according to different investigations in the study site (Acosta & Custodio, 2008; DGA, 2009; Hernández-López et al., 2014; Johnson et al., 2010). The purpose of defining this ET region is twofold: i) to reduce simulation times by not using the EVT package in locations where groundwater is deep and thus no groundwater ET is expected; and ii) to simulate groundwater evaporation that is not being fully represented by the hydrological model since it is not necessarily a result of direct precipitation.

Given the importance of ET flows in the Salar del Huasco basin (Blin et al., 2022), satellite products were used to better characterize the way ET is being represented in the groundwater model developed by Blin et al. (2022), and to support the calibration of the EXDP parameter.

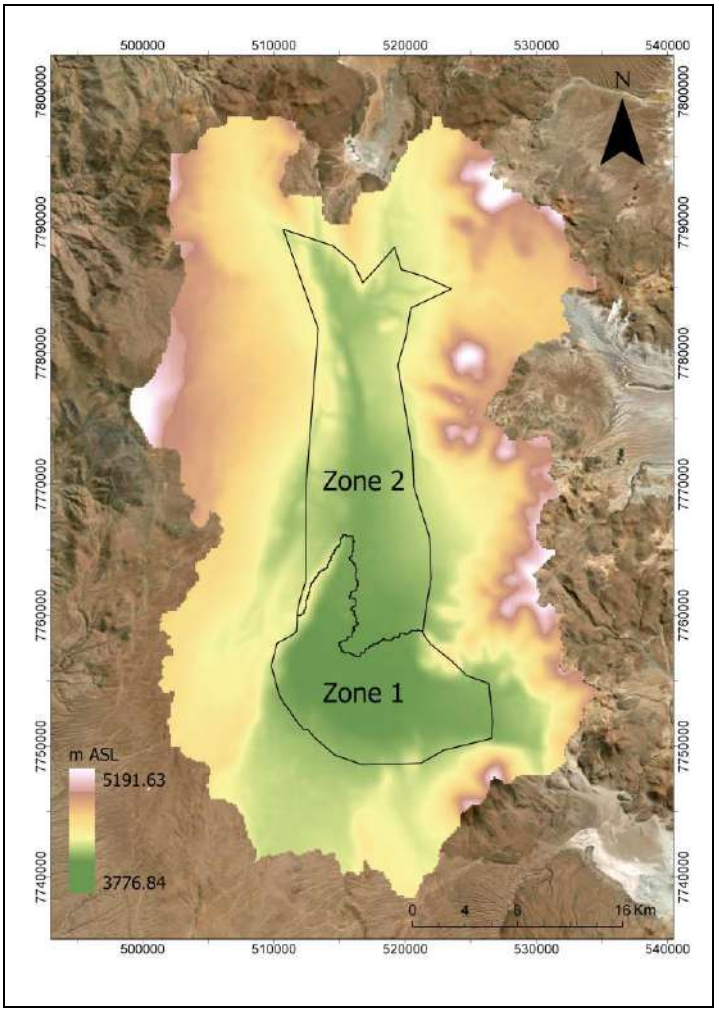

Figure 3-2: ET region defined in the groundwater flow model, represented by the EVT package in MODFLOW. The region is divided into two zones of different values of the EXDP parameter. The colormap indicates the altitude (m ASL) of the terrain inside the model domain.

3.2.2. Surface Energy Balance method: METRIC model

The ET in the basin was estimated using the METRIC model (Allen et al., 2011; Allen et al., 2007). METRIC uses the surface energy balance equation (Eq. (3-2)) to calculate the

latent heat flux, λET [Wm^{-2}], as the residue of the surface energy balance, which is estimated using satellite imagery and meteorological data products according to:

$$\lambda ET = R_n - G - H \tag{3-2}$$

where R_n is the net radiation [Wm^{-2}], G is the soil heat flux [Wm^{-2}], and H is the sensible heat flux [Wm^{-2}]. Energy balance-based models have advantages over other methods, such as crop coefficient-based methods in that knowledge of crop development stages is not required, nor do specific crop types (Allen et al., 2007; Allen et al., 2013; Zhao et al., 2020). Additionally, models based on the energy balance can detect reduced ET caused by water shortage, salinity or frost, as well as increased ET caused by bare soil evaporation (Allen et al., 2011).

The most critical factor in the physically based models is the estimation of *H* that can lead to significant errors in estimations of ET (Irmak et al., 2012). To overcome this problem, METRIC uses a near-surface temperature gradient that is indexed to radiometric surface temperature, eliminating the need for absolute surface temperature calibration, which has been the major impediment to operational satellite ET. Unlike other surface energy balance models, such as SEBAL (Bastiaanssen, 2000), which considers H = 0 Wm^{-2} at the cold pixel, METRIC uses the reference ET (ET_r) estimated with the Penman-Monteith equation (Monteith, 1965; Penman, 1948) for the estimation of *H* to account for impacts of advection in the system that are generally well represented with the Penman-Monteith equation (Allen et al., 2011; Irmak et al., 2012). Heat and moisture advection from land surfaces is strongly affected by aerodynamic processes including wind speed and turbulence which are basically invisible to satellites (Irmak et al., 2012). Thus, METRIC performs corrections on wind speed and turbulence to better represent the aerodynamic processes in mountainous regions, which are associated with local and regional-scale interactions (Allen et al., 2011; Lobos-Roco et al., 2021). Lobos-Roco et al. (2021) found

that local- and regional-scale processes govern diurnal evaporation cycles from Salar del Huasco's lagoon. Thus, accounting for impacts on these processes is particularly important in the study area. Consequently, the METRIC model was used in this research because: (1) it accounts for impacts of regional advection by using Penman-Monteith equation in the calibration of H, and (2) it makes corrections in aerodynamic processes in mountainous regions.

3.2.3. Processing EEFlux images

EEFlux was recently developed for operating the METRIC model on the GEE platform. EEFlux (https://eeflux-level1.appspot.com/) has the advantage of being a user friendly open-source platform, completely based on remote sensing, since it uses grided meteorological products for the calibration of the surface energy balance. Thus, it can be used in almost every part of the world. The use of GEE also enables a fast fetching of the satellite datasets and faster processing due to supercomputers on the Google cloud (Gorelick et al., 2017).

EEFlux processes individual Landsat scenes from any period from 1984 until present. From each Landsat image, EEFlux utilizes the thermal band to drive the surface energy balance and short-wave bands to estimate albedo, the amounts of vegetation and surface roughness to calculate λET, according to Eq. (3-2). λET is then transformed into the instantaneous actual ET (ET_a) by dividing it by the latent heat of vaporization. In EEFlux, the resulting ET_a at the moment of satellite passage is converted to an index called reference evapotranspiration fraction (ET_rF):

$$ET_rF = \frac{ET_a}{ET_r} \tag{3-3}$$

where ET_rF represents ET as a fraction of ET_r, similar to the traditional crop coefficient (K_c), which enables the conversion of the instantaneous ET into monthly or seasonal ET. In Eq. (3-3), ET_r is calculated using the "tall" alfalfa reference (ASCE – EWRI, 2005), according to the Standardized Penman-Monteith equation (Allen et al., 1998). EEFlux uses North American Land Data Assimilation System (NLDAS) (Cosgrove et al., 2003; Mitchell et al., 2004) gridded weather data in the US and Climate Forecast System version 2 (CFSV2) of NOAA (https://www.ncdc.noaa.gov/data-access/model-data/model-datasets/climate-forecast-system-version2-cfsv2) gridded weather data globally for the computations of λET.

EEFlux calculates the ET_rF at the desired location on the globe and generates a processed image that has different values of the ET_rF at each pixel. The ET_rF computed at the image time is assumed to be the same as the average value over 24 hours hours (Irmak et al., 2012), which has been demonstrated to be consistent in various studies (Allen et al., 2007; Colaizzi et al., 2006; Romero, 2004).. From a series of images available at the passing of the satellite every 16 days, the monthly ET_rF can be derived by daily interpolating them to calculate the average of the interpolated values over a specific month (Fadel et al., 2020; Irmak et al., 2012). In this research, images from both Landsat 5 and Landsat 7 were used to have more information on ET_rF in a month for the interpolation, which was performed using a spline method that better fits the typical oscillating pattern of crop coefficients during a growing season, similarly to the construction of a seasonal Kc curve (Allen et al., 1998; Allen et al., 2007; Dhungel et al., 2016; Hankerson et al., 2012; Irmak et al., 2012; Semmens et al., 2016; Wright, 1982). Consequently, the monthly ET_rF [-] can be derived according to Eq. (3-4):

$$ET_rF_{month} = \frac{\sum_{i=1}^{30} ET_rF_i \cdot ET_{r_i}}{\sum_{i=1}^{30} ET_{r_i}} \quad (3\text{-}4)$$

where ET_rF_i [-] are the daily interpolated values in a specific month and ET_{ri} are daily reference ET [mm d^{-1}]. Since Eq. (3-4) is a dimensionless ET, $ET_{r\,i}$ can be estimated with meteorological data or records of pan evaporation in that same month. Mean monthly ET can be then obtained from:

$$ET_{month} = ET_rF_{month} \cdot ET_{r\,month} \quad (3\text{-}5)$$

where ET_{month} is the mean monthly ET [mm d^{-1}] and $ET_{r\,month}$ [mm d^{-1}] is the average daily ET_r of that month.

For the Salar del Huasco basin, EEFlux images were downloaded over the period between 2002 and 2012 for the calibration of the groundwater model (i.e., calibration period). The methodology described above was applied to the images, using daily records of pan evaporation at the Collacagua meteorological station (Figure 3-1) for estimating $ET_{r\,i}$. ET_r in Eq. (3-4) was calculated at each pixel with the Blaney-Criddle (Doorenbos & Pruitt, 1977) equation, considering that temperature varies with elevation, as described in Blin et al. (2022). Using the Blaney-Criddle equation allows having pixel-wise estimates of monthly ET_r with which a more representative average value can be obtained for the ET region than using pan evaporation only at the location of the meteorological station.

3.2.4. Validation of EEFlux-ET estimates using Eddy Covariance measurements

To corroborate that magnitudes of EEFlux-ET estimates are comparable with observations, we used Eddy Covariance (EC) measurements recorded in the Salar del Huasco between November 15 and 23rd of 2018 as part of the E-DATA field campaign (Suárez et al., 2020). According to Lobos-Roco et al. (2021), the EC stations were located in three points in the basin's sink (Figure 3-3), one in the north part of the saline lake (EC-water station;

1.0 m height), other in the wet salt of the salt crust (EC-wet salt station; 1.5 m height), and other in the desert, ~5 km south of the salt flat nucleus (EC-desert station; 2.0 m height). A detailed description of the sites where the EC stations were deployed is provided in the Supplementary Material.

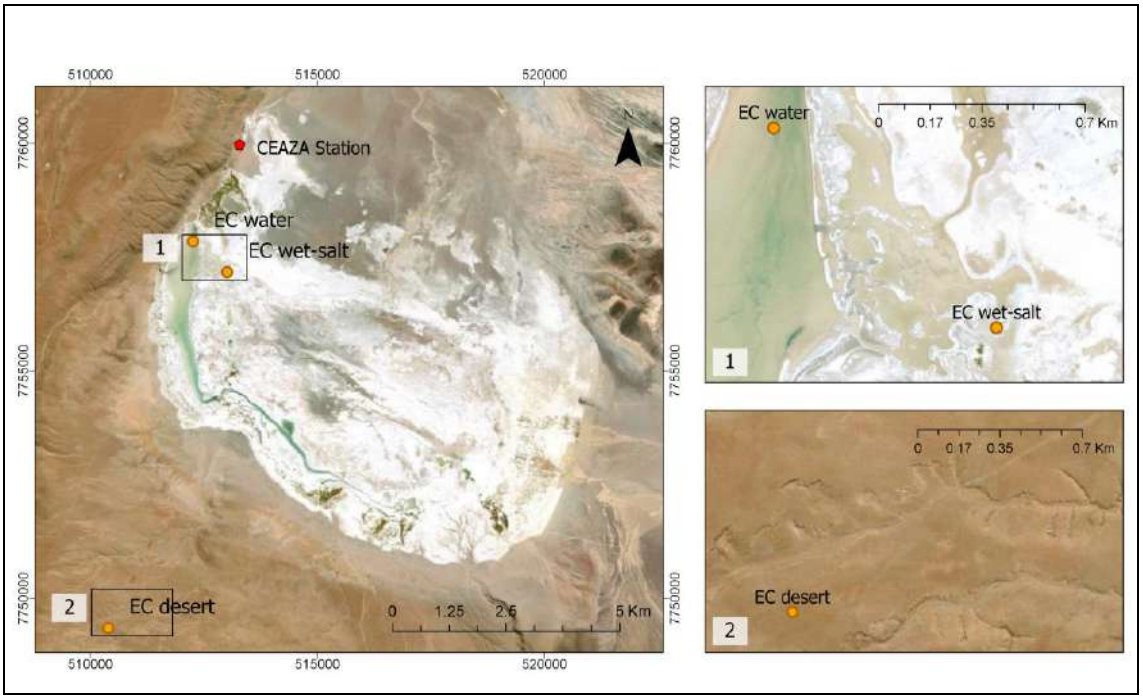

Figure 3-3: Location of the 3 EC stations with records between November 15 and November 23, 2018. The panels 1 and 2 show a zoom of each station and its surroundings, in order to show the heterogeneity at each location.

To compare the fluxes measured at these stations with estimations based on the EEFlux method, ET_rF images available within the dates of the EC records were interpolated in time to have daily interpolated values of ET_rF at each pixel of the image. To estimate daily ET at the three locations of the EC stations, a representative footprint of the EC measurement

field was defined for each of them (Figure 3-3), where the average of ET_rF in the pixels within it was calculated. The definition of the footprints was based on delimiting zones with relatively homogeneous characteristics that represent each zone measured by the stations. With the average daily ET_rF of the areas surrounding the stations, the ET_r as then calculated using daily measurements of meteorological variables obtained from the CEAZA (available at http://www.ceazamet.cl) station (Figure 3-3), according to Standardized Penman-Monteith equation (Allen et al., 1998). Unlike the image processing showed in section 2.3, Penman-Monteith was used for the validation since the CEAZA station provided daily data on more meteorological variables. Finally, daily ET at each station's footprint was calculated by multiplying ET_rF and ET_r.

Considering the few available ET data in the study area (only 8 days of continuous EC measurements), four additional zones with yearlong records were used to improve the quality of the validation of the EEFlux method for estimating ET. These zones were also located in the Altiplano of the Atacama Desert in northern Chile (see Supplementary Material), at about the same altitude, and have similar climatic and physical characteristics than those of the EC stations in Salar del Huasco. Thus, a comparison can be established to assess the capability of the method in representing evaporation fluxes in the Altiplano. As data from some of these stations were previously used by Mosre & Suárez (2021), we maintained the names given to their EC stations, and new stations were named following said nomenclature. Station CH-AT2 was installed over alluvial deposits of a transboundary river basin on a site covered by native vegetation at 4,330 m ASL, and CH-AT3 was set in a wetland at 4,250 m ASL; station CH-AT4 was located in a wetland at 4,075 m ASL, and CH-AT5 was deployed within a salt flat (with a cyclical ephemeral lagoon) at 4,235 m ASL. Similar to the EC stations at Salar del Huasco, footprints of the EC measurements were defined to enclose homogeneous pixels from EEFlux images with surfaces ranging between 0.4 -2 km2.

The validation performance was assessed with the root mean square error (RMSE) and the Nash-Sutcliffe efficiency (NSE) coefficient. The optimal values of RMSE and NSE are zero and one, respectively (Bennett et al., 2013).

3.2.5. Calibration of the groundwater flow model

The calibration of the groundwater model presented in section 3.2.1, was performed under various configurations of the calibration process, where different sets of parameters were calibrated to different observational data to assess the effect of EEFlux estimations in the process. The calibrations were carried out using the Parameter Estimation software (PEST) (Doherty, 2004). Python-based scripts were generated to create the inputs for the PEST calibration using the pyEMU module (White et al., 2016).

Since EEFlux accounts for the total water being evaporated from the system as perceived by the satellites, ET_a calculated by the basin's rainfall-runoff model (Uribe et al., 2015) was subtracted from EEFlux-ET estimates to obtain the groundwater evaporation (hereafter referred to as EEFlux-ET_{gw}). Monthly EEFlux-ET_{gw} estimates over the ET region (Figure 3-2) were used as observations in the calibration of the groundwater model, against which monthly evaporation simulated by the model over the same area were compared. However, using only EEFlux-ET_{gw} estimates to represent the observations in the PEST calibration would not lead to a unique set of parameters of the inverse problem that is to be solved for two reasons: (1) using only one monthly value as "observation" for calibrating multiple parameters represents an "ill-posed" problem, defined as a problem in which the number of estimated parameters is larger than the available data (Golmohammadi et al., 2015; Hunt et al., 2007); and (2) it corresponds to an estimation and not a raw observation or measurement in-situ. To avoid such problems, water level (heads) records at 42 wells (shown in Figure 3-1) were also used in the calibration process. A flowchart of the calibration is presented in Figure 3-4.

The calibrated parameters correspond to 23 parameters of horizontal conductivity (K_h) and 16 of vertical conductivity (K_v) distributed along the cells of the entire model domain; seven parameters of specific storage (S_s) and seven parameters of specific yield (S_y), whereas two EXDP parameters of the EVT package were utilized (one per zone of the ET region, according to Figure 3-2). This methodology is not restrictive to this set of parameters, and therefore users are encouraged to define different sets according to their specific hydrogeological settings. The calibrations were performed over the period between 2002 and 2012, using monthly MODFLOW stress periods.

As mentioned before, different configurations of set of parameters and observational data to calibrate them were defined to assess the role of EEFlux-ET_{gw} fluxes in the calibration:

- Calibration 1: only observed heads were used to calibrate hydraulic properties parameters.

- Calibration 2: only observed heads were used to calibrate hydraulic properties and EXDP parameters.

- Calibration 3: estimates of EEFlux-ET_{gw} and observed heads were used to calibrate hydraulic properties parameters.

- Calibration 4: estimates of EEFlux-ET_{gw} and observed heads were used to calibrate hydraulic properties and EXDP parameters.

Although in some approaches greater weights are assigned to the more reliable data (e.g. head records), in this study both types of observations were considered to have the same contribution to the objective function in Calibrations 3 and 4 to simplify their subsequent analysis. To achieve this, however, EEFlux-ET_{gw} estimates were weighted to account for differences between flow and head data.

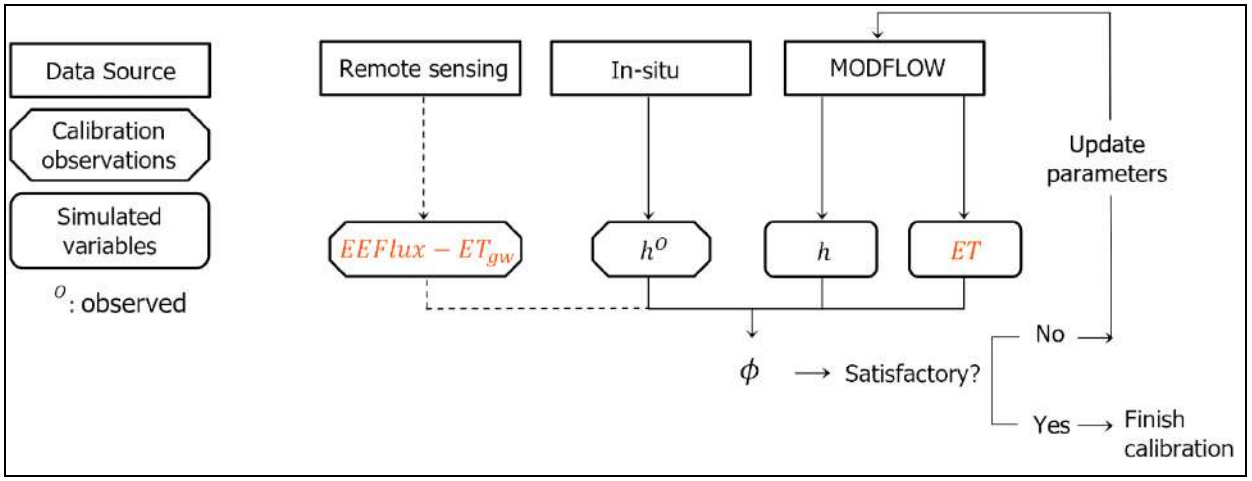

Figure 3-4: Flowchart of the calibration methodology. EEFlux-ET_{gw} estimates and observed heads are used as observations in the calibration. Heads and ET simulated by the groundwater model are compared against observations in the calibration process based on the objective function (ϕ), which minimizes the square of residuals, and parameters are updated in each PEST iteration. The dashed line refers to the different calibration configurations, in which half of them incorporate EEFlux-ET_{gw} estimates as additional data to support head observations. Data corresponding to evaporation flows are shown in orange, as opposed to heads data shown in black.

A simulation named Sim0 was performed using the initial values of the calibrated parameters to represent a baseline of the groundwater system (before the calibration of its hydraulic properties and EXDP parameters) with respect to which changes produced in the basin by the calibrated parameters were evaluated. The hydraulic properties parameters used in the Sim0 simulation correspond to the parameters used by Blin et al. (2022). Once each of the calibrations were performed, four simulations were carried out using the respective calibrated parameters obtained in the four calibrations, hereafter referred to as Sim1, Sim2, Sim3, and Sim4. These simulations differ from the four calibrations in that

their initial water table conditions were calculated using the calibrated parameters in a steady state simulation. To assess the performance of the four calibrations, the RMSE and mean absolute error (MAE) of heads were calculated in the four simulations and compared to the metrics obtained in Sim0 simulation. Normalized metrics (NRMSE and NMAE) were also calculated to account for large head differences observed in some wells that could affect the overall value of RMSE and MAE, as well as the percent bias (PBIAS). The optimal value of all these metrics is zero, while low values indicate good performance.

3.3. Results

3.3.1. Validation of the EEFlux method in the Altiplano

A comparison between measured and EEFlux-based evaporation is shown in Figure 3-5 for the validation of the EEFlux method at Salar del Huasco. The evaporation in the saline lagoon (EC-water) is slightly overestimated by EEFlux, while the almost null evaporation in the desert zone is being well simulated with the method; in the wet-salt zone, EEFlux-ET slightly overestimated the evaporation observations. The bias between measurements and EEFlux-ET estimates in the wet-salt zone could be explained by the possible existence of water pixels inside the footprint defined for estimating the mean ET_rF (since this location is particularly heterogenous), which would have immediately increased the ET estimates.

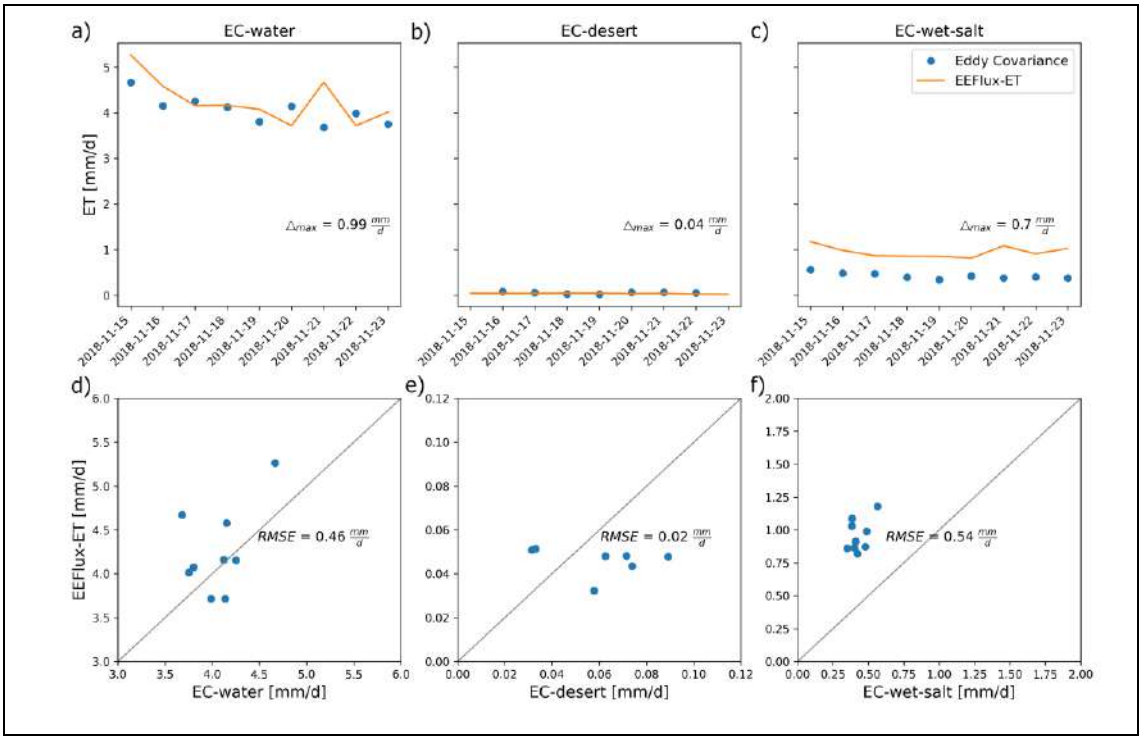

Figure 3-5: Validation of ET fluxes estimated with EEFlux in the EC stations located in the Salar del Huasco basin. Δ_{max} corresponds to the maximum bias between EC records and EEFlux-ET produced at each station.

Having less than 10 days of data is not enough to evaluate the method's performance in simulating the ET evolution throughout the year. The validation using yearlong records at the four additional EC stations, however, allows for such assessment (Figure 3-6). Figure 3-6a), c), e) and g) show the temporal evolution of the observed and estimated ET rates. The EEFlux method represents the seasonal variations of ET across the stations. Moreover, it simulates distinctive ET cycles along the year in all stations except CH-AT2. Here, Landsat images from September and November were discarded due to their high percentage of cloudiness. Nevertheless, the fact that CH-AT2 has the lowest RMSE

suggests that EEFlux-ET estimates can correctly represent ET fluxes over areas where evaporation is almost zero most of the time. Figure 3-6 b), d), f) and h) show scatter plots of EEFlux-ET (y-axis) and observed ET at the EC stations (x-axis), whose relation is represented by a linear regression curve in each case. Marginal histograms and kernel density estimation (KDE) plots were added at the top and right margins of the scatter plots to analyze the probability distribution of the observed ET and EEFlux-ET data, respectively. CH-AT4 (Figure 3-6 f)) and CH-AT5 (Figure 3-6 h)) have greater dispersion (and therefore are further from the regression curve and have negative NSE s) than the other two stations, which can be related to the large day-to-day variability observed in their corresponding time series plots (Figure 3-6 e) and g)). The best NSE and R^2 are achieved at CH-AT3, where less day-to-day variability is observed (Figure 3-6 c)). Therefore, EEFlux-ET better explains the variance of the observations at locations with low daily variability. However, the histograms and KDE at CH-AT4 show similar distributions of observed ET and EEFlux-ET with modes of around 3 and 2.5 mm/d, respectively. Although the regression curves indicate that EEFlux is not always capable of representing each daily observation, the probability density function curves of both observed ET and EEFlux-ET indicate that they have a similar behavior throughout the year. Therefore, the method correctly represents the seasonal variations and magnitudes of ET fluxes in different environments in elevated arid areas.

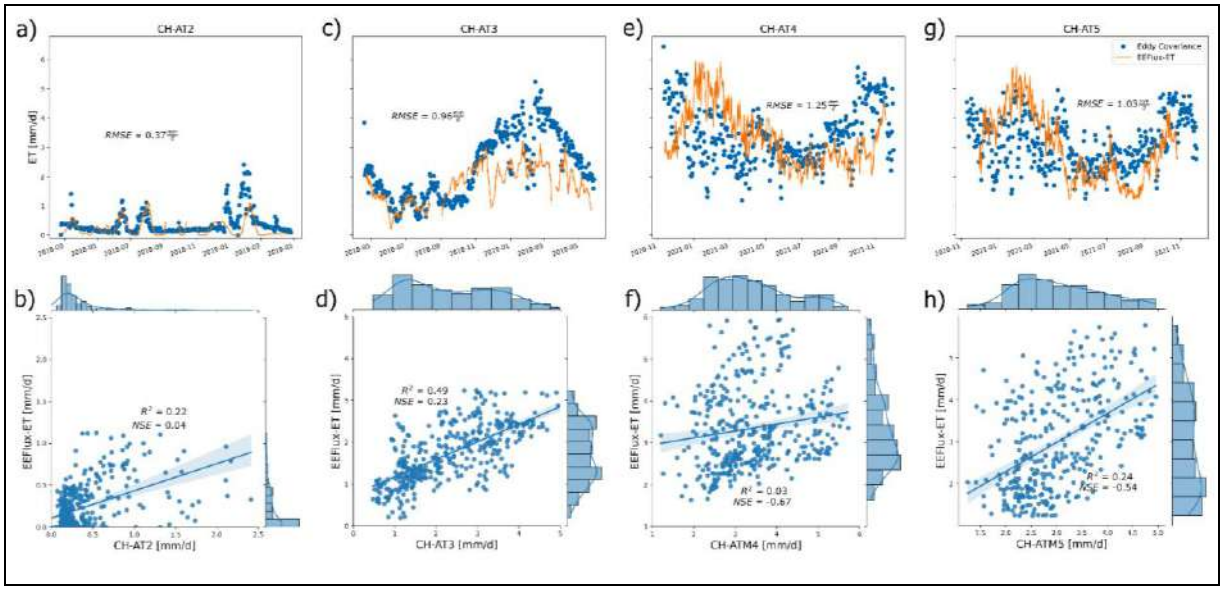

Figure 3-6: Validation of EEFlux in four additional sites in the Atacama Desert. Results at each station are presented by columns, where the upper row shows time series of observed and daily EEFlux-ET (panels a), c), e) and g)), and the lower row shows the scatter plots of estimated EEFlux-ET values to observations (EC records) (panels b), d), f) and h)), where a regression curve of their fit is showed at each station, along with their R^2 and NSE. Translucent bands around the regression line show the 95% confidence interval. Each scatter plot shows how the dependent variable, EEFlux-ET (y-axis) varies with the independent variable, observed ET (x-axis). Marginal histograms and KDE are plotted at the top and right margins of the scatter plots to show the probability distributions of EEFlux-ET at the right and observed ET at the top.

3.3.2. EFlux-ET estimates

The values of ET_rF (average of pixel values over the ET region) over the calibration period vary seasonally (Figure 3-7 a)), with averages of 0.24 and 0.21 in summer and winter

months, respectively, and an overall average of 0.22 ± 0.07 (mean ± standard deviation). The monthly average of the daily EEFlux-ET estimates over the ET region range between 0.1 and 2.1 mm/d in winter and summer, respectively, within the calibration period (Figure 3-7 b), with an average of 0.8 ± 0.38 mm/d.

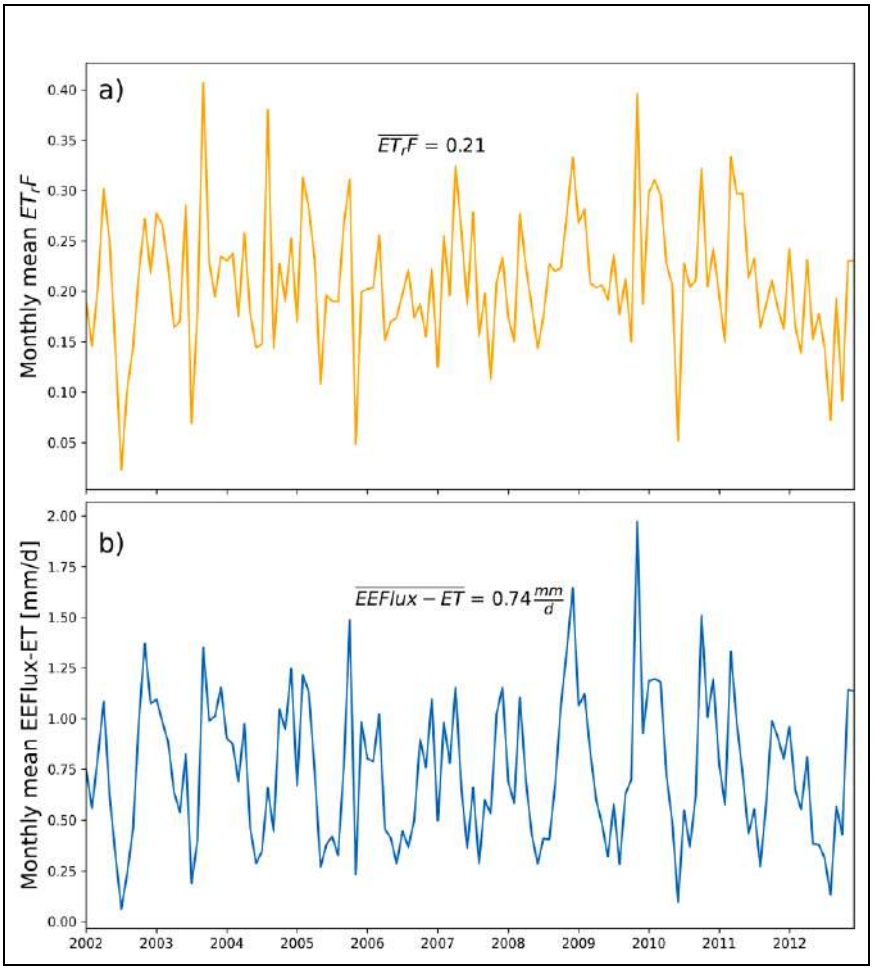

Figure 3-7: a) Monthly values of ETr F and b) monthly values of EEFlux-ET estimates in the basin's ET region.

The results shown in Figure 3-7 b) can be compared with previous ET studies performed in the Salar del Huasco basin (Table 3-1). The values obtained from EEFlux-ET estimates are more similar to bare soil evaporation reported in previous studies. Additionally, the results obtained by Johnson et al. (2010), are very similar to those of the present study, in which EEFlux-ET was also calculated over areas where different depths to the water table can be found.

Table 3-1: ET and E (evaporation) estimates carried out in previous studies in the wetlands and vegetation areas near the salt flat nucleus of the Salar del Huasco basin.

Previous studies	**ET from wetlands and vegetated areas near salt flat nucleus (mm/d)**	**E from bare soil (mm/d)**	**Methodology for estimating ET (E)**
Acosta (2004)	2.09	1.10	ET: Pan evaporation corrected by tank coefficient and crop coefficients from previous studies E: Correction of E – water table depth relations at Salar de Atacama
Collahuasi-GP Consultores (2008)	Summer: 3.45 Winter: 1.91	Summer: 2.73 Winter: 0.75	ET and E: Lysimetry
DGA (2009)	2.68	0.61	ET: Pan evaporation corrected by tank coefficient and elevation gradient E: E – water table depth curve based on portable chamber measurements
Johnson et al. (2010)	1.64 mm/d when water table depth is 0.11 m 0.86 mm/d when water table depth is 0.37 m 0.16 mm/d when water table depth is 0.99 m 0.10 mm/d when water table depth is 3.34 m		ET and E: Portable chamber method

3.3.3. PEST calibrations

The four simulations show similar performance metrics, all of them outperforming the Sim0 simulation by about 2% in the case of NRMSE and 0.7% in the case of NMAE (Table 3-2). Both RMSE and MAE are affected by the range in which the observations vary within the complex topography basin, where the observed range is 144 m (that is, the difference between the maximum and minimum observations of heads). Moreover, the NRMSE show that the RMSE of Sim1 to Sim4 is slightly above 4% of this maximum range, while the NMAE indicates that the MAE is almost 3% of the range. Among the four simulations, Sim3 achieves best performance metrics of heads, which means that better values of heads result when only hydraulic properties are calibrated using EEFlux-ET_{gw} in addition to water level records.

Additionally, considering the large observed range of heads, RMSE, NRMSE and PBIAS were calculated in four areas distributed throughout the basin to assess the performance of the simulations at different altitudes (Figure 3-8). In Sectors B, C and D the four simulations improve the model performance, while in Sector A they worsen it. In Sector B, Sim2 achieves the best performance, decreasing by 11.4% the RMSE with respect to Sim0, while in Sector C and D, Sim3 outperforms the other simulations by decreasing the RMSE by 32.2% and 38.9%, respectively. The similar and low-magnitude PBIAS in all sectors means that the average tendency of the simulated data to deviate from observations does not change greatly with altitude.

Table 3-2: Performance metrics of simulations performed using calibrated parameters from the four PEST calibrations. Metrics of the entire model are presented in the Global column, while metrics of the four sectors shown in Figure 3-8 are presented in the adjacent columns.

Simulation	*Metric*	*Sim0*	*Sim1*	*Sim2*	*Sim3*	*Sim4*
Global	*RMSE (m)*	8.9	6.2	6.1	5.9	6.4
	NRMSE (%)	6.2	4.2	4.2	4.1	4.5
	MAE (m)	5.12	4.16	4.17	4.07	4.24
	NMAE (%)	3.55	2.88	2.89	2.82	2.94
	PBIAS (%)	0.010	0.002	0.010	-0.014	-0.005
Sector A	*RMSE (m)*	2	5.1	4.7	4.9	4.9
	NRMSE (%)	0.050	0.132	0.122	0.127	0.128
	PBIAS (%)	0.036	-0.095	-0.086	-0.099	-0.095
Sector B	*RMSE (m)*	4.4	4.1	3.9	4	4
	NRMSE (%)	0.06	0.054	0.05	0.053	0.052
	PBIAS (%)	0.012	0.031	0.033	-0.011	0.031
Sector C	*RMSE (m)*	5.9	4.1	4.3	4	4.2
	NRMSE (%)	0.13	0.093	0.1	0.092	0.097
	PBIAS (%)	0.073	0.079	0.087	0.068	0.079
Sector D	*RMSE (m)*	19.8	13	12.7	12.1	13.9
	NRMSE (%)	0.17	0.11	0.11	0.1	0.12
	PBIAS (%)	-0.23	-0.15	-0.13	-0.13	-0.15

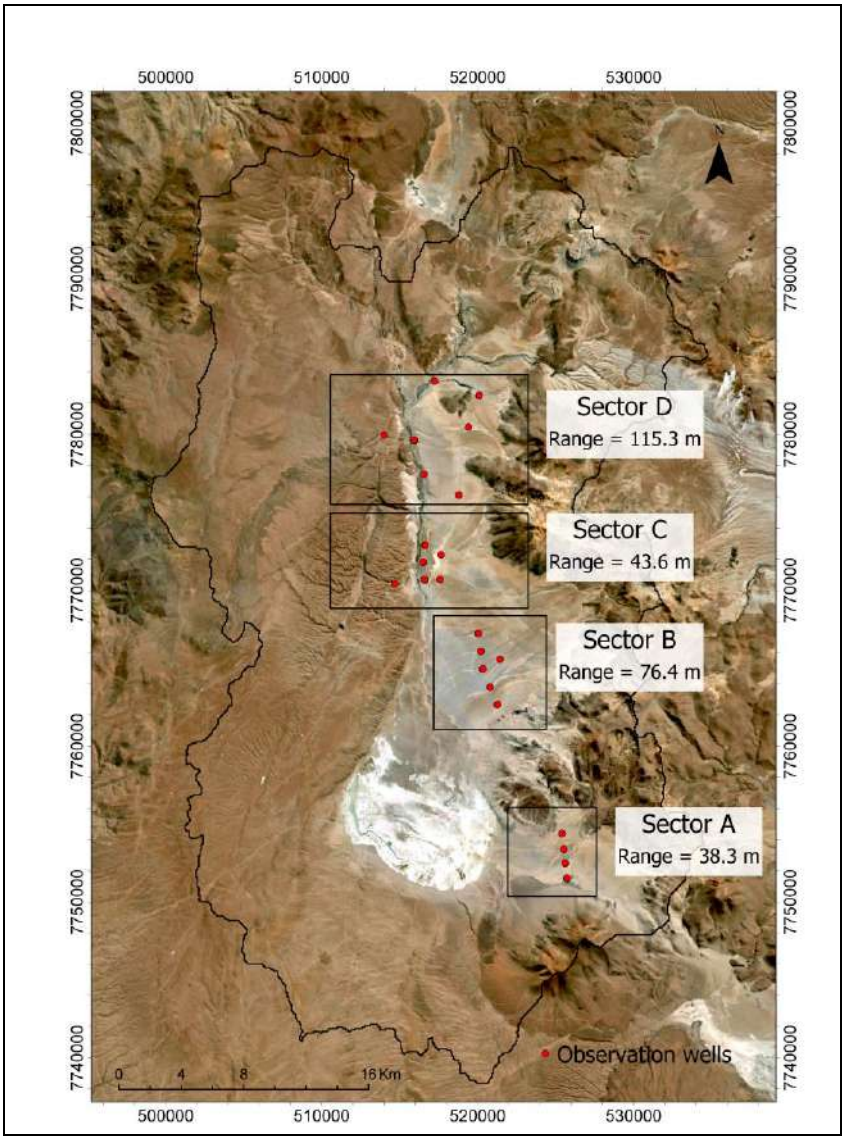

Figure 3-8: Sectors used for the assessment of the model performance at different altitudes. The ranges indicate the maximum differences in levels recorded during the calibration period in the observation wells within each sector.

Groundwater levels are directly related to groundwater evaporation. Thus, understanding simulated heads is crucial to assess groundwater evaporation in each simulation. A scatter plot of simulated and observed heads is shown in Figure 3-9 a), whereas resulting time series of groundwater ET are shown in Figure 3-9 b). On one hand, the highest ET rates occur in the Sim0 simulation (Figure 3-9 b)), which means that this simulation is the one with the highest water table at the locations where ET occurs in the model. Accordingly, overestimation of heads between 3775 and 3840 m ASL in Sim0 (Figure 3-9 a)) suggests that this process occurs mainly at lower elevations within the basin (Zone 1 of the ET region in Figure 3-2). On the other hand, the water table increases at elevations above 3850 m ASL in Sim1 through Sim4 with respect to Sim0, thus getting closer to the observations (Figure 3-9 a)). However, the highest ET is generated in Sim0, implying that a shallower water table at low altitudes will necessarily result in more ET. Furthermore, simulations with higher EXDP values in Zone 2 (Sim2 and Sim4 (Table 3-3)) do not generate higher ET rates than Sim0, which means that Zone 2 contributes little to the total ET flow.

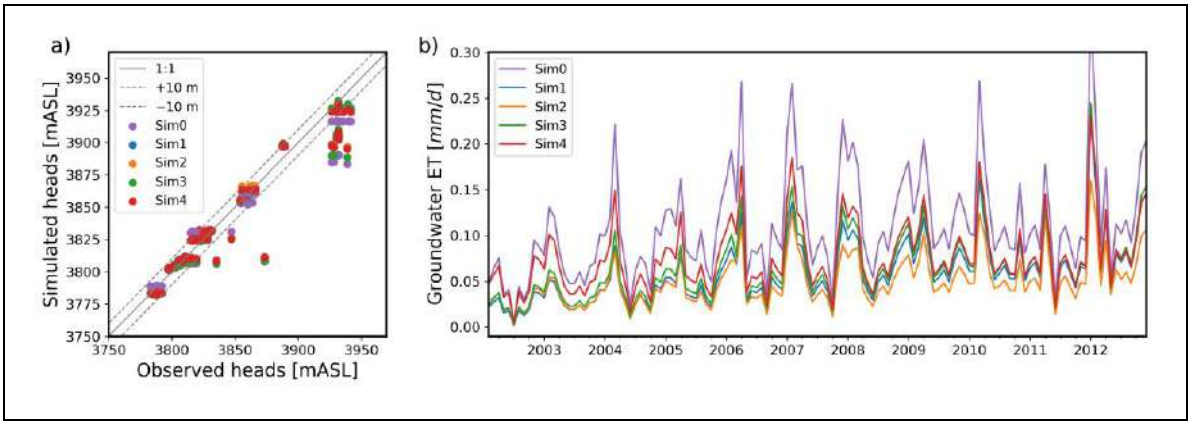

Figure 3-9: a) Scatter plot of estimated (y axis) versus observed (x axis) heads. The grey line represents the perfect fit (1:1), whereas the dash grey lines correspond to 10 m above and below 1:1; b) Time series of simulated groundwater evaporation rates from the ET region of the model.

Table 3-3: Calibrated EXDP parameters by zones of the ET region. The columns of simulations are further divided into parameters calibrated (blue), and observations used to calibrate them (red).

		Sim0	**Sim1**	**Sim2**	**Sim3**	**Sim4**
			Heads		*Heads + EEFlux*	
			Hydraulic prop.	*Hydraulic prop. + EXDP*	*Hydraulic prop.*	*Hydraulic prop. + EXDP*
EXDP Zone 1	*Value (m)*	3	3	3.03	3	4.3
	Percentage of change with respect to Sim0	-	-	1.1%	-	42.3%
EXDP Zone 2	*Value (m)*	4	4	7	4	7
	Percentage of change with respect to Sim0	-	-	75%	-	75%

When EXDP increases in Zone 1 (Sim4), ET rates do increase. Furthermore, a direct contribution of the use of EEFlux can be observed when comparing the values of the EXDP parameters in Zone 1 of the ET region in Sim2 and Sim4 (Table 3-3). When using only heads as observations in the calibration process (Sim2) the EXDP parameter in Zone 1 remains practically unchanged; while it increases by more than 40% when EEFlux-ET_{gw} estimates are used as observations (Sim4). Therefore, incorporating EEFlux-ET_{gw} estimates as observations in the calibration contributes to calibrating the EXDP parameter in areas where evaporation occurs and, consequently, to higher ET rates.

According to Figure 3-9 a) the general trend among the four calibrations is to decrease the water table at lower elevations (in the center of the basin) where Sim0 overestimates it, and

to increase it at higher elevations (towards the north), where Sim0 underestimates it, by changing the hydraulic properties parameters of K_h and storage. K_v parameters experience negligible changes of the order of 10^{-6} %, and since they do not contribute to the piezometric changes they are excluded from the analysis. The hydraulic property parameters are presented with numerical subscripts according to the zones they represent within the model, which corresponds to an arbitrary numbering assigned according to their spatial location. 35% of the calibrated K_h parameters experience the exact same percentage of change with respect their initial value across the four calibrations, regardless of the configuration of observations and parameters defined in each calibration. As these parameters are where most of the observation wells are located, observed heads are the main data used for correcting the water table in this area.

Figure 3-9 b) shows that as the simulations develop in time, they gradually converge to more similar ET flows as the water table rises and stabilizes. As a result, the EXDP parameter ceases to be a relevant factor in the generation of ET, which begins to depend solely on the hydraulic properties that govern the water flow equation, and thus the hydraulic heads. Therefore, evaluating the effect of changes in these hydraulic parameters on the resulting ET across the four simulations is key to understand the contribution of EEFlux in the calibration process.

The remaining parameters experience different percentages of change across the four calibrations based on their respective configuration of parameters and observations. We searched for common patterns between changes in the observations and parameters used in the calibrations to determine if there is a relation between them. For that purpose, simulations are grouped firstly according to the observations used in the calibration, i.e., heads against heads and EEFlux-ET_{gw} estimates, and secondly, according to their calibrated parameters, i.e., only hydraulic properties against hydraulic properties and EXDP. In both groups we searched for changes of similar magnitude and direction

(positive or negative change) experienced by the parameters. From now on, we will use the term “pattern of observations” to refer to common changes in parameters based on observations used to calibrate them, while “pattern of parameters” will be used when referring to common changes according to the parameters defined in the calibration.

From the entire set of remaining parameters, only those shown in **Table 3-4** present changes based on these patterns, whose subscripts correspond to different zones of K_h and S_y distributed throughout the basin (more information on the spatial location of these parameters can be found in the Supplementary Material, section B). Only two of them correspond to K_h (9% of K_h parameters), which suggests that it is difficult to establish a direct relation between the adjustments of K_h and the settings of the calibrations. However, K_{h2} follows the “pattern of parameters”, increasing in 100% in simulations where only hydraulic properties are calibrated (Sim1 and Sim3), while decreasing in those that also calibrate EXDP (Sim2 and Sim4). Furthermore, the decrease in K_{h2} is greater when EEFlux-ET_{gw} estimates are used (Sim4). On the contrary, K_{h18} follows the “pattern of observations”, as it increases in calibrations that use EEFlux-ET_{gw} estimates (Sim3 and Sim4), whereas it decreases in those using only head data (Sim1 and Sim2). Therefore, despite the general trend, using EEFlux-ET_{gw} estimates as observations contributes to the calibration of K_h.

Table 3-4: Parameters that behave according to the defined patterns: "pattern of observations" or "pattern of parameters". The calibrated value of the parameters is presented, as well as their percentages of change experienced with respect their initial values. The columns of simulations are further divided into parameters calibrated (blue) and observations used to calibrate them (red).

Parameter		**Sim0**	**Sim1**	**Sim2**	**Sim3**	**Sim4**
			Heads		*Heads + EEFlux*	
			Hydraulic properties	*Hydraulic prop. + EXDP*	*Hydraulic properties*	*Hydraulic prop. + EXDP*
K_{h_2}	*Value (m/d)*	0.03	0.06	0.024	0.06	0.015
	Percentage of change with respect to Sim0	-	100%	-21.6%	100%	-50%
$K_{h_{18}}$	*Value (m/d)*	3	2.35	3.31	4	5.3
	Percentage of change with respect to Sim0	-	-21.6%	10.4%	33.5%	76.%
S_{y_1}	*Value (-)*	0.03	0.033	0.01	0.032	0.017
	Percentage of change with respect to Sim0	-	9%	-66.7%	5.5%	-43.7%
S_{y_2}	*Value (-)*	0.06	0.078	0.011	0.085	0.034
	Percentage of change with respect to Sim0	-	29.8%	-82.4%	41.6%	-42.7%
S_{y_3}	*Value (-)*	0.07	0.3	0.3	0.084	0.13
	Percentage of change with respect to Sim0	-	328.6%	328.6%	20.3%	90.6%
S_{y_4}	*Value (-)*	0.1	0.294	0.186	0.168	0.124
	Percentage of change with respect to Sim0	-	193.8%	85.7%	68.2%	23.6%
S_{y_5}	*Value (-)*	0.15	0.214	0.3	0.161	0.011
	Percentage of change with respect to Sim0	-	42.6%	100%	7%	-92.5%

Unlike K_h, storage parameters, particularly S_y, do exhibit changes according to the previously defined patterns in five out of the seven S_y zones of the model (**Table 3-4**). Most of them present a "pattern of observations", where calibrations using EEFlux-ET_gw

estimates as observations (Sim3 and Sim4) exhibit a greater decrease (or a lower increase) in S_y than those using only head observations (Sim1 and Sim2). This is the case of S_{y4} and S_{y5}, which are located inside Zone 1 of the ET region, in the first layer of the model (Figure 3-10 a)). Since ET occurs when the water table is shallow (and mainly from Zone 1 of the ET region), S_y values defined in layer 1 are used to calculate the heads that generate ET flows from the water table. Thus, when EEFlux-ET_{gw} estimates are used in the calibration as observations, the S_y parameters are adjusted to simulate evaporation flows similar to these observations. Greater decreases in S_y suggest that calibrations that use EEFlux-ET_{gw} estimates attempt to represent a time-varying water table based on these observed ET fluxes. This effect can be observed in Figure 3-10, which shows water table fluctuations (WTF) across the four simulations at four points acting as virtual wells (VW) located inside S_{y4} and S_{y5} zones. WTF differences across simulations are difficult to observe in S_{y4} since its value increased in all of them. However, differences are observed in the wells located in S_{y5}. While slightly larger WTF are observed in Sim3 in comparison to Sim1 and Sim2, pronounced WTF are clearly observed in Sim4 since it is the only simulation in which S_{y5} decreased (**Table 3-4**). On the contrary, when the water table is deeper, there is no groundwater ET and the S_{y2} values are adjusted according to heads (**Table 3-4**). It is noteworthy that S_{y1}'s behavior follows the "pattern of parameters" despite being in layer 1, which implies that there is a direct relation between the adjustment of S_y in areas where evaporation occurs, and the EEFlux-ET_{gw} estimates are used as observations in the calibration.

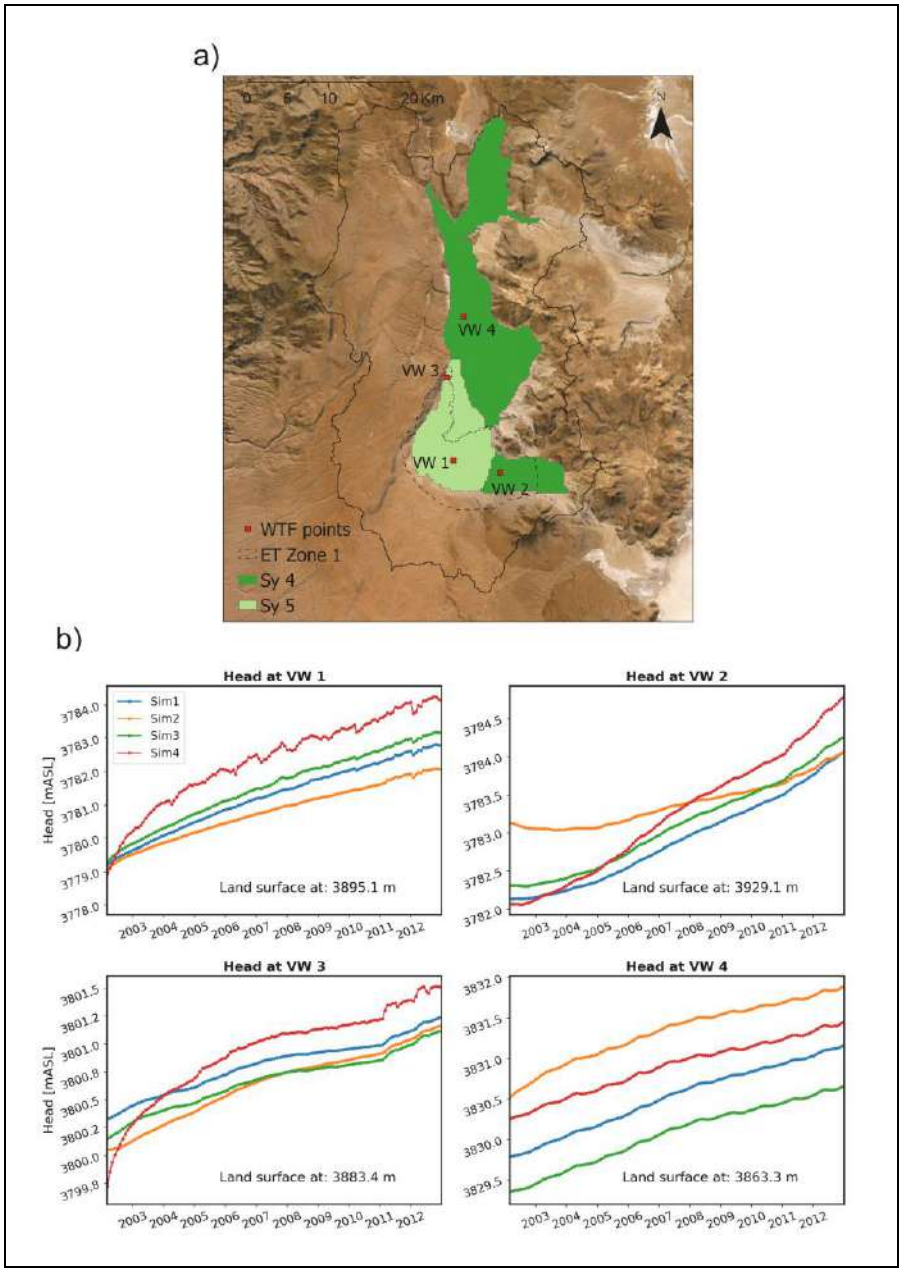

Figure 3-10: a) Location of the virtual wells (VW) in the basin. b) Water table fluctuations at virtual wells.

3.4. Discussion

3.4.1. Uncertainties in the application of the EEFlux method

EEFlux is a worldwide useful and easy-to-use tool that has been applied for different purposes. Limitations of its application associated with the uncertainty in the EEFlux-ET_{gw} estimates must be considered in each case, according to the purpose for which it is used. In this research, the objective was to contribute to the calibration of groundwater models, whose stress periods typically have time scales of months or seasons. Therefore, we justified the use of EEFlux-ET_{gw} estimates as observational data in the calibration based on the capacity of the EEFlux method in reproducing seasonal trends observed in EC stations used for its validation. However, since EEFlux-ET_{gw} estimates are not raw observations, they inherently carry uncertainty associated with their estimation. Consequently, they were not used in the calculation of performance metrics of the four calibrations. Here, we identify and discuss the sources of these uncertainties with the aim of contributing to a better future application of this tool.

The frequency with which images are available, according to the passage of the satellites over the study area, adds uncertainty to the daily scale EEFlux-ET_{gw} estimates. In this study, 315 images from Landsat 5 and 7 were used, which correspond to an average of two images per month. According to Irmak et al. (2012), one satellite image per month should suffice to construct an accurate ET_rF curve for purposes of estimating seasonal ET. However, they note that during periods of rapid vegetation change, a more frequent image interval may be desirable (Allen et al., 2007; Irmak et al., 2012). de la Fuente et al. (2021) studied the spatiotemporal variability of water bodies and vegetation patches at Salar del Huasco. They found that these patches vary seasonally, but the magnitude of the increase in the area covered by vegetation was not as intense as that observed for open water bodies. Accordingly, two images per month are sufficient to represent monthly ET at Salar

del Huasco for the purpose of our research. However, it is important to recall this limitation as a source of uncertainty that must be analyzed in each case. Cloud cover percentage of the available images must also be accounted for, since clouds add noise and alter the information used when processing the EEFlux data. Carrasco-Benavides et al. (2022) selected images of clear sky conditions (≤30% of clouds) for estimating ET_a from EEFlux in central Chile, while de Oliveira Costa et al. (2020a) gave priority to images without clouds for their selection within the EEFlux platform. Similarly, in this research, images with clouds over the Salar del Huasco basin were discarded.

EEFlux images provide an evaporation factor equivalent to the crop coefficient. The obtained ET value is thus a combination of: (1) the ET_rF factor; and (2) in-situ ET_r computations. (1) is calculated as a fraction of instantaneous ET_a estimated by METRIC and satellite-derived ET_r estimated using Penman-Monteith with meteorological data from CFSV2 grided products (Eq. (3-2)). The standardized Penman-Monteith method for computing ET_r assumes that the near-surface profiles for air temperature, humidity, and wind speed are in equilibrium with the well-watered surface represented by ET_r and it has been found that its application over dry areas results in overestimation of ET_r (Allen et al., 2021; Blankenau et al. , 2020). Allen et al. (1983) reported ET_r calculated with Penman-Monteith nearly 17% greater when using weather data from non-irrigated environments, as opposed to that collected over irrigated environments. Blankenau et al. (2020) found that summer season ET_r computed with Penman-Monteith from gridded weather data in 103 sites exceeded by 10–30% that computed from weather stations. In the case of (2), the method and available data used for computing in-situ ET_r should also be considered as sources of uncertainty in the EEFlux-ET estimates. In this study, the Blaney-Criddle equation was used to calculate ET_r because it only requires monthly mean temperatures, making it especially useful in regions with poor hydrometeorological information. This is not only the case of the Salar del Huasco basin, but also that of many other areas where the use of EEFlux would be an important contribution to the lack of detailed in-situ

information. However, the simplicity of the Blaney-Criddle method also makes it inaccurate, especially in extreme climates (Brouwer & Heibloem, 1986). Some studies have reported overestimated values of ET_r in arid regions (Gao et al., 2017; Hashemi & Habibian, 1979; Tabari et al., 2013), whereas other investigations have reported underestimated ET_r values in arid regions (Brouwer & Heibloem, 1986; Heydari et al., 2015; Li et al., 2016; Zhan & Shelp, 2009).

3.4.2. Contribution of $EEFlux - ET_{gw}$ estimates to the calibration of hydraulic properties

The use of heads and EEFlux-ET_{gw} estimates as observations in the calibration process of a groundwater model contributes to improving the simulation of aquifer levels both in space (through calibration of K) and in time (through calibration of S_y). The S_y parameter is defined as the space available for the gain or loss of groundwater associated with the rise or fall of a water table, respectively (Liu et al., 2022; Lv et al., 2021). Thus, it is responsible for the fluctuations of the water table over time, whose simulation is essential to estimate groundwater ET. Multiple water balance studies based on water table fluctuations have pointed S_y as one of the main sources of uncertainty in the estimation of flows such as recharge and ET (Diouf et al., 2020; Gribovszki, 2018; Gumuła-Kawęcka et al., 2022; Jiang et al., 2017; Li et al., 2009; Shah et al., 2007; Su et al., 2022; Yonghong et al., 2022), concluding that there is a strong relationship between this parameter and groundwater ET, which is consistent with our finding. Therefore, determining and calibrating its value has also been the focus of multiple studies (Durand et al., 2017; Gong et al., 2021; Liu et al., 2022; Pozdniakov et al., 2019; Su et al., 2022; Sun et al., 2010). However, to the best of our knowledge, this is the first study that used satellite observations of evaporation fluxes in a numerical groundwater model to calibrate S_y.

On the contrary, K did not experience changes that could be directly attributed to the use of EEFlux-ET_{gw} estimates in the calibration. This is consistent with the study of Carroll et al. (2015), which reported no appreciable link between K and parameters associated to the estimation of ET, which suggested that K could be calibrated only to water level records while ET-related parameters to EVI-derived ET from Landsat images. In the present work however, the fact that Sim3 achieved the bests performance metrics suggests that incorporating EEFlux-ET_{gw} estimates contribute to the calibration of K, and thus there is a relation between them, which is mostly indirect.

3.5. Conclusions

EEFlux images were utilized to assess the applicability of remote sensing products to support calibration of groundwater models in an arid zone of complex topography. Validation of the EEFlux method indicates that the approach can represent the magnitude and seasonal variations of evaporation over the Altiplano. This finding is supported by relatively low RMSE's values ranging between 0.46 and 1.25 mm/d. Therefore, coherent ET rates can be obtained in areas of complex topography, where access to them is often limited. Thus, this methodology allows supplementing the existing information for the calibration of numerical models in remote aquifers.

The results of this study also show that EEFlux contributes to a better calibration of the hydraulic parameters of the numerical groundwater model, as there is more observational data used in the calibration process. The groundwater model simulations performed with the parameters resulting from the four calibration configurations outperformed the baseline simulation Sim0. Nevertheless, the best performance metrics were achieved in Sim3 (NRMSE = 4.1%), in which only hydraulic properties parameters were calibrated using both heads and EEFlux-ET_{gw} estimates. Additionally, EEFlux contributes to the calibration of the EXDP parameter in areas where evaporation occurs (e.g., see Sim 3).

Although the contribution of EEFlux-ET_{gw} estimates to the calibration of hydraulic conductivity is indirect and difficult to distinguish from that of observed levels, a direct effect on the calibration of specific yield parameters is observed in 74% of these parameters. Calibrations that incorporated EEFlux-ET_{gw} estimates as observations resulted in lower values of calibrated S_y inside Zone 1 of evaporation in comparison to those that used only heads. Lower values of S_y parameters cause more pronounced fluctuations of the water table in time and, as a result, more variations in evaporation fluxes. Therefore, its use as additional information in the calibration process contributes to a more complete representation of the spatiotemporal water table dynamics. Furthermore, to the best of our knowledge, this is the first study to calibrate S_y in a numerical groundwater model using satellite observations of evaporation fluxes.

This research confirms that satellite images can be a valuable tool in the calibration and definition of elements in groundwater models. This work not only expanded the uses of EEFlux to disciplines different to agriculture, but also developed a methodology that can be applied in other areas around the world, thanks to the coverage of the images used by EEFlux.

3.6. Acknowledgments

The authors thank the Agencia Nacional de Investigación y Desarrollo (ANID) for funding grants FONDECYT/1210221 and FSEQ210018. The authors also acknowledge support from the Centro de Desarrollo Urbano Sustentable (CEDEUS – ANID/FONDAP/15110020) and the Centro de Excelencia en Geotermia de los Andes (CEGA – ANID/FONDAP/15200001).

4. GROUNDWATER RESPONSE TO CLIMATE CHANGE AND THE TIME OF EMERGENCE OF ANTHROPOGENIC SIGNALS IN AQUIFER LEVELS: CAN GROUNDWATER SUPPORT WETLANDS' RESILIENCE TO CLIMATE CHANGE IN NATURAL-STATE BASINS?

4.1. Introduction

Groundwater is the largest source of freshwater that supplies most of the global population and plays a crucial role in supporting ecosystems (Atawneh et al., 2021; Cuthbert et al., 2019; McDonough et al., 2020). Groundwater is strongly connected to surface waters through discharges into springs, floodplains, streams (mainly as baseflow) and wetlands (Scanlon et al., 2023). With the ongoing changes in the Earth's climate, the amount and distribution of groundwater recharge is likely to fluctuate or change, affecting groundwater storage, water table levels, and eventually, the interactions between groundwater and surface water (Amanambu et al., 2020; Condon et al., 2020; Cuthbert et al., 2019). Consequently, groundwater-dependent ecosystems, such as wetlands and riparian zones, will be affected by these changes, which could significantly alter their ecological functioning (Havril et al., 2018; Kløve et al., 2014; Salimi et al., 2021).

Wetlands play a vital role in mitigating climate change (Huang et al., 2021; Ma et al., 2022; Salimi et al., 2021). They are capable of regulating the atmospheric concentrations of greenhouse gases that contribute to global warming, such as methane, carbon dioxide and nitrous oxide. These ecosystems store about a third of the global soil carbon and more than half of the carbon in the atmosphere, being thus a crucial long-term carbon sink (Cuthbert et al., 2019; Huang et al., 2021; Ma et al., 2022; Mitsch et al., 2013; Moomaw et al., 2018). However, wetlands are threatened by climate change and human activities,

which have led to a loss of approximately 35% of the world's natural wetlands between 1970 and 2015 (Fluet-Chouinard et al., 2023; Huang et al., 2021).

It is still unclear how wetlands will respond to climate change (Gallego-Sala et al., 2018; Ma et al., 2022; Salimi et al., 2021). Studies suggest that wetlands in arid regions are generally more resilient than those in temperate or tropical regions, as they have been capable to adapt to extreme climate events, such as drought and flooding episodes, and they have a greater capacity to recover from disturbances (Sandi et al., 2020). In these regions, most wetlands depend on groundwater, and it has been found that changes in groundwater levels significantly impact the hydrology and functioning of wetlands (Chen et al., 2021; Froend et al., 2016; House et al., 2016; Ma et al., 2022; Paquis et al., 2023; Sandi et al., 2020; Scanlon et al., 2023; Stirling et al., 2020; Zhu et al., 2020). Therefore, assessing the groundwater response to climate change is crucial to better understand the potential impacts on groundwater-dependent wetlands.

Recently, the concept of time of emergence (ToE) of the climate change signal has been found to be crucial to anticipate and adapt to climate change impacts. The ToE is defined as the time at which the signal of anthropogenic climate change is emerging against the background of natural climate variability (noise) (Hawkins & Sutton, 2012; Lehner et al., 2017; Sui et al., 2014). Identifying when the climate change signal will emerge from the background could be particularly difficult in environments with large natural variability, such as in regions strongly influenced by large-scale oceanic-atmospheric phenomena.

The ToE of climate change signal in atmospheric variables has been widely explored, particularly in temperature and precipitations (Barrow & Sauchyn, 2019; Gaetani et al., 2020; Hawkins et al., 2020; Hawkins & Sutton, 2012; Li et al., 2021; Sui et al., 2014). More recently, its application has expanded to hydrological studies. For example, Chadwick et al. (2021) assessed the ToE of climate change in a Chilean reservoir under

future streamflow time series to identify when its operational rule will no longer be able to maintain its performance. They observed that the signal of climate change would emerge earlier in the reservoir's performance than in precipitations, and therefore they remark the importance of identifying the ToE in variables directly related to water resources availability. Walker et al. (2022) employed the ToE to examine the timing of the onset of modern rates of sea-level rise, both globally and locally. They found that local records in the North Atlantic had a larger variability than the global signal, and therefore the spatial variability in sea-level rise should be considered when assessing the impacts on coastal communities and infrastructure. Recently, John et al. (2023) evaluated the ToE of climate change across Australian catchments. Their results showed that signals emerge earlier in systems with low natural variability, however, earlier emergence is likely to be observed in streamflow than in precipitations. Martínez et al. (2023) studied the ToE of the sclerophyllous forest in central Chile to improve the understanding of when the forest will be displaced by climate change, which extends the application of ToE into forest hydrology. These studies give valuable insights of the importance of studying the ToE in hydrological variables for better managing of water resources.

Given the crucial role that groundwater resources are expected to play in the future, it becomes relevant to incorporate the concept of ToE in groundwater studies to gain a better understanding of how climate change-induced shifts in groundwater could affect their dependent ecosystems. While studies assessing the ToE in variables other than climatic have increased, its application in groundwater studies remains largely unexplored. To the best of our knowledge, the study by Ascott et al. (2022) was the first to estimate the ToE in groundwater levels, and it still stands as one of the few—if not the sole—studies on the subject to date. With data from the CMIP5 ensemble, the authors of this study forced a lumped conceptual groundwater model to simulate future levels at eight borehole sites in Burkina Faso, West Africa, and estimated the ToE using a signal-to-noise approach. They found no consistent direction of climate change impact on groundwater levels across the

boreholes studied when different climate models were used to force the model, highlighting the need for improved GCMs and long-term monitoring.

Despite the important insights provided by Ascott et al. (2022), the study has some limitations, such as employing eight boreholes to represent what could happen in an entire region. Also, the use of a lumped conceptual groundwater model may not properly represent complex hydrogeological systems, which could lead to inaccurate predictions of future groundwater changes for management purposes. Additionally, the study did not consider the impacts of extreme climate events on groundwater, nor how human activities could affect groundwater recharge. In addition, climate models from CMIP5 may not be the most up-to-date or accurate models. Therefore, it is necessary to increase the understanding of the ToE in groundwater levels for adaptation strategies by performing studies that can more accurately simulate groundwater dynamics, using up-to-date climate models.

Our study focuses on the aquifer of the Salar del Huasco basin, located in the hyper-arid Chilean Altiplano. This basin is home to groundwater-dependent wetlands that are protected by the Ramsar convention due to their ecological value. These wetlands have adapted to extreme climatic conditions, including low annual precipitation and its high interannual variability, by relying on groundwater discharges. However, their adaptive capacity may be threatened by changes in groundwater levels that exceed their natural variability. Therefore, it is crucial to determine when the anthropogenic signals emerge from the groundwater response to climate change in order to protect these ecosystems.

Previous studies in Salar del Huasco have investigated changes in groundwater flows and dynamics (Acosta & Custodio, 2008; Blin et al., 2022), wetland dynamics (de la Fuente & Meruane, 2017; de la Fuente et al., 2021; Lobos-Roco et al., 2021; Lobos-Roco et al., 2022; Paquis et al., 2023), adaptation of microbial communities (Dorador et al., 2009;

Dorador et al., 2010; Molina et al., 2021), among others. However, no studies have yet evaluated the ToE in groundwater levels to identify when wetlands might be affected by changes beyond the natural variability. Accordingly, the main goal of this research is to evaluate the response of groundwater dynamics to climate change and assess the time in which the anthropogenic signal will emerge from the natural variability of groundwater levels. To achieve this, we use up-to-date climatic data from the CMIP6 ensemble to drive a transient numerical groundwater model of the Salar del Huasco aquifer. Employing a groundwater numerical model, previously calibrated by Blin & Suárez (2023) using borehole records at 42 wells, we estimate the ToE of the climate change signal in the simulated groundwater levels. Since our study site is at its natural state due to its RAMSAR protected status, our findings could provide crucial information for developing adaptation strategies to preserve wetlands not only in Salar del Huasco, but also in areas of similar climatic and hydrogeological properties.

4.2. Methods

4.2.1. Study site

The Salar del Huasco basin is located in the extremely arid Chilean Altiplano within the Atacama Desert, between 19.98°S and 20.43°S of latitude and between 68.94°W and 68.7°W of longitude (Figure 4-1). The basin extends over 1470 km^2 at a mean elevation of 4165 m ASL. Previous isotopic studies have discarded a possible groundwater connection between the Salar del Huasco basin and its neighbors, and it is therefore considered a hydrologically closed (endorheic) basin (Risacher et al., 1999; Scheihing et al., 2017; Uribe et al., 2015). Accordingly, the aquifer discharges into the basin's topographic low, where a salt flat of 50 – 60 km^2 has formed by the long-term evaporation of water enriched with salts and brines (Corenthal et al., 2016; Marazuela et al., 2020). Groundwater-fed wetlands and lagoons located in the salt flat zone have a great ecological value as they

sustain the life of unique species of flora and fauna, for which they are protected by the RAMSAR convention (CONAF, 2005), as well as by the Chilean government who recently declared the basin a National Park (Blin et al., 2022; Blin & Suárez, 2023).

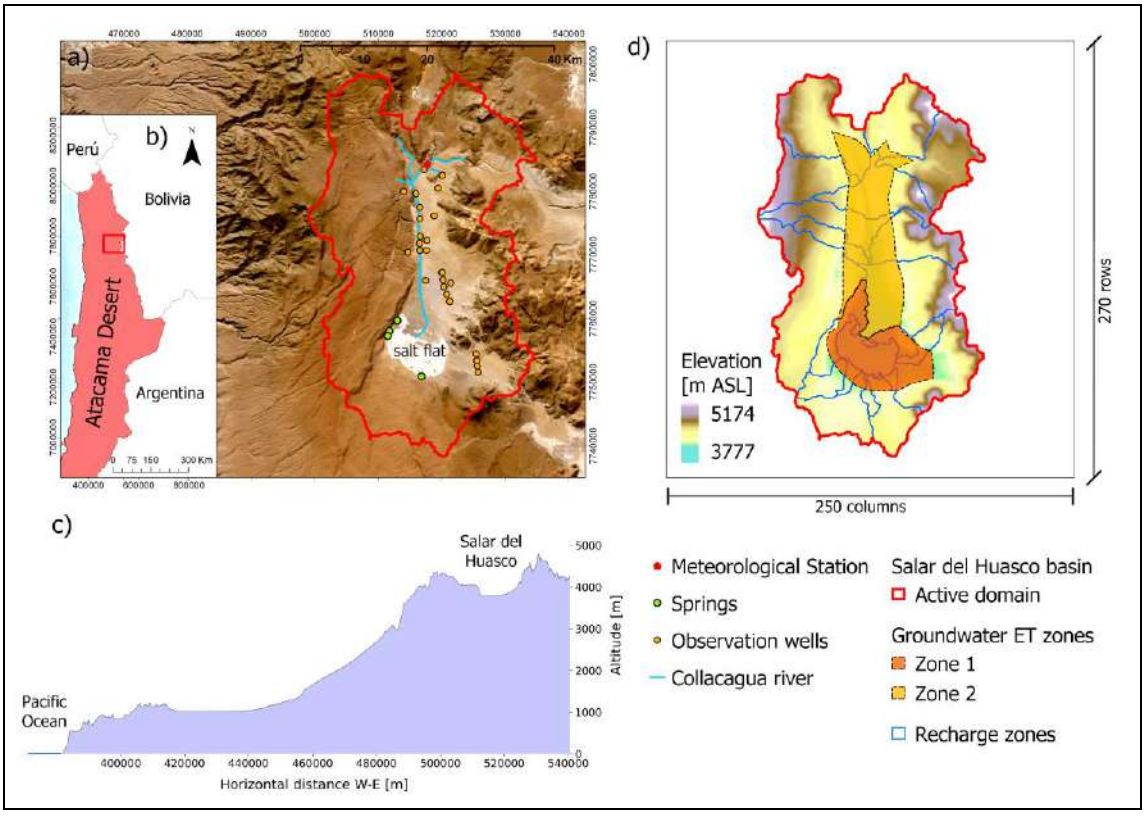

Figure 4-1: Study site. Panel a) Salar del Huasco basin, where observation wells are depicted as orange circles, Collacagua meteorological station is shown as a red pentagon and springs as green circles near the wetlands at the salt flat nucleus. b) Location of the Salar del Huasco basin (enclosed by a red rectangle) in the Atacama Desert, northern Chile, South America. c) Elevation profile from the Pacific Ocean (left) to the Salar del Huasco basin (right) in the Altiplano. d) Altitude of the basin's topography in meters above sea level (m ASL), the recharge zones delineated in blue represent the subbasins of the rainfall – runoff model.

Depending on the altitude, mean daily temperatures within the Salar del Huasco basin can range between 4–14°C, with high daily thermal oscillation (DGA, 2009). Precipitation in this part of the Altiplano occurs in the austral summer (November through March) as heavy convective storms, with a high interannual variability that ranges from 11 to 400 mm/year as a consequence of the El Niño-Southern Oscillation (ENSO) phenomenon (Blin et al., 2022; Garreaud et al., 2003; Hernández-López et al., 2014). Additionally, long-term climate fluctuations in the Altiplano have been associated to the Pacific Decadal Oscillation (PDO) phenomenon, which has a strong influence on decadal and inter-decadal variability (Garreaud & Aceituno, 2001; Rojas-Murillo et al., 2022; Torres-Batlló & Martí-Cardona, 2020).

In the Salar del Huasco, as in most of the Altiplano basins, groundwater flows mainly through fractured volcanic aquifers, unconsolidated sediments, and alluvial fans (Acosta & Custodio, 2008; Blin et al., 2022; Herrera et al., 2016; Houston, 2009; Urrutia et al., 2022). The hydrogeological system is mainly characterized by a shallow aquifer of recent sedimentary deposits, a middle aquifer formed by Collacagua Formation and clay, and a deep aquifer formed by Collacagua Formation and Huasco Ignimbrite (Acosta & Custodio, 2008; DGA, 2009).

4.2.2. Groundwater flow model

The groundwater dynamics were simulated using a numeric groundwater flow model developed by Blin et al. (2022) and later modified by Blin & Suárez (2023). The model was built in MODFLOW (Harbaugh et al., 2000) using FloPy (Bakker et al., 2016), a python library for building, running and processing MODFLOW-based models. The model of the Salar del Huasco basin discretizes the three main aquifers of the hydrogeological system into 10 layers, 253 columns and 270 rows. No-flow conditions were defined in the

boundaries of the domain to represent the hydrogeological disconnection between the basin and its neighbors.

Recharge was estimated with the rainfall-runoff model developed by Uribe et al. (2015) for the Salar del Huasco basin, which is based on the HEC-HMS model's routines. For each hydrological response unit (HRU) within the model domain, mass balance equations are applied to reservoirs that represent processes occurring at the surface and the subsurface. The model uses daily precipitation, temperature, and potential evapotranspiration to calculate surface runoff, actual evaporation and deep percolation, i.e., groundwater recharge. Future potential evapotranspiration is estimated using the Blaney-Criddle modified equation (Doorenbos & Pruitt, 1977), whose parameters were calibrated by Blin et al. (2022) for the Salar del Huasco basin. Groundwater evaporation is thus the difference between the potential evapotranspiration and the actual evaporation from the subsurface estimated by the rainfall-runoff model, to represent what can still be evaporated from the groundwater system. For a more detailed description of the rainfall-runoff model we refer readers to the works of Uribe et al. (2015) and Blin et al. (2022).

The resulting recharge is simulated as a specified flux in the MODFLOW model using the Recharge Package (RCH) (Harbaugh et al., 2000), where different recharge rates are applied to zones that represent the rainfall-runoff model's subbasins (Figure 4-1d). Groundwater evaporation is simulated as a head-dependent boundary condition using the EvapoTranspiration package (EVT) (Harbaugh et al., 2000) package. The EVT package establishes a linear relationship between heads and evaporation rate: no evaporation occurs if heads are below a specific extinction depth (EXDP parameter), while evaporation increases linearly as heads increase from that depth to the surface. The maximum evaporation rate that occurs at the surface results from the rainfall runoff model (as the difference between the potential evapotranspiration and the actual evaporation). The EVT package is applied where the water table is shallow, which occurs in the topographic low

of the basin and in the riparian surroundings of the Collacagua river (zones 1 and 2 in Figure 4-1d). The EVT area is divided into zones 1 and 2, where different values of the EXDP parameter were defined and calibrated by Blin & Suárez (2023).

The interaction between the aquifer and the Collacagua river was simulated with the River Package (RIV) (Harbaugh et al., 2000). The RIV package is a head-dependent boundary condition in which water can be exchanged between the river and the aquifer based on the water table height. Finally, the groundwater discharge to the springs was simulated using the Drain package (DRN) (Harbaugh et al., 2000) which is also a head-dependent boundary condition in which only discharge from the aquifer can occur when heads are above the spring's elevation. Four drains represent the main springs in the wetland area (Figure 4-1a).

Simulation time was discretized into monthly stress periods in the historical and future simulations. The historical simulation covers the period between 1980 and 2014, while future simulations cover continuously the period between 2014 and 2100. However, the period between 2014 and 2024 is considered as a warm-up period, and thus future analysis of groundwater dynamics begins from 2025.

4.2.3. Climate change data

4.2.3.1. Bias-adjustment of climate model data

We used the climQMBC package (https://github.com/saedoquililongo/climQMBC) for the bias- adjustment of monthly precipitation and temperature projections of CMIP6 models. This climQMBC package offers five quantile-mapping based methods to adjust systematic biases in the future variables to historical observations.

While preserving the absolute changes in quantiles of temperature through the regular Quantile Mapping (QM) (Panofsky & Brier, 1968; Wood et al., 2002), is a straightforward process, maintaining the relative changes or trends projected by the GCMs is more challenging for precipitation than for temperature. Consequently, in this study, we chose different bias- adjustment methods for temperature and precipitation given their different nature: the Quantile Delta Mapping (QDM) method was used for precipitation as it performs a QM method that preserves model-projected relative changes in the quantiles, and the Detrended Quantile Mapping (DQM) (Bürger et al., 2013) was used for adjusting systematic biases in temperature means (Cannon et al., 2015).

The climQMBC package applies the QDM method according to Cannon et al. (2015). The method begins with detrending future model outputs by quantile and bias-adjusting to match observations using QM with the inverse of the cumulative distribution function (CDF) of observations over the historical period ($F_{o,h}^{-1}[\ ]$), according to:

$$\hat{x}_{o:m,h:p}(t) = F_{o,h}^{-1}[\tau_{m,p}(t)] \qquad (4\text{-}1)$$

where $\tau_{m,p}(t)$ is the non-exceedance probability of a particular precipitation event modeled at a time t in the future ($x_{m,p}(t)$); and $\hat{x}_{o:m,h:p}(t)$ is the historical bias-adjusted value of $x_{m,p}(t)$. An independent probability distribution function is assigned to each month and projected period, which is selected by using the Kolmogorov-Smirnov test (for more detail see Chadwick et al., 2023).

Next, the relative changes in quantiles between the historical period and a future time t ($\Delta_m(t)$) are calculated as the ratio between $x_{m,p}(t)$ and the model's CDF over the historical period ($F_{m,h}^{-1}[\ ]$):

$$\Delta_m(t) = \frac{x_{m,p}(t)}{F_{m,h}^{-1}[\tau_{m,p}(t)]} \quad (4\text{-}2)$$

These $\Delta_m(t)$ are subsequently superimposed (multiplicatively) to the historical bias-adjusted value ($\hat{x}_{o:m,h:p}(t)$):

$$\hat{x}_{m,p}(t) = \hat{x}_{o:m,h:p}(t)\Delta_m(t) \quad (4\text{-}3)$$

Biases in temperature data were adjusted using the DQM method, preserving the model's projected changes in temperature means. This is achieved by examining the difference between the long-term trends of the modeled temperature data in the historical and future periods as the model-projected changes:

$$\Delta_m(t) = \bar{x}_{m,p}(t) - \bar{x}_{m,h} \quad (4\text{-}4)$$

where $\bar{x}_{m,h}$ and $\bar{x}_{m,p}(t)$ are, respectively, estimates of the long-term modeled mean over the historical period and at time *t* in the projected period *p*, respectively.

Finally, the bias-adjusted temperature and precipitation were disaggregated from monthly to daily basis using a K-Nearest Neighbors (KNN) approach, according to Chadwick et al. (2021).

4.2.3.2. Selection of ensemble members

We We evaluated the potential implications of climate change on the Salar del Huasco basin by considering the SSP2 4.5 and SSP5 8.5 scenarios from the sixth phase of the Coupled Model Intercomparison Project (CMIP6). These scenarios are a combination of the Socio Economic Pathways (SSP, O'Neill et al., 2020) and the Representative

Concentration Pathways (RCP, Moss et al., 2010). The SSP scenarios offer insights into various societal factors, including demographics, political shifts, and economic development, and are structured as narratives that emphasize future challenges of both adaptation and mitigation. In CMIP6's framework, greenhouse gas concentrations from CMIP5's RCP (Moss et al., 2010) are incorporated, facilitating its use in comprehensive studies (O'Neill et al., 2020). SSP2 4.5 projects a future where social, technological, and economic trajectories follow historical patterns, resulting in moderate challenges in mitigation and adaptation. On the contrary, the SSP5 8.5 scenario anticipates a future defined by rapid economic growth through the extensive use of fossil fuels, posing high mitigation challenges (O'Neill et al., 2017). The projected warming under these scenarios by the century's end varies between 2 – 2.9℃ for SSP2 4.5, and 4 – 4.3℃ for SSP5 8.5 in the GISS-E2.1 GCM (Nazarenko et al., 2022).

In the current study, small ensembles of six bias-adjusted GCMs were generated for each scenario. Their respective members were selected from a set of 45 GCM projections according to the GCM changes between the future period (2015-2100) and the historical period (1980 – 2014). Subsequently, six models projecting climate change signals corresponding to 10^{th}, 25^{th}, 50^{th}, 75^{th}, 90^{th} and 100^{th} percentiles were selected to generate ensembles of SSP2 4.5 and SSP5 8.5 scenarios. Thus, both scenarios comprise different magnitudes of change in the future.

Since precipitation and temperature behave differently, the signal that a model projects for precipitation is not the same as that for temperature and so percentiles of ΔP differ from percentiles of ΔT. Taking that into account, the models of both ensembles were selected based on ΔP since precipitation has a direct effect on the aquifer's incoming recharge. Table 4-1 presents the models used as ensemble members for the SSP2 4.5 and SSP5 8.5 climate change scenario.

Table 4-1: Models used as ensemble members of the two SSP climate change scenarios used in this research. The rip indexes (which indicate the realization, initialization method, physics version and forcing index of the model run) are showed inside parenthesis to identify different realizations of a same model for the corresponding scenario.

Scenario	Ensemble-member	Model	ΔP	ΔT
SSP2 4.5	$q_{10^{th}}$	CESM2_WACCM	0.89	0.93
	$q_{25^{th}}$	KACE_1_0_G	0.92	1.09
	$q_{50^{th}}$	GDL_ESM4	0.97	0.64
	$q_{75^{th}}$	CanESM5 (r3i1p1f1)	1.01	1.15
	$q_{90^{th}}$	INM_CM4_8	1.04	0.55
	$q_{100^{th}}$	CanESM5 (r2i1p1f1)	1.13	0.99
SSP5 8.5	$q_{10^{th}}$	ACCESS_CM2	0.81	2.30
	$q_{25^{th}}$	MPI_ESM1_2_LR	0.89	1.75
	$q_{50^{th}}$	KACE_1_0_G	0.97	2.04
	$q_{75^{th}}$	MIROC6	1.05	1.29
	$q_{90^{th}}$	CanESM5	1.10	2.59
	$q_{100^{th}}$	FIO_ESM_2_0	1.13	1.67

4.2.4. Estimation of the time of emergence of the climate change signal on groundwater levels

Unlike the water budget flows of the basin, which have a seasonal and decadal variability, the water level records observed in the Salar del Huasco basin have been characterized by remaining relatively steady between 1980 and 2014 (Acosta & Custodio, 2008; Blin et al., 2022; DGA, 2009). Therefore, we seek to understand when the projected increase or

decrease in aquifer heads ceases being a natural response of the aquifer to natural climate variability and begins to be a consequence of climate change.

A signal-to-noise approach was used to estimate the ToE of the climate change signal on groundwater heads to assess when and where the climate change signal is emerging from the background noise of natural variability (Ascott et al., 2022; Gaetani et al., 2020; Hawkins et al., 2020). The signal-to-noise approach assumes that the variable, i.e., groundwater levels, is composed of a low-frequency (LF) component, which represents the externally forced climate signal, and a high-frequency (HF) component representing natural variability (Gaetani et al., 2020; Hawkins et al., 2020; Hawkins & Sutton, 2012). The time at which the LF signal exceeds the HF threshold uninterruptedly until the end of the century is considered as the ToE (Gaetani et al., 2020).

In this research, we used two approaches for estimating the LF component: (1) we applied a 4th-degree polynomial smoothing to the time series to accommodate the long-term trend and multi-decadal variability within the LF component, thereby constraining the natural variability to interannual changes. A smoothing fit is often used to account for interannual variability because it is capable of capturing more complex patterns that might exist within the data over shorter time scales. Yet, considering the substantial role of the decadal variability ascribed to the Pacific Decadal Oscillation (PDO) in the Altiplano (Rojas-Murillo et al., 2022), (2) we used a linear fit of the time series to account for the decadal variability as the HF component (Gaetani et al., 2020). By fitting a linear trend, we are considering that, over the long term, many of the short-term fluctuations tend to cancel each other, and what remains visible is a longer-term trend.

The procedure for estimating the ToE at each well is as follows:

- Estimate the LF component in the historical period (1980 – 2014), LF_{hist}, by fitting a polynomial function to the levels simulated at each well. The polynomial degree can vary depending on the nature of the data, here, we used a 4^{th}-degree polynomial or smoothing, and a linear trend.
- Calculate the residuals as the difference between the simulated groundwater levels and the fitted polynomial. These residuals represent the variability in historical groundwater levels that LF_{hist} does not capture. The well's HF component corresponds to the standard deviation of these residuals, which represents the short-term fluctuations in the historical groundwater levels.
- Estimate the LF component in the future period (2025 – 2100), LF_{fut}, by fitting the polynomial to future simulated heads.
- Estimate the climate change signal, *S*, by subtracting LF_{hist} to LFfut.
- The signal-to-noise ratio is calculated as the ratio of *S* and the HF component. The ToE corresponds to the year of the onset in which the signal-to-noise ratio is uninterruptedly greater than 1:

$$ToE: \quad S/HF > 1 \tag{4-5}$$

Following the approach of Gaetani et al. (2020), we define a robust multi-model ToE as the median ToE for models that concur on the trend direction, assuming this agreement involves at least 50% of the ensemble. Given the use of six ensemble members in this study, a multi-model ToE is established when a minimum of three members are in concurrence. Without such consensus, climate change emergence is not determined.

4.3. Results

4.3.1. Bias-adjusted temperature and precipitation projections

Under both future scenarios the mean temperatures are projected to increase along with the minimum and maximum temperatures (2015-2100 period) with respect to the historical period (1980-2014 period) (Table 4-2). Among the statistics of precipitation, however, only the maximum monthly event projects a clear increasing change with respect to the historical period in both scenarios, forecasting thus more intense precipitation events. In addition, a larger range of the mean precipitation within the ensembles (~4 mm in SSP2 4.5 and ~8 mm in SSP5 8.5) is projected in comparison to temperatures (~2°C in both ensembles). Accordingly, there is currently more uncertainty related to the forecasting of future precipitations than temperatures.

Table 4-2: Maximum and minimum threshold of main statistics of bias-adjusted mean monthly temperature and total monthly precipitation projected by ensembles SSP2 4.5 and SSP5 8.5 between 2015 to 2100. Statistics from historical variables (period 1980 – 2014) are presented in the bottom row, shaded in grey.

Future period		**Mean monthly temperature** (°C)					**Total monthly precipitation (mm)**				
Scenario ensemble	*Ensemble range*	*Mean*	*Std.*	*Min.*	*Median*	*Max.*	*Mean*	*Std.*	*Min.*	*Median*	*Max.*
SSP2 4.5	lower	6.1	2.9	-1.3	6.1	12.3	9.4	21.6	0.0	0.0	176.2
	upper	8.0	3.3	0.1	8.0	14.9	13	26.5	0.0	0.7	242
SSP5 8.5	lower	7.2	3.1	-1.6	7.5	14.5	7.2	17.9	0.0	0.0	191.2
	upper	9.6	3.5	1.1	9.9	17.3	15.5	30.9	0.0	0.4	315.2
Historical period		4.71	3.09	-3.76	4.72	11.2	11.47	25.3	0.0	0.0	154.5

As observed in Figure 4-2, although statistics reveal increasing temperatures in both scenarios, their trends suggest that the increasing rate in SSP2 4.5 will eventually diminish by around 2040, whereas temperatures will increase until the end of the century in SPP5 8.5. Figure 4-2 also shows that the uncertainty in future precipitations can be clearly noted from the extent of the shaded area encompassing the individual trends projected by the six members of each ensemble over time. The larger the extent of this area, the larger the disagreement in precipitation projections among ensemble members. Even though similar areas (and thus uncertainty of ensemble forecasts) are projected for precipitations under both scenarios in the near future, the uncertainty of future precipitations slightly diminishes under SSP2 4.5 by the second half on the century as the shaded area slightly contracts around the ensemble mean. Contrarily, in SSP5 8.5 the uncertainty increases by the second half on the century, reaching a 16.5 mm difference between the minimum and maximum trends of the ensemble. The uncertainty surrounding these projections reinforces the importance of using ensembles to provide ranges of future changes for better assessing their potential impacts.

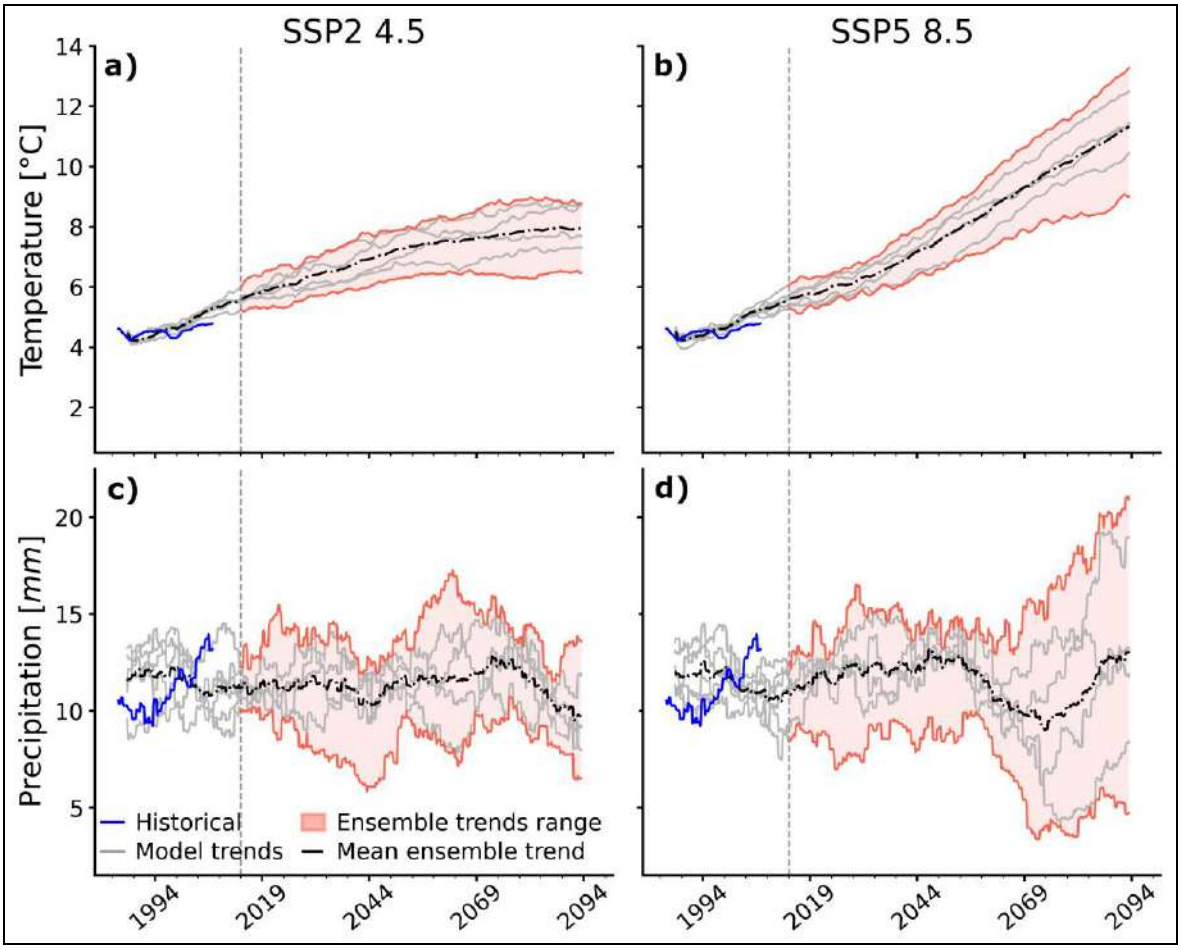

Figure 4-2: Temperature trends (a and b) and precipitation trends (c and d)) estimated over a 15-year window. The first and second row represent the future trends projected in SSP2 4.5 and SSP5 8.5, respectively. Trends in the historical reference period (delimited by dashed vertical lines) are presented in blue in all a) – d) plots. The shaded areas encompass the individual trends projected by the six members of each ensemble, representing thus the range of projections covered by the ensembles.

The ensemble means presented in Figure 4-3 indicate that mean temperatures are expected to increase in average by ~1.5 and ~2.5°C in SSP2 4.5 and SSP5 8.5, respectively, throughout the year in the future projections (between 2025 and 2100) with respect to the

reference period. In addition, both ensemble means of total monthly precipitation project a slight increase (of ~3 mm in both ensemble means) in winter precipitations (particularly in June and August), and a larger increase (of ~20 mm in both ensemble means) in summer precipitations in January and February. However, the ensemble ranges depicted in Figure 4-3c-d suggest that the greater the projected increase in the ensemble mean of total monthly precipitation, the more uncertain the magnitude of such increase within the ensemble.

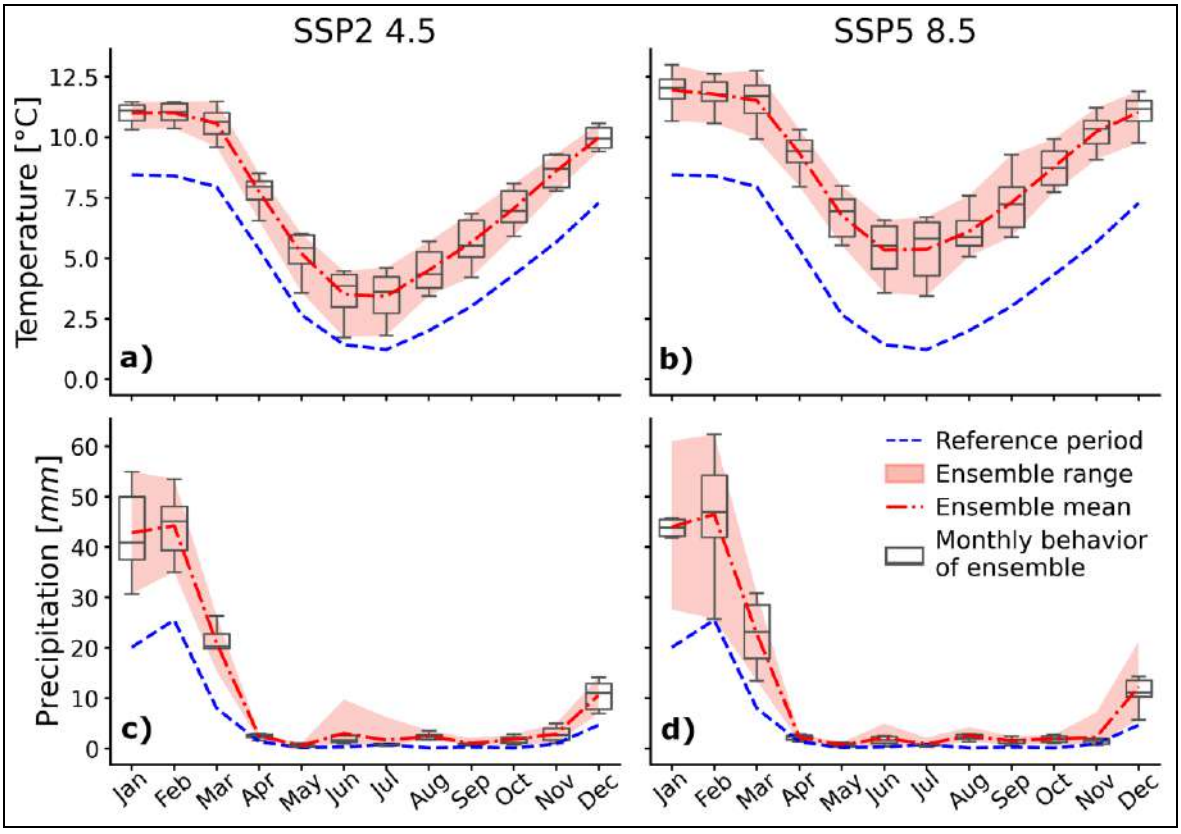

Figure 4-3: Comparison between the monthly means of temperature and total monthly precipitation observed in the reference period (1980 – 2014) and projected in the future (2025 – 2100) by ensembles SSP2 4.5 (a and c) and SSP5 8.5 (b and d). The reference period means are presented in dashed blue lines, and ensemble means in dash-dotted red lines. Boxplots

show the distribution of the ensemble members' projections for each month, while the red shaded area represents their range (maximum difference between projections).

4.3.2. Projected changes in the groundwater balance flows

As it is the main discharge mechanism of the Salar del Huasco basin (de la Fuente et al., 2021; Lobos-Roco et al., 2022; Lobos-Roco et al., 2021; Suárez et al., 2020), assessing groundwater evaporation is crucial to understand the future response of the water table. Recharge trends (Figure 4-4) are primarily driven by precipitation. Although the pattern of groundwater evaporation trends is more similar to that of precipitation than that of temperature, there is less variability among the members of the evaporation ensembles.

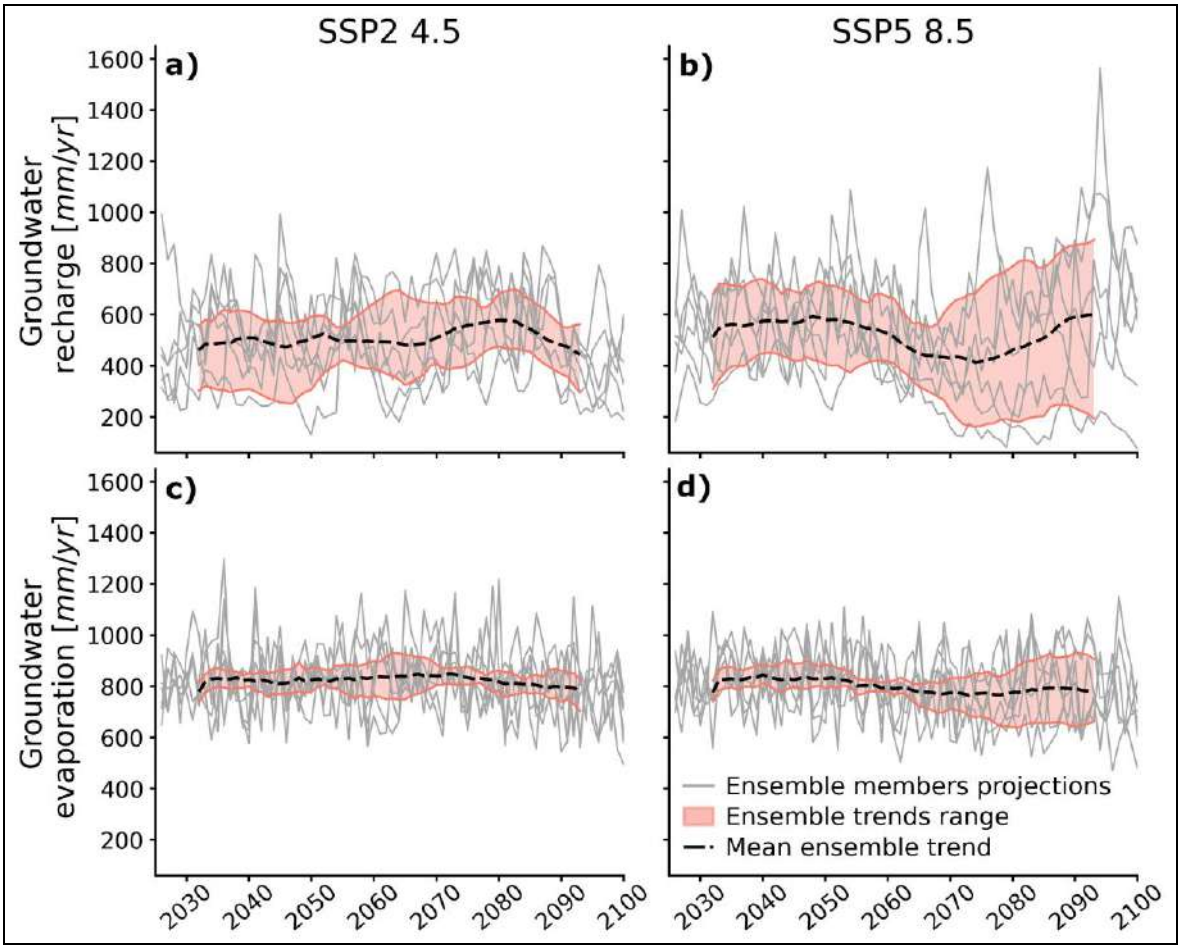

Figure 4-4: Groundwater recharge (a and b) and groundwater evaporation (c and d) estimated over the future period (2025 2100). Panels a) and c) presents results of SSP2 4.5, while b) and d) those of SSP5 8.5. The monthly projections of ensemble members are depicted in grey to show the short – term fluctuations within each ensemble. The long – term fluctuations are represented by the shaded area, which encompasses all individual trends projected by the ensemble, while the dashed black line corresponds to the mean ensemble trend (estimated with a 15-year window).

It is anticipated that future recharge rates will be significantly impacted by changes in climatic variables in winter moths (Figure 4-5). Specifically, the most substantial changes in recharge relative to the reference period are expected to occur during winter (from May

until October) due to warmer temperatures. In fact, winter recharge may increase by around 9 – 192% in SSP2 4.5 and 7 – 223% in SSP5 8.5, being July the month of largest increase, more than three times compared to the reference period. The results also suggest that under the SSP5 8.5 scenario, more extreme recharge episodes are likely to occur, as reflected by the large ensemble range (Figure 4-5b). By contrast, as the increasing summer temperatures enhance surface evapotranspiration, recharge is likely to decrease during summer by around 3 – 18% in SSP2 4.5 and 2 – 11% in SSP5 8.5.

The ensemble range of evaporation in both scenarios is much thinner than the range of recharge, and the difference between the ensemble means of both scenarios is negligible, which suggest that the groundwater response through evaporation is expected to be less uncertain than that of recharge. Despite of the slight recharge decrease in summer, the higher temperatures are expected to enhance groundwater evaporation, which is to increase in ~15 – 75% regarding the evaporation of the reference period due to the higher temperatures. As groundwater evaporation is a linear function of the depth to the surface, then it could be derived that groundwater levels could be rising.

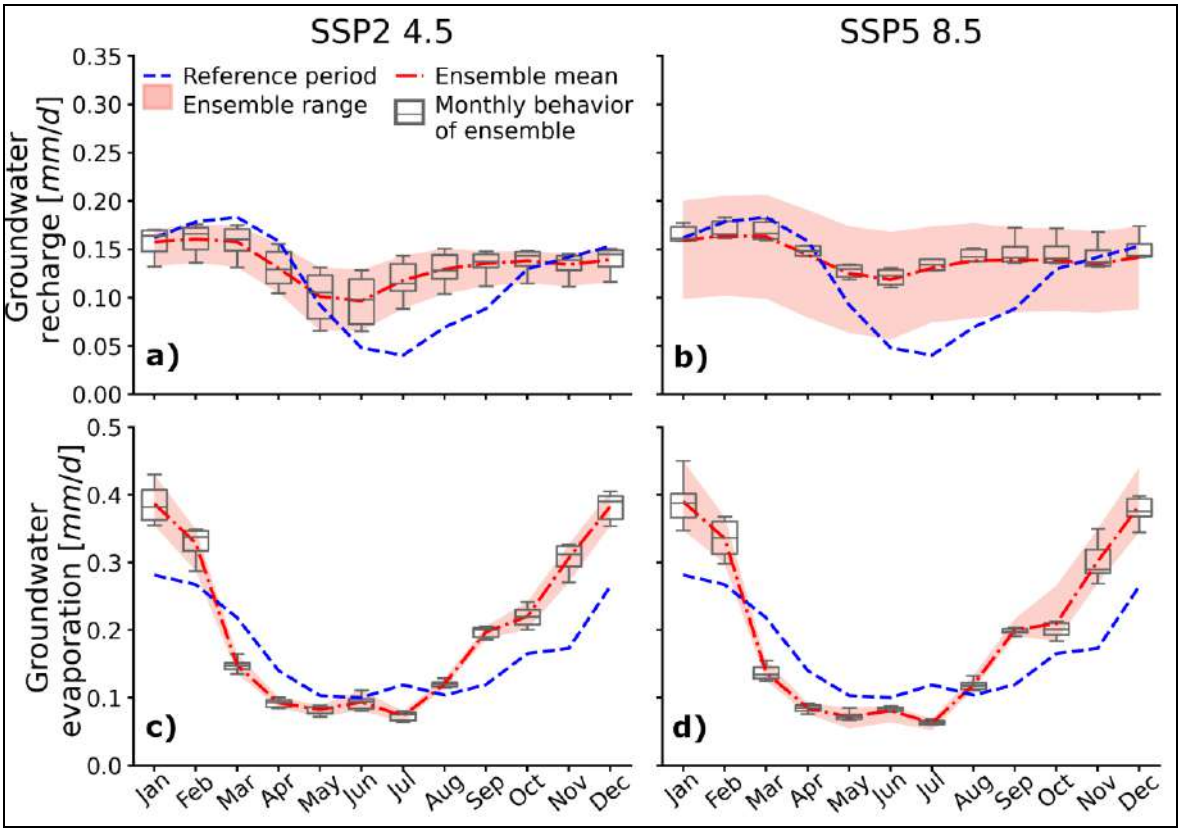

Figure 4-5: Comparison of future groundwater recharge and groundwater evaporation rates (in mm/d) of ensembles SSP2 4.5 (panels a and c) and SSP5 8.5 (panels b and d) throughout the year against the reference period (1980 – 2014), portrayed as blue dashed lines. The red dashed line represents the ensemble mean and the boxplots depict the monthly behavior of the ensemble for each month of the year simulated over the entire future period (2025 – 2100), while the shaded area corresponds to the ensemble range, given by the whiskers of the boxplots (depicting 1.5 times the interquartile range (IQR)). Panels a and b show groundwater recharge, which is the sole flux entering to the aquifer in the MODFLOW model, while panels c and d show the groundwater's response through evaporation.

Although groundwater discharges into the Collacagua river and into the springs are smaller in magnitude than evaporation, their monthly mean statistics are expected to increase

according to **Table 4-3**. The monthly maximum discharge of groundwater to the springs is projected to have the most significant increase, with a change of 370% under both scenarios. The similarity in changes projected by both scenarios suggests that the system is not highly sensitive to differences between the climate scenarios above a certain threshold, which could be beneficial for the development of management and adaptation plans since the system's response is likely to be similar to possible extreme events between climate change scenarios.

Table 4-3: Percentual change projected in the future period (2025 – 2100) in monthly mean groundwater (GW) discharge to the springs and the Collacagua river with respect to the reference period (1980 – 2014).

	Change in mean GW discharge to the springs (%)		**Change in mean GW discharge to the river (%)**	
Monthly statistic	SSP2 4.5	SSP5 8.5	SSP2 4.5	SSP5 8.5
Min.	63%	72%	44%	47%
Median	81%	83%	64%	66%
Max.	370%	370%	174%	181%

4.3.3. Spatial variations projected in groundwater levels and ToE of the climate change signal at observation wells

Under ensemble SSP2 4.5, a basin-wide mean groundwater level change with increasing levels of around 5 – 9 m is projected between December 2025 (near future) and December 2100 (end of the century), while changes with increasing levels of ~ 3 – 12 m are expected under SSP5 8.5 between the same time-periods (Figure 4-6). Nevertheless, future changes in groundwater levels will vary spatially with topography and geological features, which are represented in the modeling by HRUs (and thus recharge subbasins) and hydraulic

properties of the aquifer. Moreover, groundwater levels are expected to drop in both scenarios at the northeast of the basin by the end of the century by approximately 1 – 20 m in SSP2 4.5, and 5 – 20 m in SSP5 8.5. Even though most of precipitations occur at higher elevations in the north of the basin, the water table at the northeast will be prone to decline under lower recharge conditions projected from January to May (Figure 4-6a, b, c, g and h)

Contrarily, groundwater levels at the basin's lowlands will likely increase, according to the heads simulated across all models within the current study. The high permeability of the sedimentary materials deposited in the salt flat nucleus area and around the Collacagua river (DGA, 2009) will contribute to the increase in aquifer levels under future conditions in which recharge is expected to be more evenly distributed throughout the year (Figure 4-5). Additionally, wells near the river are not likely to respond to climate change as the water table is controlled by the river stage.

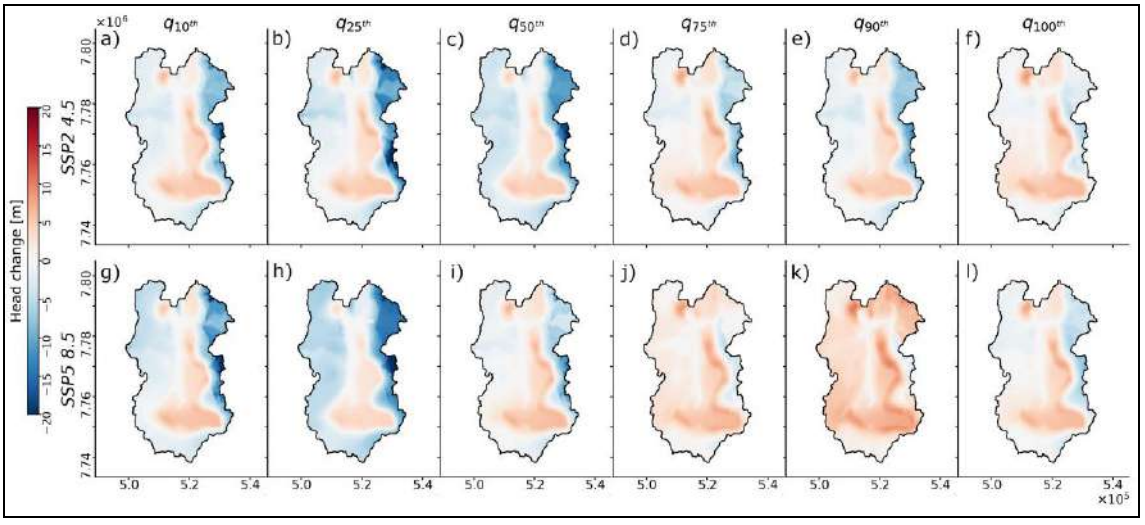

Figure 4-6: Spatial variations of the projected changes in the water table between December 2025 and December 2100 across ensemble members of scenarios SSP2 4.5 (panels a to f) and SSP5 8.5 (panels g to l).

The significance of water table variations in the Salar del Huasco aquifer can be interpreted using the multi-model ToEs at local wells (Figure 4-7), in terms of where and when the climate change signal departs from natural variability. When accounting for interannual fluctuations as natural variability in the basin, as represented by the smoothing (4th-degree polynomial) approach (Figure 4-7a). the climate change signal does not emerge. Conversely, when accounting for interannual and interdecadal fluctuations within the natural variability with the linear approach (Figure 4-7b), the signal of climate change is expected to emerge by 2034 in SSP2 4.5 and in 2035 in SSP5 8.5. A positive climate change signal (water table rise) was identified under both scenarios in all the wells with multi-model ToE.

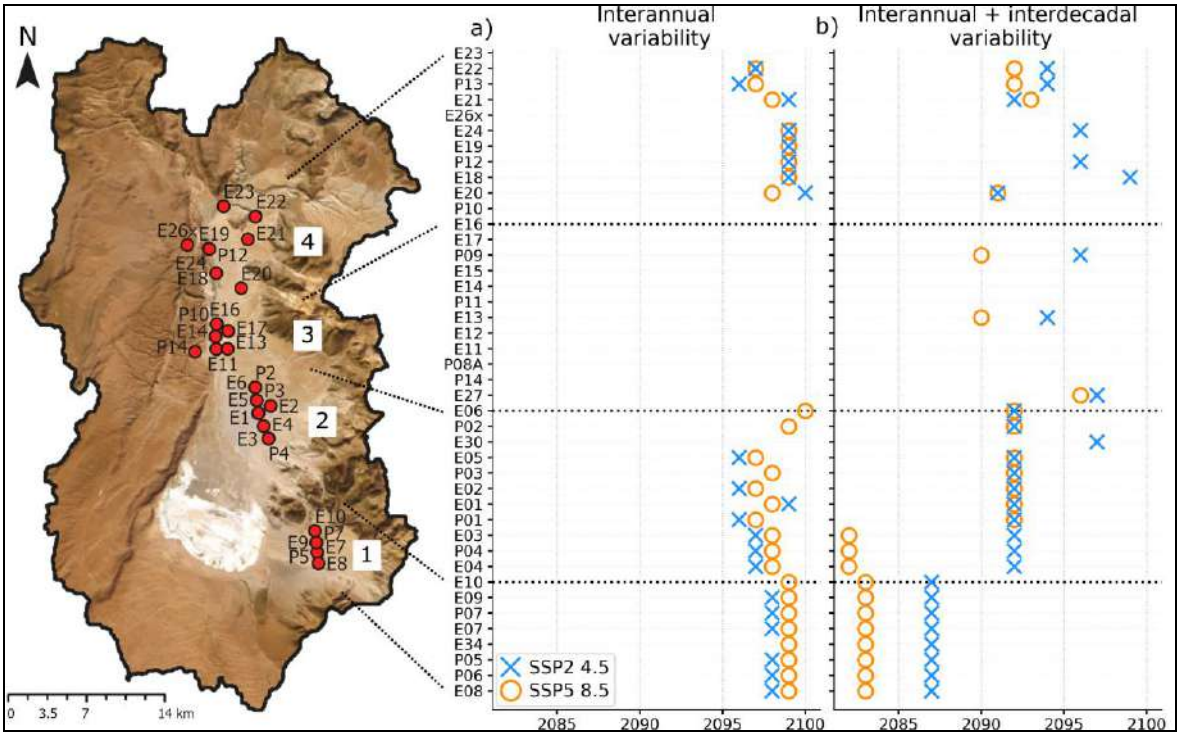

Figure 4-7: Time of emergence (ToE) of the climate change signal when: a) only interannual fluctuations are accounted for the natural variability (4th-degree polynomial smoothing approach), and b) interannual and interdecadal fluctuations are accounted for (linear approach)

in each monitoring well in the basin. The wells are depicted in the y-axis from south to north, with black dotted lines delimitating zones of wells and their location within the basin at the left.

Our analysis demonstrates a spatially consistent relationship between the ToE and the specific location of the wells within the basin, regardless of the varying well depths, with a sooner emergence for the southern wells (Figure 4-7b). This finding suggests that the ToE values observed in proximate wells are likely to exhibit strong similarities. When analyzing the correlation between the ToE and the average historical level in each well Figure 4-8, no discernible correlation between these two variables is observed. Consequently, our research posits that that climate change emergence is not primarily tied to the groundwater level itself. Instead, we predict a spatially consistent emergence of climate change signals across the entire basin.

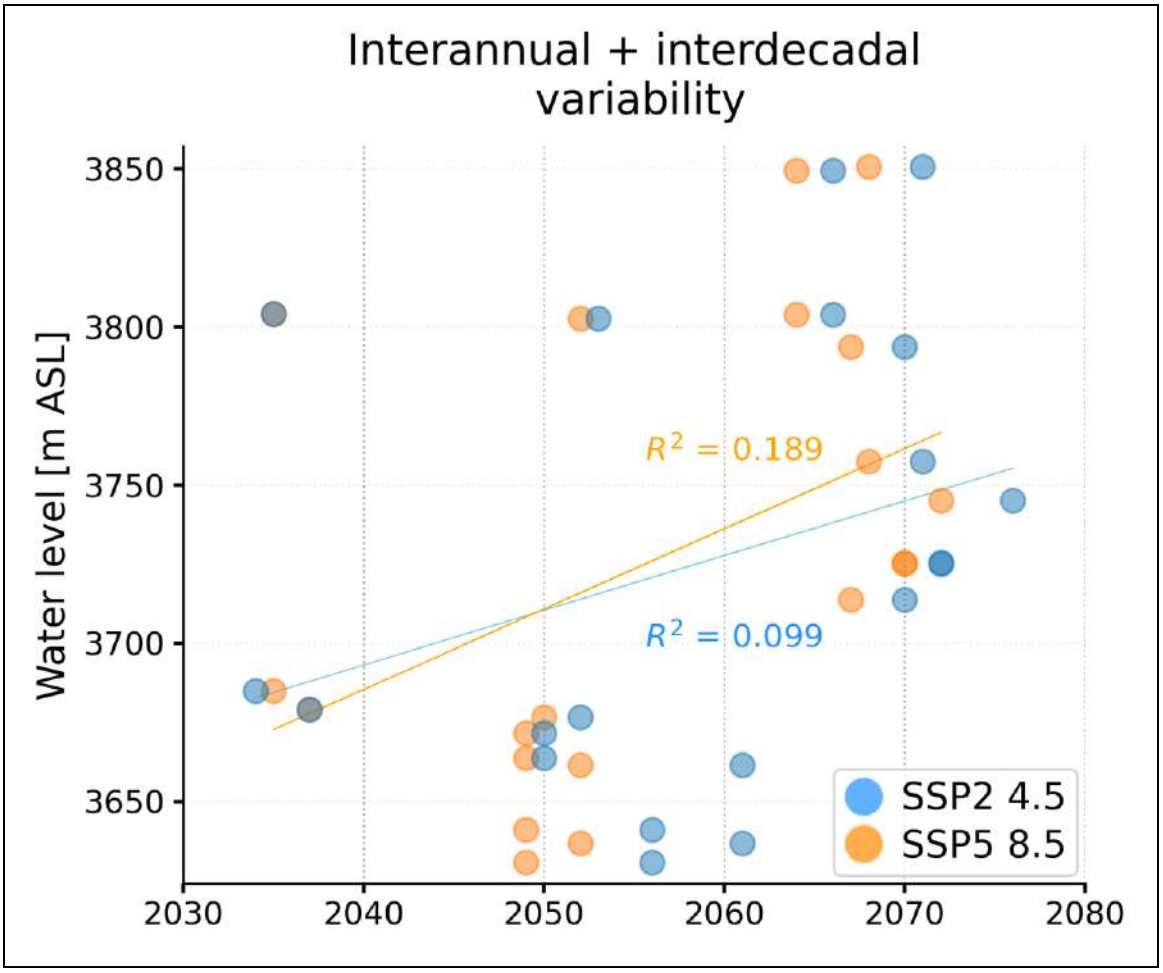

Figure 4-8: Time of emergence (ToE) of the climate change signal according to the average historical levels of the wells when interannual and interdecadal fluctuations are accounted for (linear approach) in each monitoring well in the basin.

Based on these results, groundwater-dependent ecosystems would not be endangered by water table fluctuations beyond the natural variability of the system until the end of the century if only interannual fluctuations are considered as natural variability. However, if interdecadal variabilities are also accounted for, climate change-induced fluctuations are expected up to 60 years earlier.

4.4. Discussion

4.4.1. Considerations on the estimation of the ToE of the climate change signal in groundwater levels

The two approaches employed to estimate the ToE of climate change in groundwater levels depict the low-frequency (LF) and high-frequency (HF) components of the signal differently based on the extent to which natural variability is accounted for in the system. The availability and dynamics of water resources in the Altiplano are strongly influenced by the El Niño-Southern Oscillation (ENSO) and the Pacific Decadal Oscillation (PDO), which are large-scale oceanic-atmospheric phenomena (Garreaud, 2009; Garreaud & Aceituno, 2001; Garreaud et al., 2003; Rojas-Murillo et al., 2022). ENSO is a shorter-term phenomenon with a cycle of about 3-7 years that has been mainly associated to interannual variability of summer rainfall (Rojas-Murillo et al., 2022). In contrast, PDO has a longer timescale, with a cycle of around 20-30 years and has been associated with decadal and interdecadal climatic variability. As crucial components of the natural variability of the Altiplano, ENSO and PDO should be accounted for in the HF component of groundwater levels. However, the available records in the Salar del Huasco basin are insufficient to simulate a reference period that includes several PDO cycles, which may affect the accuracy of the linear approach in representing the decadal and interdecadal variability of Salar del Huasco climate. By using the linear and smoothing approaches, we aimed to address the limitation of the former while contributing to a more comprehensive understanding of the ToE of climate change in groundwater levels, particularly when different representations of the natural variability are employed.

The importance of understanding the natural climate variability when employing the ToE has also been addressed in previous studies (Chadwick et al., 2021; Collins, 2021; Gaetani et al., 2020; John et al., 2023). Hawkins and Sutton (2012) observed that the differences in

the magnitude of projected warming and natural variability among climate models within an ensemble could lead to uncertainty in ToE estimates. Accordingly, they showed that by separating the natural variability of each model it is possible to identify whether the variability in projections arises from inter-model differences or from natural climate fluctuations, improving thus the accuracy of the ToE estimates. A later research by Lehner et a. (2017) accounted for large-scale atmospheric circulation variability within the natural variability for estimating the ToE of anthropogenic warming in North America and Europe. They found that removing the atmospheric circulation influence resulted in delayed or advanced ToE, demonstrating that the influence of natural variability can mask the anthropogenic signal when it is not properly isolated. More recently, Gaetani et al. (2020) highlighted the challenges in estimating the ToE of climate change in West African precipitations due to their complex variability. They found that low-resolution models underestimated the ToE as they fail to capture the natural variability of precipitations, hampering the detection of the anthropogenic signal from the noise of natural variability.

In addition, the fact that our findings indicate that the emergence of climate change signals is subject to the geographical location of the water table suggests that local properties of the aquifer, such as the hydraulic conductivity, could play a role in the ToE. However, this might be inherent to the Salar del Huasco aquifer as it has not been subjected to anthropogenic pressures, preserving its natural state due to its specific status as a RAMSAR protected area. The fact that Ascott et al. (2022) found no direct influence of defined hydrogeological properties on the timing of climate change signal emergence in their conceptual groundwater models further supports the idea that each ecosystem may respond differently based on its unique set of circumstances. Therefore, our results underline the importance of considering the unique characteristics and conservation status of each ecosystem when developing climate change adaptation strategies.

Given these unique circumstances of the Salar del Huasco basin, our research offers valuable insights into how groundwater in similar, minimally-disturbed ecosystems may respond to climate change. For such regions, the early emergence of climate change signals could necessitate specific mitigation measures and proactive management strategies to preserve the ecosystem's integrity and resilience in the face of climate change.

It is important to note that the lack of multi – model ToE results when S/HF ≤ 1 or when there is no agreement in either the sign of the change or the year of emergence among ensemble members. With the ensembles generated in this study, 100% of the wells with no multi-model ToE resulted from model disagreement in both ensembles, and with both approaches. Therefore, a larger ensemble would be required to achieve a more robust multi-model ToE. Nevertheless, although the ensembles used in this study have only six members, these members represent very different projections within a same scenario, and so the fact that multi-model ToEs were identified suggests that said ToEs could be representative of other intermediate models comprised within range of current ensembles. Also, discrepancies between climate projections in an ensemble have shown to have a significant impact in the timing of the ToE climatic detection (Chadwick et al., 2019), hence, more models per ensemble are recommended for robust results.

Finally, we utilize the simulated levels yielded from the groundwater model, calibrated against actual observations, rather than employing the observations themselves. This strategy ensures we mitigate any possible discrepancies stemming from the model's imperfect reflection of the observed data.

4.4.2. Implications of a positive climate change signal in groundwater levels on the key role of wetlands against climate change

The emergence of a positive climate change signal in groundwater levels at Salar del Huasco suggests that the basin's lagoons and wetlands are not likely to dry out by the end of the century, on the contrary, they would experience positive changes that could lead to increases in their size, vegetation patches, and water levels. According to de la Fuente et al. (2021) the long-term spatiotemporal variability of Salar del Huasco's wetlands (in terms of the size of the wetlands) is mainly regulated by groundwater. Consequently, we estimated the changes in the total flooded area (where the water table reaches the surface within the salt flat nucleus zone) simulated by the groundwater model compared to the reference period to assess the effects of the climate change signal identified at local wells on the size of the wetlands (Figure 4-9). According to simulations from ensembles SSP2 4.5 and SSP5 8.5, the total wet surface area is projected to increase in size, stabilizing around 5.25 – 6.25 km^2 (ensemble mean ± standard deviation) by ~2080, which is also when the earliest ToEs were identified in the aquifer. This corresponds to a 10 – 12 % growth in the wet surface relative to the reference period, with wetlands and other components such as the salt crust potentially contributing to this increase. As a result, it could be posited that wetlands are to experience structural changes by the end of the century.

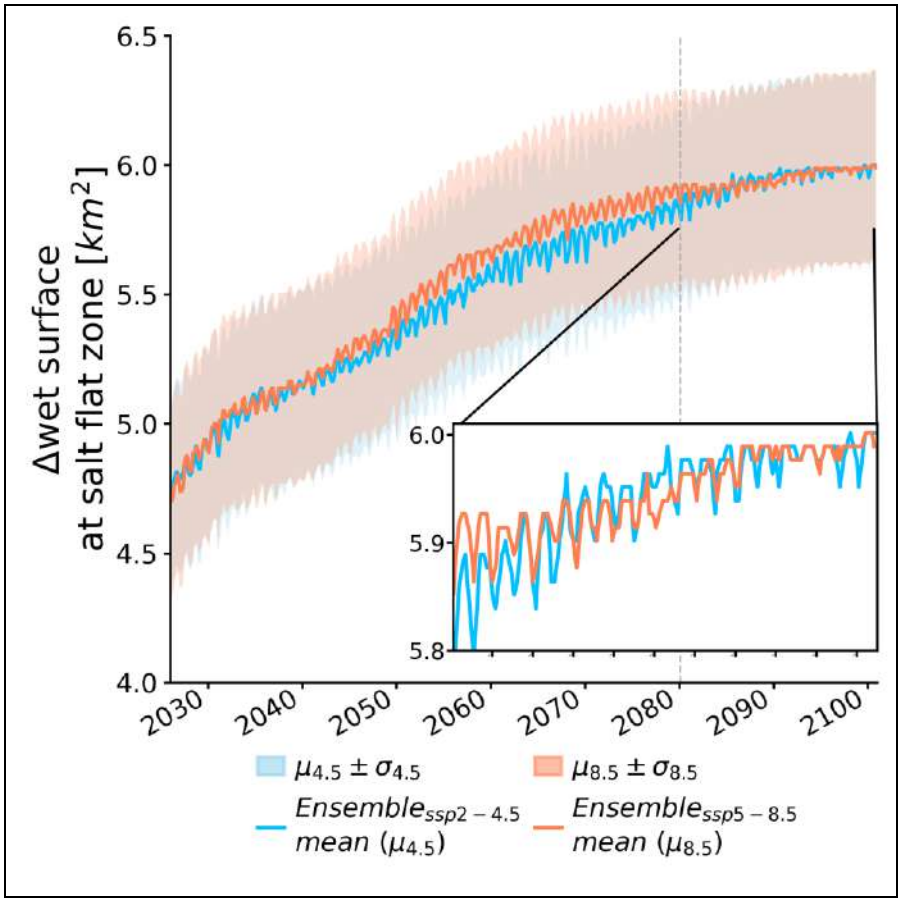

Figure 4-9: Projected change of the total flooded area within the salt flat nucleus zone. The blue dashed line represents the mean flooded area in the historical period. Flooded areas represent wetlands and lagoons.

Under warmer conditions structural changes, e.g., size increase or shrinkage, might alter the wetland's functioning, which could have far-reaching consequences that will affect ecosystems and the wetland's role in carbon and nitrogen cycles (Chen et al., 2021; House et al., 2016; Ma et al., 2022; Ren et al., 2022; Salimi et al., 2021). it has been found that in wetlands with high water tables, warmer conditions will enhance methane emissions (Chen et al., 2021; Huang et al., 2021). and can also lead to waterlogged soils, which could

decrease the amount of oxygen available for microbial decomposition, affecting the wetland's function as carbon sink (Salimi et al., 2021). However, it is still uncertain whether the future changes in wetlands will lead to positive or negative feedback to climate change. Therefore, future studies should take into account the spatiotemporal variability of the water levels into the modeling of the wetlands' dynamics to better understand of the implications of the increasing water levels in Salar del Huasco wetlands.

4.5. Conclusions

The Salar del Huasco basin is expected to undergo changes in precipitation's magnitude and seasonality throughout the year, and warming temperatures due to climate change. These changes are anticipated to affect the timing of groundwater's recharge and discharges, which are expected to occur three months earlier throughout a year. We found that during winter (May – September) recharge could increase by up to three times compared to the reference period (1980 – 2014). While recharge is likely to decrease in summer (November – March), groundwater evaporation will increase between 15% in winter, and 75% in summer. Additionally, the steadier trends observed of projected groundwater evaporation in comparison to those of recharge suggest that even though recharge remains uncertain, the aquifer's response through evaporation will likely be more consistent.

The water table is not expected to suffer major negative changes in areas where groundwater discharges to the surface. On the contrary, our results suggest that the water table could slightly rise in these areas. We found these changes to be within the background noise of natural variability until nearly 2040, year after which ToE of the climate change signal are identified. We also demonstrated that different ToE result when interannual and interdecadal are accounted in the natural variability. When only interannual variability is accounted for natural variability, the climate change signal does

not emerge, whereas it emerges nearly 60 years before the end of the century when interdecadal variability is also considered.

Overall, groundwater-dependent ecosystems in Salar del Huasco would not undergo significant change at least until ~2040. However, although higher groundwater levels may alleviate concerns about the drying out of wetlands, potential structural changes in the wetlands could have negative consequences on the environment, such as a positive climate change feedback. Further research is required to assess the implication of wetlands' structural changes induced by water levels on the environment.

Finally, as a protected area, the Salar del Huasco aquifer remains in its natural state. Therefore, our findings provide valuable insights into how groundwater in similar ecosystems may respond to climate change and guide the development of adaptation strategies.

4.6. Acknowledgments

The authors thank the Agencia Nacional de Investigación y Desarrollo (ANID) for funding grants FONDECYT/1210221 and FSEQ210018. The authors also acknowledge support from the Centro de Desarrollo Urbano Sustentable (CEDEUS – ANID/FONDAP/15110020) and the Centro de Excelencia en Geotermia de los Andes (CEGA – ANID/FONDAP/15200001).

5. CONCLUSIONS

The focal point of this dissertation was to address the overarching question: *How will climate change affect groundwater dynamics in arid regions?* To this end, the Salar del Huasco basin, in the arid Chilean Altiplano, was used as a study case. Derived from the central question, three specific research questions were developed and addressed within the preceding chapters, each focusing on a distinct aspect of groundwater dynamics and their interaction with climate change.

5.1. Distilled insights and main conclusions per research question

Chapter 2 addressed the first derived research question: ***How will climate change affect groundwater dynamics in arid regions? More specifically, what future conditions will contribute to significant variations in groundwater discharges and water levels in natural basins?*** Utilizing synthetic hybrid climate scenarios, we studied the potential impacts on the Salar del Huasco aquifer and observed its sensitivity and responses to varied extreme conditions. We discovered the aquifer adjusts to external conditions by modulating its water discharges. Groundwater evaporation emerged as the primary discharge mechanism, effectively balancing the recharge inputs. Notably, we observed that although lower projected recharge rates caused a reduction in groundwater levels, the water table around the wetlands remained stable. Consequently, the discharge to the spring became the most consistent flow from the groundwater system, demonstrating its stability. These results support **H1**, as they confirm the equilibrium between recharge and discharge fluxes.

Chapter 3 engaged with the second research question: ***Could satellite products based on energy balance models, e.g., EEFlux, contribute to improve local-scale models? How can they better support numerical groundwater modeling?*** Validation of the EEFlux

method demonstrated its ability to represent both the magnitude and seasonal variations of evaporation over the Altiplano. The monthly EEFlux-ET estimates over the Salar del Huasco ranged between 0.1 and 2.1 mm/d in winter and summer, respectively, which was consistent with previous studies in the basin. We found that simulations performed with parameters calibrated with EEFlux outperformed the original simulation by about 2% in the case of Normalized Root Square Error (NRMSE). Moreover, the use of EEFlux contributed to more accurate representations of spatiotemporal water table dynamics by facilitating the calibration of specific yield parameters in regions where evaporation occurs. These findings underscore the utility of satellite imagery as a tool for calibrating groundwater models, validating thus **H2**.

Chapter 4 tackled the third research question: ***What role does groundwater play in mitigating the effects of climate change on dependent ecosystems in arid regions? Particularly, are the wetlands of Salar del Huasco naturally resilient to climate change due to this groundwater influence, and can this resilience persist through the century?*** Unlike Chapter 1, where we used hybrid scenarios to discern the response of the groundwater system, we addressed this question by focusing on the climate change projections outlined in the CMIP6 scenarios (SSP2 4.5 and SSP5 8.5). Our analysis indicated that the expected shifts in precipitation patterns, combined with warming temperatures, will likely alter the timing of groundwater recharge and discharges, potentially advancing these events by approximately three months. This shift could result in up to a threefold increase in recharge during the winter months. Conversely, in the summer, while recharge may decrease, we predict that groundwater evaporation will increase, varying between approximately 15 – 75%. Despite these substantial changes, the water table in the vicinity of the wetlands is expected to exhibit considerable resilience, remaining relatively stable or possibly rising slightly. This suggests that these wetlands possess a natural capacity to mitigate some effects of climate change given by

groundwater. This resilience, in turn, supports the first part of **H3**, which posits that groundwater plays a mitigating role for dependent ecosystems in arid regions.

We further examined the time of emergence (ToE) of the climate change signal, taking into account both interannual and interdecadal variabilities as part of the natural variability of the Salar del Huasco. Interestingly, we found that the second part of **H3**, which predicts a decline of the groundwater's buffering capacity over the course of the century, could be either rejected or confirmed depending on the interpretation of natural variability. If only interannual variability is considered, the effects of climate change would not emerge within this century, effectively rejecting **H3**. However, if interdecadal variability is also taken into account, the climate change effects would emerge before 2040, thus confirming **H3**. Overall, we found that groundwater-dependent ecosystems in the Salar del Huasco are expected to be resilient to climate change at least until nearly 2040.

5.2. Concluding remarks and future perspectives

To summarize, this dissertation has offered an in-depth exploration into the complex relationship between groundwater dynamics and climate change in arid regions, with a focus on the Salar del Huasco basin. Our findings demonstrate the complex balancing act of groundwater systems in response to environmental fluctuations and highlighted the potential of satellite-based tools, such as EEFlux, in supporting local-scale models in remote areas. More importantly, the inherent resilience of wetland ecosystems to climate-induced changes, due to their connection with groundwater, underlines the significance of protecting these groundwater-dependent ecosystems. Through our findings, we hope to guide further research and inform policies aimed at preserving these vital ecosystems and ensuring sustainable groundwater management in the face of climate change.

Nevertheless, our research also highlights that the timing of climate change's impacts on these systems can vary significantly, subject to the interpretation of natural variability. As the effects of climate change continue to escalate, such estimates become crucial information for anticipating its ecological impacts, for which better understanding of the natural climate variability is imperative.

Additionally, the Salar del Huasco basin represents an exceptional study area as it has been largely free from direct human intervention. Its relative isolation and its status as a protected area has allowed a unique opportunity to examine the influence of climate change on groundwater dynamics without the confounding factors of anthropogenic pressures often encountered in other regions. This unique setting thereby strengthening the value of our results for understanding the pristine processes in play. However, recognizing that many similar ecosystems globally do face human-induced pressures, it would be beneficial for future studies to explore these influences alongside climate change in other settings. Hence, future studies, while leveraging the findings from the Salar del Huasco, should also consider the interplay between anthropogenic pressures and climate change in regions subject to activities like mining or agricultural expansion, to gain a more comprehensive understanding of how these factors shape groundwater dynamics. Such insights would be crucial to formulate sustainable management strategies that consider both the impending threat of climate change and human-induced challenges in various regions.

REFERENCES

Acosta, O, & Custodio, E. (2008). *Impactos ambientales de las extracciones de agua subterránea en el Salar del Huasco (norte de Chile)*. Retrieved from http://bibliotecadigital.ciren.cl/bitstream/handle/123456789/6525/HUM2-0035.pdf?sequence=1

Acosta, Orlando. (2004). *Impactos de las extracciones de agua subterránea en el Salar del Huasco (norte de Chile)*. Universidad Politéctica de Catalunya.

Adams, K. H., Reager, J. T., Rosen, P., Wiese, D. N., Farr, T. G., Rao, S., … Rodell, M. (2022). Remote Sensing of Groundwater: Current Capabilities and Future Directions. *Water Resources Research*, *58*(10), e2022WR032219. https://doi.org/https://doi.org/10.1029/2022WR032219

Aedo, S., Chadwick, C., González-Leiva, F., & Gironás, J. (2021). climQMBC a new package to Bias Correct climatic variables while preserving raw GCM changes in the mean and standarsd deviation for R, Python and MATLAB [Poster presentation]. *AGU Fall Meeting December 13-17*. New Orleans, USA.

Aghlmand, R., & Abbasi, A. (2019). Application of MODFLOW with Boundary Conditions Analyses Based on Limited Available Observations: A Case Study of Birjand Plain in East Iran. *Water 2019, Vol. 11, Page 1904*, *11*(9), 1904. https://doi.org/10.3390/W11091904

Alam, S., Gebremichael, M., Li, R., Dozier, J., & Lettenmaier, D. P. (2019). Climate change impacts on groundwater storage in the Central Valley, California. *Climatic Change*, *157*(3–4), 387–406. https://doi.org/10.1007/s10584-019-02585-5

Amanambu, A. C., Obarein, O. A., Mossa, J., Li, L., Ayeni, S. S., Balogun, O., … Ochege, F. U. (2020). *Groundwater system and climate change: Present status and future considerations*. https://doi.org/10.1016/j.jhydrol.2020.125163

Atawneh, D. Al, Cartwright, N., & Bertone, E. (2021). Climate change and its impact on the projected values of groundwater recharge: A review. *Journal of Hydrology*, *601*, 126602. https://doi.org/https://doi.org/10.1016/j.jhydrol.2021.126602

Bennett, N. D., Croke, B. F., Guariso, G., Guillaume, J. H., Hamilton, S. H., Jakeman, A. J., … Land, C. (2013). Characterising performance of environmental models q. *Environmental Modelling and Software*, *40*, 1–20. https://doi.org/10.1016/j.envsoft.2012.09.011

Bennett, T. H., & Peters, J. C. (2004). Continuous soil moisture accounting in the Hydrologic Engineering Center Hydrologic Modeling System (HEC-HMS). *Joint Conference on Water Resource Engineering and Water Resources Planning and Management 2000: Building Partnerships*, *104*. https://doi.org/10.1061/40517(2000)149

Bloomfield, J. P., Marchant, B. P., & Mckenzie, A. A. (2019). Changes in groundwater drought associated with anthropogenic warming. *Hydrol. Earth Syst. Sci*, *23*, 1393–1408. https://doi.org/10.5194/hess-23-1393-2019

Boronina, A., & Ramillien, G. (2008). Application of AVHRR imagery and GRACE measurements for calculation of actual evapotranspiration over the Quaternary aquifer (Lake Chad basin) and validation of groundwater models. *Journal of Hydrology*, *348*(1–2), 98–109. https://doi.org/10.1016/J.JHYDROL.2007.09.061

Camici, S., Brocca, L., Melone, F., & Moramarco, T. (2014). Impact of Climate Change on Flood Frequency Using Different Climate Models and Downscaling Approaches. *Journal of Hydrologic Engineering*, *19*(8), 04014002. https://doi.org/10.1061/(ASCE)HE.1943-5584.0000959

Carroll, R. W. H., Pohll, G. M., Morton, C. G., & Huntington, J. L. (2015). Calibrating a Basin-Scale Groundwater Model to Remotely Sensed Estimates of Groundwater Evapotranspiration. *JAWRA Journal of the American Water Resources Association*,

51(4), 1114–1127. https://doi.org/10.1111/JAWR.12285

Chen, H., Xu, X., Fang, C., Li, B., & Nie, M. (2021). Differences in the temperature dependence of wetland CO2 and CH4 emissions vary with water table depth. *Nature Climate Change 2021 11:9*, *11*(9), 766–771. https://doi.org/10.1038/s41558-021-01108-4

Collahuasi - GP Consultores. (2008). *Información sobre evaporación provista por Compañía Minera Doña Inés de Collahuasi. Informes inéditos.*

CONAF. (2005). *Ficha informativa de los Humedales de Ramsar (FIR)*.

Condon, L. E., Atchley, A. L., & Maxwell, R. M. (2020). Evapotranspiration depletes groundwater under warming over the contiguous United States. *Nature Communications 2020 11:1*, *11*(1), 1–8. https://doi.org/10.1038/s41467-020-14688-0

Condon, L. E., Kollet, S., Bierkens, M. F. P., Fogg, G. E., Maxwell, R. M., Hill, M. C., … Abesser, C. (2021). Global Groundwater Modeling and Monitoring: Opportunities and Challenges. *Water Resources Research*, *57*(12), e2020WR029500. https://doi.org/https://doi.org/10.1029/2020WR029500

Corenthal, L. G., Boutt, D. F., Hynek, S. A., & Munk, L. A. (2016). Regional groundwater flow and accumulation of a massive evaporite deposit at the margin of the Chilean Altiplano. *Geophysical Research Letters*, *43*(15), 8017–8025. https://doi.org/10.1002/2016GL070076

Crosbie, R. S., Dawes, W. R., Charles, S. P., Mpelasoka, F. S., Aryal, S., Barron, O., & Summerell, G. K. (2011). Differences in future recharge estimates due to GCMs, downscaling methods and hydrological models. *Geophysical Research Letters*, *38*(11), n/a-n/a. https://doi.org/10.1029/2011GL047657

Crosbie, R. S., Scanlon, B. R., Mpelasoka, F. S., Reedy, R. C., Gates, J. B., & Zhang, L. (2013). Potential climate change effects on groundwater recharge in the High Plains Aquifer, USA. *Water Resources Research*, *49*(7), 3936–3951.

https://doi.org/10.1002/wrcr.20292

Cuthbert, M., Gleeson, T., Moosdorf, N., Befus, K. M., Schneider, A., Hartmann, J., & Lehner, B. (2019). Global patterns and dynamics of climate–groundwater interactions. *Nature Climate Change*, *9*(2), 137–141. https://doi.org/10.1038/s41558-018-0386-4

Cuthbert, M., Taylor, R., Favreau, G., Todd, M., Shamsudduha, M., Villholth, K., … Kukuric, N. (2019). Observed controls on resilience of groundwater to climate variability in sub-Saharan Africa. *Nature*, *572*(7768), 230–234. https://doi.org/10.1038/s41586-019-1441-7

de la Fuente, A., & Meruane, C. (2016). *Investigación en el Salar del Huasco: Entendiendo los procesos fundamentales que mantienen a los Salares y que explican la vida en torno a estos ecosistemas altiplánicos*.

de la Fuente, A., & Meruane, C. (2017). Spectral model for long-term computation of thermodynamics and potential evaporation in shallow wetlands. *Water Resources Research*, *53*(9), 7696–7715. https://doi.org/10.1002/2017WR020515

de la Fuente, A., Meruane, C., & Suárez, F. (2021). *Long-term spatiotemporal variability in high Andean wetlands in northern Chile*. *756*, 143830. Retrieved from https://linkinghub.elsevier.com/retrieve/pii/S0048969720373617

de Silva, C. S., & Rushton, K. R. (2007). Groundwater recharge estimation using improved soil moisture balance methodology for a tropical climate with distinct dry seasons. *Hydrological Sciences Journal*, *52*(5), 1051–1067. https://doi.org/10.1623/hysj.52.5.1051

DGA. (2009). Sistema Piloto I Región: Salar del Huasco. In *Levantamieno hidrogeológico para el desarrollo de nuevas fuentes de agua en áreas prioritarias de la zona norte de Chile, Regiones XV, I, II y III*.

DGA. (2017). *Actualización del Balance Hídrico Nacional, SIT Nº 417*. Santiago, Chile.

Erler, A. R., Frey, S. K., Khader, O., d'Orgeville, M., Park, Y. J., Hwang, H. T., … Sudicky, E. A. (2019). Evaluating Climate Change Impacts on Soil Moisture and Groundwater Resources Within a Lake-Affected Region. *Water Resources Research*, *55*(10), 8142–8163. https://doi.org/10.1029/2018WR023822

Feldman, A. D. (2000). *Hydrologic modeling system HEC-HMS: technical reference manual*. US Army Corps of Engineers, Hydrologic Engineering Center.

Fowler, H. J., Blenkinsop, S., & Tebaldi, C. (2007). Linking climate change modelling to impacts studies: recent advances in downscaling techniques for hydrological modelling. *International Journal of Climatology*, *27*(12), 1547–1578. https://doi.org/10.1002/joc.1556

Froend, R. H., Horwitz, P., & Sommer, B. (2016). *Groundwater Dependent Wetlands BT - The Wetland Book: II: Distribution, Description and Conservation* (C. M. Finlayson, G. R. Milton, R. C. Prentice, & N. C. Davidson, Eds.). https://doi.org/10.1007/978-94-007-6173-5_246-1

Fu, J., Liu, J., Wang, X., Zhang, M., Chen, W., & Chen, B. (2020). Ecological risk assessment of wetland vegetation under projected climate scenarios in the Sanjiang Plain, China. *Journal of Environmental Management*, *273*, 111108. https://doi.org/10.1016/j.jenvman.2020.111108

Gallego-Sala, A. V., Charman, D. J., Brewer, S., Page, S. E., Prentice, I. C., Friedlingstein, P., … Zhao, Y. (2018). Latitudinal limits to the predicted increase of the peatland carbon sink with warming. *Nature Climate Change 2018 8:10*, *8*(10), 907–913. https://doi.org/10.1038/S41558-018-0271-1

Gardeweg, M., & Sellés, D. (2015, October). Estratigrafía y evolución estructural del área Collacagua-Rinconada, alta cordillera de Iquique, 20 00'-20 30'S–Región de Tarapacá. *XIV Congreso Geológico Chileno*.

Garreaud, R. D. (2009). The Andes climate and weather. *Advances in Geosciences*, *22*, 3–

11. https://doi.org/10.5194/adgeo-22-3-2009

Garreaud, R., Vuille, M., & Clement, A. C. (2003). The climate of the Altiplano: observed current conditions and mechanisms of past changes. *Palaeogeography, Palaeoclimatology, Palaeoecology*, *194*(1–3), 5–22. https://doi.org/10.1016/S0031-0182(03)00269-4

Garreaud, René D., Boisier, J. P., Rondanelli, R., Montecinos, A., Sepúlveda, H. H., & Veloso-Aguila, D. (2020). The Central Chile Mega Drought (2010–2018): A climate dynamics perspective. *International Journal of Climatology*, *40*(1), 421–439. https://doi.org/10.1002/joc.6219

Garreaud, René D., Vuille, M., Compagnucci, R., & Marengo, J. (2009). Present-day South American climate. *Palaeogeography, Palaeoclimatology, Palaeoecology*, *281*(3–4), 180–195. https://doi.org/10.1016/j.palaeo.2007.10.032

Goderniaux, P., Brouyère, S., Wildemeersch, S., Therrien, R., & Dassargues, A. (2015). Uncertainty of climate change impact on groundwater reserves - Application to a chalk aquifer. *Journal of Hydrology*, *528*, 108–121. https://doi.org/10.1016/j.jhydrol.2015.06.018

Green, T., Taniguchi, M., Kooi, H., Gurdak, J., … D. A.-J. of, & 2011, U. (2011). Beneath the surface of global change: Impacts of climate change on groundwater. *Elsevier*. Retrieved from https://www.sciencedirect.com/science/article/pii/S0022169411002988

Hamlet, A., Salathé, E., & Carrasco, P. (2010). *Statistical downscaling techniques for global climate model simulations of temperature and precipitation with application to water resources planning studies*. Retrieved from https://digital.lib.washington.edu/researchworks/bitstream/handle/1773/38428/2010-5.pdf?sequence=1

Harbaugh, A., Banta, E., Hill, M., & McDonald, M. (2000). MODFLOW-2000, The US

Geological Survey Modular Ground-Water Model-User Guide to Modularization Concepts and the Ground-Water Flow Process. In *Open-file Report 00-92. wipp.energy.gov*. Retrieved from http://wipp.energy.gov/library/CRA/2009_CRA/references/Others/Harbaugh_Banta_Hill_and_McDonald_2000_MODFLOW_2000_Open_File_Report_00_92.pdf

Hartmann, A., Gleeson, T., Wada, Y., & Wagener, T. (2017). Enhanced groundwater recharge rates and altered recharge sensitivity to climate variability through subsurface heterogeneity. *Proceedings of the National Academy of Sciences of the United States of America*, *114*(11), 2842–2847. https://doi.org/10.1073/pnas.1614941114

Hashemi, H., Uvo, C. B., & Berndtsson, R. (2015). Coupled modeling approach to assess climate change impacts on groundwater recharge and adaptation in arid areas. *Hydrol. Earth Syst. Sci*, *19*, 4165–4181. https://doi.org/10.5194/hess-19-4165-2015

Hausner, M. B., Wilson, K. P., Gaines, D. B., Suárez, F., Scoppettone, G. G., & Tyler, S. W. (2014). Life in a fishbowl: Prospects for the endangered Devils Hole pupfish (*Cyprinodon diabolis*) in a changing climate. *Water Resources Research*, *50*(8), 7020–7034. https://doi.org/10.1002/2014WR015511

Hausner, M. B., Wilson, K. P., Gaines, D. B., Suárez, F., Scoppettone, G. G., & Tyler, S. W. (2016). Projecting the effects of climate change and water management on Devils Hole pupfish (Cyprinodon diabolis) survival. *Ecohydrology*, *9*(4), 560–573. https://doi.org/10.1002/eco.1656

Hernández-López, M. F., Gironás, J., Braud, I., Suárez, F., & Muñoz, J. F. (2014). Assessment of evaporation and water fluxes in a column of dry saline soil subject to different water table levels. *Hydrological Processes*, *28*(10), 3655–3669.

Herrera, C., Custodio, E., Chong, G., Lambán, L. J., Riquelme, R., Wilke, H., … Lictevout, E. (2016). Groundwater flow in a closed basin with a saline shallow lake in

a volcanic area: Laguna Tuyajto, northern Chilean Altiplano of the Andes. *Science of the Total Environment*, *541*, 303–318. https://doi.org/10.1016/j.scitotenv.2015.09.060

Herrera, C., Gamboa, C., Custodio, E., Jordan, T., Godfrey, L., Jódar, J., … Sáez, A. (2018). Groundwater origin and recharge in the hyperarid Cordillera de la Costa, Atacama Desert, northern Chile. *Science of the Total Environment*, *624*, 114–132. https://doi.org/10.1016/j.scitotenv.2017.12.134

Herrera, C., Godfrey, L., Urrutia, J., Custodio, E., Jordan, T., Jódar, J., … Barrenechea, F. (2021). Recharge and residence times of groundwater in hyper arid areas: The confined aquifer of Calama, Loa River Basin, Atacama Desert, Chile. *Science of the Total Environment*, *752*, 141847. https://doi.org/10.1016/j.scitotenv.2020.141847

Holman, I. P. (2006). Climate change impacts on groundwater recharge-uncertainty, shortcomings, and the way forward? *Hydrogeology Journal*, *14*(5), 637–647. https://doi.org/10.1007/s10040-005-0467-0

House, A. R., Thompson, J. R., & Acreman, M. C. (2016). Projecting impacts of climate change on hydrological conditions and biotic responses in a chalk valley riparian wetland. *Journal of Hydrology*, *534*, 178–192. https://doi.org/10.1016/J.JHYDROL.2016.01.004

Huang, J., Yu, H., Guan, X., Wang, G., Change, R. G.-N. C., & 2016, U. (2015). Accelerated dryland expansion under climate change. *Nature*. Retrieved from https://www.nature.com/articles/nclimate2837

Huang, Y., Ciais, P., Luo, Y., Zhu, D., Wang, Y., Qiu, C., … Qu, L. (2021). Tradeoff of CO2 and CH4 emissions from global peatlands under water-table drawdown. *Nature Climate Change 2021 11:7*, *11*(7), 618–622. https://doi.org/10.1038/S41558-021-01059-W

Hydrologic Engineering Center (US). (2001). *The Hydrologic Modeling System (HEC-HMS)*.

IPCC. (2014). IPCC, 2014: climate change 2014:synthesis report. Contribution of Working Groups I. II and III to the Fifth Assessment Report of intergovernmental panel on Climate Change. In *Team, Core Writing Pachauri, Rajendra K. Meyer, L. A.* Geneva, Switzerland.

Johnson, E., Yáñez, J., Ortiz, C., & Muñoz, J. (2010). Evaporation from shallow groundwater in closed basins in the Chilean *Altiplano*. *Hydrological Sciences Journal*, *55*(4), 624–635. https://doi.org/10.1080/02626661003780458

Jyrkama, M. I., & Sykes, J. F. (2007). The impact of climate change on spatially varying groundwater recharge in the grand river watershed (Ontario). *Journal of Hydrology*, *338*(3–4), 237–250. https://doi.org/10.1016/j.jhydrol.2007.02.036

Kløve, B., Ala-Aho, P., Bertrand, G., Gurdak, J. J., Kupfersberger, H., Kværner, J., … Pulido-Velazquez, M. (2014). Climate change impacts on groundwater and dependent ecosystems. *Journal of Hydrology*, *518*(PB), 250–266. https://doi.org/10.1016/J.JHYDROL.2013.06.037

Koutroulis, A. G. (2019). Dryland changes under different levels of global warming. *Science of the Total Environment*, *655*, 482–511. https://doi.org/10.1016/j.scitotenv.2018.11.215

Kovalevskii, V. S. (2007). Effect of Climate Changes on Groundwater. *Water Resources*, *34*(2), 140–152. https://doi.org/10.1134/S0097807807020042

Li, H. T., Brunner, P., Kinzelbach, W., Li, W. P., & Dong, X. G. (2009). Calibration of a groundwater model using pattern information from remote sensing data. *Journal of Hydrology*, *377*(1–2), 120–130. https://doi.org/10.1016/J.JHYDROL.2009.08.012

Lobos-Roco, F., Hartogensis, O., Suárez, F., Huerta-Viso, A., Benedict, I., de la Fuente, A., & Vilà-Guerau de Arellano, J. (2022). Multi-scale temporal analysis of evaporation on a saline lake in the Atacama Desert. *Hydrology and Earth System Sciences*, *26*(13), 3709–3729. https://doi.org/10.5194/HESS-26-3709-2022

Lobos-Roco, F., Hartogensis, O., Vilà-Guerau de Arellano, J., de la Fuente, A., Muñoz, R., Rutllant, J., & Suárez, F. (2021). Local evaporation controlled by regional atmospheric circulation in the Altiplano of the Atacama Desert. *Atmospheric Chemistry and Physics Discussions*, 1–38. https://doi.org/10.5194/acp-2020-1300

Ma, L., Zhu, G., Chen, B., Zhang, K., Niu, S., Wang, J., … Zuo, H. (2022). A globally robust relationship between water table decline, subsidence rate, and carbon release from peatlands. *Communications Earth & Environment 2022 3:1*, *3*(1), 1–14. https://doi.org/10.1038/s43247-022-00590-8

Mao, D., Tian, Y., Wang, Z., Jia, M., Du, J., & Song, C. (2020). Wetland changes in the Amur River Basin: Differing trends and proximate causes on the Chinese and Russian sides. *Journal of Environmental Management*, 111670. https://doi.org/10.1016/j.jenvman.2020.111670

Marazuela, M. A. A., Vázquez-Suñé, E., Ayora, C., García-Gil, A., & Palma, T. (2019). *The effect of brine pumping on the natural hydrodynamics of the Salar de Atacama: The damping capacity of salt flats*. *654*, 1118–1131. Retrieved from https://www.sciencedirect.com/science/article/pii/S0048969718345522

Marazuela, M. A., Vázquez-Suñé, E., Ayora, C., & García-Gil, A. (2020). Towards more sustainable brine extraction in salt flats: Learning from the Salar de Atacama. *Science of the Total Environment*, *703*, 135605. https://doi.org/10.1016/j.scitotenv.2019.135605

Marazuela, M. A., Vázquez-Suñé, E., Ayora, C., García-Gil, A., & Palma, T. (2019). Hydrodynamics of salt flat basins: The Salar de Atacama example. *Science of The Total Environment*, *651*, 668–683. https://doi.org/10.1016/J.SCITOTENV.2018.09.190

Marchionni, V., Daly, E., Manoli, G., Tapper, N. J., Walker, J. P., & Fatichi, S. (2020). Groundwater Buffers Drought Effects and Climate Variability in Urban Reserves.

Water Resources Research, *56*(5), e2019WR026192. https://doi.org/https://doi.org/10.1029/2019WR026192

McDonough, L. K., Santos, I. R., Andersen, M. S., O'Carroll, D. M., Rutlidge, H., Meredith, K., … Baker, A. (2020). Changes in global groundwater organic carbon driven by climate change and urbanization. *Nature Communications 2020 11:1*, *11*(1), 1–10. https://doi.org/10.1038/s41467-020-14946-1

McKenna, O. P., & Sala, O. E. (2018). Groundwater recharge in desert playas: current rates and future effects of climate change. *Environmental Research Letters*, *13*(1), 014025. https://doi.org/10.1088/1748-9326/aa9eb6

Mitsch, W. J., Bernal, B., Nahlik, A. M., Mander, Ü., Zhang, L., Anderson, C. J., … Brix, H. (2013). Wetlands, carbon, and climate change. *Landscape Ecology*, *28*(4), 583–597. https://doi.org/10.1007/s10980-012-9758-8

Moomaw, W. R., Chmura, G. L., Davies, G. T., Finlayson, C. M., Middleton, B. A., Natali, S. M., … Sutton-Grier, A. E. (2018). Wetlands In a Changing Climate: Science, Policy and Management. *Wetlands 2018 38:2*, *38*(2), 183–205. https://doi.org/10.1007/S13157-018-1023-8

Mosre, J., & Suárez, F. (2021). Actual Evapotranspiration Estimates in Arid Cold Regions Using Machine Learning Algorithms with In Situ and Remote Sensing Data. *Water*, *13*(6), 870. https://doi.org/10.3390/w13060870

Mu, S., Li, B., Yao, J., Yang, G., Wan, R., & Xu, X. (2020). Monitoring the spatio-temporal dynamics of the wetland vegetation in Poyang Lake by Landsat and MODIS observations. *Science of the Total Environment*, *725*, 138096. https://doi.org/10.1016/j.scitotenv.2020.138096

Nkhonjera, G. K., & Dinka, M. O. (2017). *Significance of direct and indirect impacts of climate change on groundwater resources in the Olifants River basin: A review*. https://doi.org/10.1016/j.gloplacha.2017.09.011

Paquis, P., Hengst, M. B., Florez, J. Z., Tapia, J., Molina, V., Pérez, V., & Pardo-Esté, C. (2023). Short-term characterisation of climatic-environmental variables and microbial community diversity in a high-altitude Andean wetland (Salar de Huasco, Chile). *Science of The Total Environment*, *859*, 160291. https://doi.org/10.1016/J.SCITOTENV.2022.160291

Peng, K., Jiang, W., Deng, Y., Liu, Y., Wu, Z., & Chen, Z. (2020). Simulating wetland changes under different scenarios based on integrating the random forest and CLUE-S models: A case study of Wuhan Urban Agglomeration. *Ecological Indicators*, *117*, 106671. https://doi.org/10.1016/j.ecolind.2020.106671

Persaud, E., Levison, J., MacRitchie, S., Berg, S. J., Erler, A. R., Parker, B., & Sudicky, E. (2020). Integrated modelling to assess climate change impacts on groundwater and surface water in the Great Lakes Basin using diverse climate forcing. *Journal of Hydrology*, *584*, 124682. Retrieved from https://linkinghub.elsevier.com/retrieve/pii/S0022169420301426

Post, V. E. A., Galvis, S. C., Sinclair, P. J., & Werner, A. D. (2019). Evaluation of management scenarios for potable water supply using script-based numerical groundwater models of a freshwater lens. *Journal of Hydrology*, *571*, 843–855. https://doi.org/10.1016/J.JHYDROL.2019.02.024

Prăvălie, R. (2016). *Invited review Drylands extent and environmental issues. A global approach*. https://doi.org/10.1016/j.earscirev.2016.08.003

Prăvălie, R., Bandoc, G., Patriche, C., & Sternberg, T. (2019). Recent changes in global drylands: Evidences from two major aridity databases. *Catena*, *178*, 209–231. https://doi.org/10.1016/j.catena.2019.03.016

Rabemaharitra, T. P., Zou, Y., Yi, Z., He, Y., & Khan, U. (2022). Optimized Pilot Point Emplacement Based Groundwater Flow Calibration Method for Heterogeneous Small-Scale Area. *Applied Sciences 2022, Vol. 12, Page 4648*, *12*(9), 4648.

https://doi.org/10.3390/APP12094648

Reclamation. (2014). *Downscaled CMIP3 and CMIP5 Hydrology Projections Release of Hydrology Projections, Comparison with Preceding Information, and Summary of User Needs Bureau of Reclamation Climate Analytics Group Climate Central*. Retrieved from http://gdo-dcp.ucllnl.org/downscaled_cmip_projections/.

Risacher, F., Alonso, H., & Salazar, C. (1999). *Geoquímica de aguas en cuencas cerradas: I, II y III regiones-Chile*.

Rivera, J. A., Arnould, G., & Leal, R. (2020). *Evaluation of the ability of CMIP6 models to simulate precipitation over Southwestern South America: Climatic features and long-term trends (1901-2014)*. https://doi.org/10.1016/j.atmosres.2020.104953

Rossman, N. R., Zlotnik, V. A., & Rowe, C. M. (2018). Using cumulative potential recharge for selection of GCM projections to force regional groundwater models: A Nebraska Sand Hills example. *Journal of Hydrology*, *561*, 1105–1114. https://doi.org/10.1016/j.jhydrol.2017.09.019

Sáez, A., Godfrey, L. V., Herrera, C., Chong, G., & Pueyo, J. J. (2016). Timing of wet episodes in Atacama Desert over the last 15 ka. The Groundwater Discharge Deposits (GWD) from Domeyko Range at 25°S. *Quaternary Science Reviews*, *145*, 82–93. https://doi.org/10.1016/j.quascirev.2016.05.036

Salimi, S., Almuktar, S. A. A. A. N., & Scholz, M. (2021). Impact of climate change on wetland ecosystems: A critical review of experimental wetlands. *Journal of Environmental Management*, *286*, 112160. https://doi.org/10.1016/J.JENVMAN.2021.112160

Samuel, A., Blin, N., Muñoz, J. F., & Suárez, F. (2020). An unsaturated/saturated coupled hydrogeological model for the llamara salt flat, Chile, to investigate prosopis tamarugo survival. *Geosciences (Switzerland)*, *10*(1). https://doi.org/10.3390/geosciences10010001

Sandi, S. G., Rodriguez, J. F., Saintilan, N., Wen, L., Kuczera, G., Riccardi, G., & Saco, P. M. (2020). Resilience to drought of dryland wetlands threatened by climate change. *Scientific Reports*, *10*(1), 13232. https://doi.org/10.1038/s41598-020-70087-x

Scanlon, B. R., Fakhreddine, S., Rateb, A., de Graaf, I., Famiglietti, J., Gleeson, T., … Zheng, C. (2023). Global water resources and the role of groundwater in a resilient water future. *Nature Reviews Earth & Environment*, *4*(2), 87–101. https://doi.org/10.1038/s43017-022-00378-6

Scanlon, B. R., Healy, R. W., & Cook, P. G. (2002). Choosing appropriate technique for quantifying groundwater recharge. *Hydrogeology Journal*, *10*, 18–39. https://doi.org/10.1007/s10040-0010176-2

Scanlon, B. R., Keese, K. E., Flint, A. L., Flint, L. E., Gaye, C. B., Edmunds, W. M., & Simmers, I. (2006). Global synthesis of groundwater recharge in semiarid and arid regions. *Hydrological Processes*, *20*(March), 3335–3370. https://doi.org/10.1002/hyp

Scheihing, K., & Tröger, U. (2018). Local climate change induced by groundwater overexploitation in a high Andean arid watershed, Laguna Lagunillas basin, northern Chile. *Hydrogeology Journal*, *26*(3), 705–719. https://doi.org/10.1007/s10040-017-1647-4

Scheihing, K. W., Moya, C. E., & Tröger, U. (2017). Insights into Andean slope hydrology: reservoir characteristics of the thermal Pica spring system, Pampa del Tamarugal, northern Chile. *Hydrogeology Journal*, *25*(6), 1833–1852. https://doi.org/10.1007/s10040-017-1533-0

Scibek, J., Allen, D., Cannon, A., & Whitfield, P. (2007). Groundwater–surface water interaction under scenarios of climate change using a high-resolution transient groundwater model. *Journal of Hydrology*. Retrieved from https://www.sciencedirect.com/science/article/pii/S0022169406004069

Scibek, J., & Allen, D. M. (2006). Modeled impacts of predicted climate change on

recharge and groundwater levels. *Water Resources Research*, *42*(11). https://doi.org/10.1029/2005WR004742

SEA. (2019). *"Desarrollo de Infraestructura y Mejoramiento de Capacidad Productiva de Collahuasi" ADENDA. Elaborado por: SGA*.

SEA, S. (2012). *Guía para el uso de modelos de aguas subterráneas en el SEIA*.

Shanafield, M., Cook, P. G., Gutiérrez-Jurado, H. A., Faux, R., Cleverly, J., & Eamus, D. (2015). Field comparison of methods for estimating groundwater discharge by evaporation and evapotranspiration in an arid-zone playa. *Journal of Hydrology*, *527*, 1073–1083. https://doi.org/10.1016/j.jhydrol.2015.06.003

Sheffield, J., Wood, E. F., Pan, M., Beck, H., Coccia, G., Serrat-Capdevila, A., & Verbist, K. (2018, December 1). Satellite Remote Sensing for Water Resources Management: Potential for Supporting Sustainable Development in Data-Poor Regions. *Water Resources Research*, Vol. 54, pp. 9724–9758. https://doi.org/10.1029/2017WR022437

Shen, G., Yang, X., Jin, Y., Xu, B., & Zhou, Q. (2019). Remote sensing and evaluation of the wetland ecological degradation process of the Zoige Plateau Wetland in China. *Ecological Indicators*, *104*, 48–58. https://doi.org/10.1016/j.ecolind.2019.04.063

Shen, M., Chen, J., Zhuan, M., Chen, H., Xu, C. Y., & Xiong, L. (2018). Estimating uncertainty and its temporal variation related to global climate models in quantifying climate change impacts on hydrology. *Journal of Hydrology*, *556*, 10–24. https://doi.org/10.1016/j.jhydrol.2017.11.004

Smith, W. K., Dannenberg, M. P., Yan, D., Herrmann, S., Barnes, M. L., Barron-Gafford, G. A., … Yang, J. (2019). Remote sensing of dryland ecosystem structure and function: Progress, challenges, and opportunities. *Remote Sensing of Environment*, *233*, 111401. https://doi.org/10.1016/J.RSE.2019.111401

Somers, L. D., McKenzie, J. M., Mark, B. G., Lagos, P., Ng, G. H. C., Wickert, A. D., …

Silva, Y. (2019). Groundwater Buffers Decreasing Glacier Melt in an Andean Watershed—But Not Forever. *Geophysical Research Letters, 46*(22), 13016–13026. https://doi.org/10.1029/2019GL084730

Souvignet, M., Oyarzún, R., Verbist, K. M. J., Gaese, H., & Heinrich, J. (2012). Hydro-meteorological trends in semi-arid north-central Chile (29-32°S): Water resources implications for a fragile Andean region. *Hydrological Sciences Journal*, *57*(3), 479–495. https://doi.org/10.1080/02626667.2012.665607

Stirling, E., Fitzpatrick, R. W., & Mosley, L. M. (2020). *Drought effects on wet soils in inland wetlands and peatlands*. https://doi.org/10.1016/j.earscirev.2020.103387

Stocker, T. (2014). *Climate change 2013: the physical science basis: Working Group I contribution to the Fifth assessment report of the Intergovernmental Panel on Climate Change*. Cambridge university press.

Suárez, F., Lobos, F., de la Fuente, A., Vilà-Guerau de Arellano, J., Prieto, A., Meruane, C., & Hartogensis, O. (2020). E-DATA: A Comprehensive Field Campaign to Investigate Evaporation Enhanced by Advection in the Hyper-Arid Altiplano. *Water*, *12*(3), 745. https://doi.org/10.3390/w12030745

Sun, A. Y., Green, R., Swenson, S., & Rodell, M. (2012). Toward calibration of regional groundwater models using GRACE data. *Journal of Hydrology*, *422–423*, 1–9. https://doi.org/10.1016/J.JHYDROL.2011.10.025

Sun, W., Fan, J., Wang, G., Ishidaira, H., Bastola, S., Yu, J., … Xu, Z. (2018). Calibrating a hydrological model in a regional river of the Qinghai–Tibet plateau using river water width determined from high spatial resolution satellite images. *Remote Sensing of Environment*, *214*, 100–114. https://doi.org/10.1016/J.RSE.2018.05.020

Sutanudjaja, E. H., Van Beek, L. P. H., De Jong, S. M., Van Geer, F. C., & Bierkens, M. F. P. (2014). Calibrating a large-extent high-resolution coupled groundwater-land surface model using soil moisture and discharge data. *Water Resources Research*,

50(1), 687–705. https://doi.org/10.1002/2013WR013807

Taheri Tizro, A., Fryar, A. E., Pour, M. K., Voudouris, K. S., & Mashhadian, M. J. (2019). Groundwater conditions related to climate change in the semi-arid area of western Iran. *Groundwater for Sustainable Development*, *9*, 100273. https://doi.org/10.1016/j.gsd.2019.100273

Tapia, J., Schneider, B., Inostroza, M., Álvarez-Amado, F., Luque, J. A., Aguilera, F., … Bravo, M. (2020). Naturally elevated arsenic in the Altiplano-Puna, Chile and the link to recent (Mio-Pliocene to Quaternary) volcanic activity, high crustal thicknesses, and geological structures. *Journal of South American Earth Sciences*, 102905. https://doi.org/10.1016/j.jsames.2020.102905

Taylor, K. E., Stouffer, R. J., & Meehl, G. A. (2012, April 1). An overview of CMIP5 and the experiment design. *Bulletin of the American Meteorological Society*, Vol. 93, pp. 485–498. https://doi.org/10.1175/BAMS-D-11-00094.1

Taylor, R. G., Scanlon, B., Döll, P., Rodell, M., van Beek, R., Wada, Y., … Treidel, H. (2013). Ground water and climate change. *Nature Climate Change*, *3*(4), 322–329. https://doi.org/10.1038/nclimate1744

Tillman, F. D., Gangopadhyay, S., & Pruitt, T. (2016). Changes in groundwater recharge under projected climate in the upper Colorado River basin. *Geophysical Research Letters*, *43*(13), 6968–6974. https://doi.org/10.1002/2016GL069714

Tohver, I., & Hamlet, A. (2014). Impacts of 21st-century climate change on hydrologic extremes in the Pacific Northwest region of North America. *Wiley Online Library*. Retrieved from https://onlinelibrary.wiley.com/doi/abs/10.1111/jawr.12199

Torres-Batlló, J., & Martí-Cardona, B. (2020). Precipitation trends over the southern Andean Altiplano from 1981 to 2018. *Journal of Hydrology*, *590*, 125485. https://doi.org/10.1016/j.jhydrol.2020.125485

Uribe, J. (2012). *Estimación de la recarga del acuífero del Salar del Huasco en base a un*

modelo de precipitación-escorrentía y una caracterización isotópica. Pontificia Universidad Católica de Chile.

Uribe, J., Muñoz, J. F., Gironás, J., Oyarzún, R., Aguirre, E., & Aravena, R. (2015). Assessing groundwater recharge in an Andean closed basin using isotopic characterization and a rainfall-runoff model: Salar del Huasco basin, Chile. *Hydrogeology Journal*, *23*(7), 1535–1551. https://doi.org/10.1007/s10040-015-1300-z

Urrutia, J., Herrera, C., Custodio, E., Jódar, J., & Medina, A. (2019). Groundwater recharge and hydrodynamics of complex volcanic aquifers with a shallow saline lake: Laguna Tuyajto, Andean Cordillera of northern Chile. *Science of the Total Environment*, *697*, 134116. https://doi.org/10.1016/j.scitotenv.2019.134116

Urrutia, R., & Vuille, M. (2009). Climate change projections for the tropical Andes using a regional climate model: Temperature and precipitation simulations for the end of the 21st century. *Journal of Geophysical Research: Atmospheres*, *114*(D2).

Usman, M., Qamar, M. U., Becker, R., Zaman, M., Conrad, C., & Salim, S. (2020). Numerical modelling and remote sensing based approaches for investigating groundwater dynamics under changing land-use and climate in the agricultural region of Pakistan. *Journal of Hydrology*, *581*, 124408. https://doi.org/10.1016/j.jhydrol.2019.124408

Velis, M., Conti, K. I., & Biermann, F. (2017). Groundwater and human development: synergies and trade-offs within the context of the sustainable development goals. *Sustainability Science*, *12*(6), 1007–1017. https://doi.org/10.1007/s11625-017-0490-9

Viguier, B., Daniele, L., Jourde, H., Leonardi, V., & Yáñez, G. (2019, October 1). Changes in the conceptual model of the Pampa del Tamarugal Aquifer: Implications for Central Depression water resources. *Journal of South American Earth Sciences*, Vol. 94, p. 102217. https://doi.org/10.1016/j.jsames.2019.102217

Viguier, B., Jourde, H., Leonardi, V., Daniele, L., Batiot-Guilhe, C., Favreau, G., & De

Montety, V. (2019). Water table variations in the hyperarid Atacama Desert: Role of the increasing groundwater extraction in the pampa del tamarugal (Northern Chile). *Journal of Arid Environments*, *168*, 9–16. https://doi.org/https://doi.org/10.1016/j.jaridenv.2019.05.007

Vormoor, K., & Skaugen, T. (2013). Temporal Disaggregation of Daily Temperature and Precipitation Grid Data for Norway. *Journal of Hydrometeorology*, *14*(3), 989–999. https://doi.org/10.1175/JHM-D-12-0139.1

Vuille, M., Francou, B., Wagnon, P., Juen, I., Kaser, G., Mark, B. G., & Bradley, R. S. (2008). Climate change and tropical Andean glaciers: Past, present and future. *Earth-Science Reviews*, *89*(3–4), 79–96.

Weise, K., Höfer, R., Franke, J., Guelmami, A., Simonson, W., Muro, J., … Hilarides, L. (2020, September 15). Wetland extent tools for SDG 6.6.1 reporting from the Satellite-based Wetland Observation Service (SWOS). *Remote Sensing of Environment*, Vol. 247, p. 111892. https://doi.org/10.1016/j.rse.2020.111892

Wilby, R. L., Wigley, T. M. L., Conway, D., Jones, P. D., Hewitson, B. C., Main, J., & Wilks, D. S. (1998). Statistical downscaling of general circulation model output: A comparison of methods. *Water Resources Research*, *34*(11), 2995–3008. https://doi.org/10.1029/98WR02577

Winston, R. B. (2009). *ModelMuse: a graphical user interface for MODFLOW-2005 and PHAST*.

Wood, A. W., Maurer, E. P., Kumar, A., & Lettenmaier, D. P. (2002). *Long-range experimental hydrologic forecasting for the eastern United States*. *107*, ACL 6-1. https://doi.org/10.1029/2001JD000659

Wu, H. bing, & Zheng, B. hui. (2020). Wetland area identification and waterbird protection management in consideration of lake topography and water level change. *Global Ecology and Conservation*, *23*, e01056.

https://doi.org/10.1016/j.gecco.2020.e01056

Xie, Y., Cook, P. G., Simmons, C. T., Partington, D., Crosbie, R., & Batelaan, O. (2018). Uncertainty of groundwater recharge estimated from a water and energy balance model. *Journal of Hydrology*, *561*, 1081–1093. https://doi.org/10.1016/j.jhydrol.2017.08.010

Xu, W., & Su, X. (2019). Challenges and impacts of climate change and human activities on groundwater-dependent ecosystems in arid areas – A case study of the Nalenggele alluvial fan in NW China. *Journal of Hydrology*, *573*, 376–385. https://doi.org/10.1016/j.jhydrol.2019.03.082

Yao, Y., Tian, Y., Andrews, C., Li, X., Zheng, Y., & Zheng, C. (2018). Role of Groundwater in the Dryland Ecohydrological System: A Case Study of the Heihe River Basin. *Journal of Geophysical Research: Atmospheres*, *123*(13), 6760–6776. https://doi.org/https://doi.org/10.1029/2018JD028432

Zamani Losgedaragh, S., & Rahimzadegan, M. (2018). Evaluation of SEBS, SEBAL, and METRIC models in estimation of the evaporation from the freshwater lakes (Case study: Amirkabir dam, Iran). *Journal of Hydrology*, *561*, 523–531. https://doi.org/10.1016/J.JHYDROL.2018.04.025

Zhang, H., Wang, B., Liu, D. L., Zhang, M., Feng, P., Cheng, L., … Eamus, D. (2019). Impacts of future climate change on water resource availability of eastern Australia: A case study of the Manning River basin. *Journal of Hydrology*, *573*, 49–59. https://doi.org/10.1016/j.jhydrol.2019.03.067

Zhu, J., Wang, X., Zhang, Q., Zhang, Y., Liu, D., Cai, A., & Zhang, X. (2020). Assessing wetland sustainability by modeling water table dynamics under climate change. *Journal of Cleaner Production*, *263*, 121293. https://doi.org/10.1016/J.JCLEPRO.2020.121293

APPENDICES

APPENDIX A: ASSESSING POTENTIAL IMPACTS OF CLIMATE CHANGE ON WATER RESOURCES AND THEIR INTERACTION WITHIN THE GREAT LAKES REGION: THE POTENTIAL BUFFERING CAPACITY OF GROUNDWATER ON SURFACE WATER PROCESSES

Nicole Blin, Jenny Soonthornrangsan, Christopher Lowry, Jorge Gironás, Cristián Chadwick, Francisco Suárez

To be submitted to: Hydrological processes

Abstract

Management of water resources, including evaluating potential impacts of climate change in water-rich regions such as the Great Lakes, is critical for long-term sustainability. In Western New York (WNY), stream and groundwater discharges to Lake Erie and Ontario are major components of the lakes' water balance. The aim of this research is to assess the hydrological response of the WNY basin under climate change to provide useful insight to aid stakeholders and policymakers in developing adaptation strategies. To represent the uncertainty of future projections, ensembles of scenarios SSP2 4.5 and SSP5 8.5 were used to drive a coupled Groundwater and Surface-water FLOW (GSFLOW) model of WNY. Our results show variability in projected precipitation across ensemble members. Future warming conditions will increase evaporation rates in WNY under both scenarios, affecting processes at the soil and unsaturated zones. However, groundwater is expected to be less sensitive to climatic changes, acting as a buffer to impacts on surface water and stream discharges to the Great Lakes if future recharge increases by ~15% in SSP2 4.5 and between ~32 – 37% in SSP5 8.5. Consequently, groundwater could sustain discharges to the Great Lakes. Nevertheless, if precipitation increases below ~ 27% and ~80% in the respective the resulting recharge will not be enough to sustain groundwater storage, limiting thus the buffering capacity of the aquifer.

Keywords: CMIP6, climate change, Great Lakes, Western New York aquifer, GSFLOW, groundwater – surface water interaction

A 1. Introduction

Groundwater is essential for the survival of human and natural systems as it provides half of the world's potable water (Amanambu et al., 2020). In the United States, groundwater provides up to 40% of the total freshwater supply (Sutton et al., 2021), which is becoming increasingly limited, not only in arid regions but also in humid areas where precipitation is abundant (Sweet et al., 2017). In humid and arid regions, climate change is impacting surface water and groundwater due to changes in precipitation rates and warming temperatures (Aygün et al., 2019; Dubois et al., 2022). Projected changes in seasonal temperature as well as changes in the timing, magnitude, and distribution of precipitation may lead to important water cycle modifications (Meixner et al., 2016; Persaud et al., 2020; Tabari, 2020). Moreover, in a warming climate, increased evapotranspiration may shift recharge patterns, which in the long-term could change groundwater levels, and subsequently, groundwater-surface water interactions and soil moisture (Cherkauer & Sinha, 2010; Condon et al., 2020; Meixner et al., 2016; Portmann et al., 2013). Consequently, potential changes at the surface will likely impact groundwater-dependent ecosystems and groundwater use for human consumption, industry, and agriculture (Dubois et al., 2022).

The Great Lakes account for 18% of the world's and 90% of the United States' freshwater supply (Cherkauer & Sinha, 2010; Kayastha et al., 2022; Niu et al., 2014). Although abundant with freshwater, the Great Lakes are not excluded from the stresses being imposed upon global water resources, and are expected to be affected by climate change (Gronewold et al., 2016a; Seglenieks & Temgoua, 2022; Soonthornrangsan & Lowry, 2021; Xu et al., 2021). Understanding changes in water budget components and storage is

key for assessing the resilience of watersheds under climate change (Niu et al., 2014; Tague et al., 2008). This is particularly crucial in the Great Lakes Basin (GLB) as it is heavily invested in agricultural production that adds strain on water resources (Cherkauer & Sinha, 2010; Persaud et al., 2020). Approximately 4100 km3 are stored in aquifers in the U.S. side of the GLB (Costa et al., 2021), and accordingly, groundwater not only plays a key role in maintaining its water quality and ecological environment, but it is also a major component of the GLB water budget either through direct discharges or indirectly as stream baseflow (Grannemann, 2000). Increasing water demands are overburdening regional groundwater supplies, in some cases reversing groundwater flows that previously recharged the Great Lakes (Cherkauer & Sinha, 2010). Considering the importance of groundwater resources in the water balance of the GLB, studying their sensitivity to climate change becomes crucial for predicting impacts on its water resources and evaluating the resiliency of the basin. This becomes more pressing as changes in the magnitude of extreme climatic events and lake levels have already been observed, and even more pronounced changes have been predicted (Gronewold et al., 2016a; Kayastha et al., 2022; Seglenieks & Temgoua, 2022; Xu et al., 2021).

Climate change impacts on water resources have been the focus of previous work on the Great Lakes (Cherkauer & Sinha, 2010; Cochand et al, 2019; Dubois et al., 2022; Erler et al., 2019; Farhadzadeh, 2017; Kayastha et al., 2022; Niu et al., 2014; Notaro et al., 2015; Persaud et al., 2020; Seglenieks & Temgoua, 2022; Soonthornrangsan & Lowry, 2021). Cherkauer & Sinha (2010) used a large-scale hydrological model to simulate changes in the spatial distribution of total runoff and baseflow under climate change scenarios from IPCC AR4 in four states surrounding Lake Michigan. Their results showed increasing annual stream flow in all rivers by late-century mainly in winter and spring, while more variability was observed in summer flows. Cochand et al. (2019) incorporated snowfall and melting processes into a fully integrated surface- groundwater model of the Saint-Charles River catchment, in Quebec, to analyze climate change impacts on water resources

under three scenarios from IPCC AR4. They found that stream discharges and groundwater heads will likely increase as warmer winters are expected, while warmer summers will lead to more evaporation, and a subsequent fall in stream discharges and groundwater heads. Soonthornrangsan & Lowry (2021) developed a coupled Groundwater and Surface-water FLOW (GSFLOW) model of the Western New York (WNY) basin to study the potential impacts on surface-groundwater interaction, water storage and discharges to the Great Lakes under NA-CORDEX outputs of RCP 4.5 and RCP 8.5, and varying the percentages of future impervious surfaces. While their results showed no statistically significant changes in surface water and groundwater systems under RCP 4.5, substantial losses were expected under RCP 8.5. More recently, Dubois et al. (2022) studied future changes in groundwater recharge in southern Quebec under RCP4.5 and RCP8.5 using a water budget model. They found that the direction and magnitude of the changes will be subject to precipitation increases, resulting in higher recharge to the aquifer only when precipitation increases over a certain threshold. These studies provide valuable insights for better understanding the hydrological response of the Great Lakes region under climatic changes. However, given the complexity and spatial extent of the GLB, potential impacts on their water resources should be continuously evaluated with new information and updated inputs to adapt current management strategies accordingly and thus reduce negative impacts in the region.

Assessment of climate change and its potential impacts has strongly relied on Global Climate Models (GCMs), coordinated by the Coupled Model Intercomparison Project (CMIP), which has been assisting global change research by making such outputs available to the public (Eyring et al., 2016). With its new sixth phase, CMIP responded to the main challenges previously identified by integrating climate and societal factors in the development of new future scenarios to support the research community and to be extendable to a wider range of applications (O'Neill et al., 2020, 2017). However, since CMIP6 outputs were recently made available for public use, their application in studies on

climate change impacts on water resources is still limited. Therefore, more studies that provide information on climate and societal conditions are required to support decision-making strategies in areas such as the Great Lakes region (O'Neill et al., 2020). Additionally, previous studies have concluded that assessing climate change impacts using a wide range of possible outcomes reduces the uncertainty of future projections (Chadwick et al., 2018). For example, Erler et al. (2019) forced a fully integrated surface water-groundwater model of a watershed within the GLB with a small ensemble of RCP 8.5. They found that models employing different moist physics led to different simulation results, with summer precipitation the main source of future uncertainty. Persaud et al. (2020) used a combination of Regional Climate Models (RCM), synthetic, and analogue scenarios to drive a HydroGeoSphere (Brunner & Simmons, 2012) model of the Upper Parkhill watershed. Comparing simulations forced with RCM against those forced with synthetic scenarios contributes to understanding the response and sensitivity of the system. However, employing different models of the same scenario (from CMIP5 or CMIP6) would serve that purpose and also provide information on the local (or regional) performance of models developed by different modeling centers in a particular climate. This information could be useful in the selection of the climate models in future climate change studies. Moreover, while the studies mentioned constitute a valuable contribution towards reducing future uncertainty of climate change impacts, to the best of our knowledge none has yet employed the new scenarios of CMIP6 using an ensemble approach in the Great Lakes, and therefore, the current research would be the first.

The main objective of this research is to assess potential impacts of climate change on surface and groundwater resources in the WNY basin, within the Lower Great Lakes. More specifically, we investigate changes in groundwater and surface water interactions and their discharges to the Great Lakes, which are major contributors to the water balance of the GLB. To this aim, a previously developed GSFLOW model of the basin is forced with

ensembles of scenarios SSP2 4.5 and SSP5 8.5 from CMIP6 defined to represent the uncertainty of future projections in the WNY basin.

A 2. Study site

The study area of WNY is located between two of the Great Lakes, Lake Ontario and Lake Erie, which are connected by the Niagara River (Figure 1c). WNY has a surface area of about 7919 km^2, comprising eight counties: Cattaraugus, Chautauqua, Erie, Genesee, Monroe, Niagara, Orleans, and Wyoming. As shown in Figure 1c), this area is home to the metropolitan cities of Buffalo, Rochester, and Niagara Falls, with a population of ~2.2 million people (2019 Census estimates). The geologic setting consists of Paleozoic rocks dipping toward the south and consisting of dolomite with interbedded shale and sandstone. The surficial geology and modern drainage network are dominated by pre-glacial erosion in the Pleistocene, followed by glaciation. The major geologic feature within the study area is the Niagara Escarpment that transverses the model domain from Niagara Falls to Rochester. The Niagara Escarpment separates the lowlands of Lake Ontario from higher elevations to the south, making up the edge of the Appalachian plateau, which drains to Lake Erie and the Niagara River (Eckhardt et al., 2008).

The climate of WNY is humid, with a mean annual precipitation of about 1016 mm and air temperatures moderated by Lake Ontario and Lake Erie (Eckhardt et al., 2008). Precipitation patterns across the study site are dominated by lake effect snow and rain traveling east off Lake Erie and depositing precipitation across the southern region of the model domain. The annual precipitation gradient decreases, moving north toward Lake Ontario.

An important hydrologic connection exists between the Great Lakes, its tributary streams, and groundwater, being groundwater a major contributor to both. The shallow water table,

which lies between ~ 5 – 60 m below the surface (Eckhardt et al., 2008), also sustains abundant surface water that serves as the primary source of drinking water. WNY is considered a water-rich environment due to its position between the Great Lakes and seasonally consistent precipitation inputs.

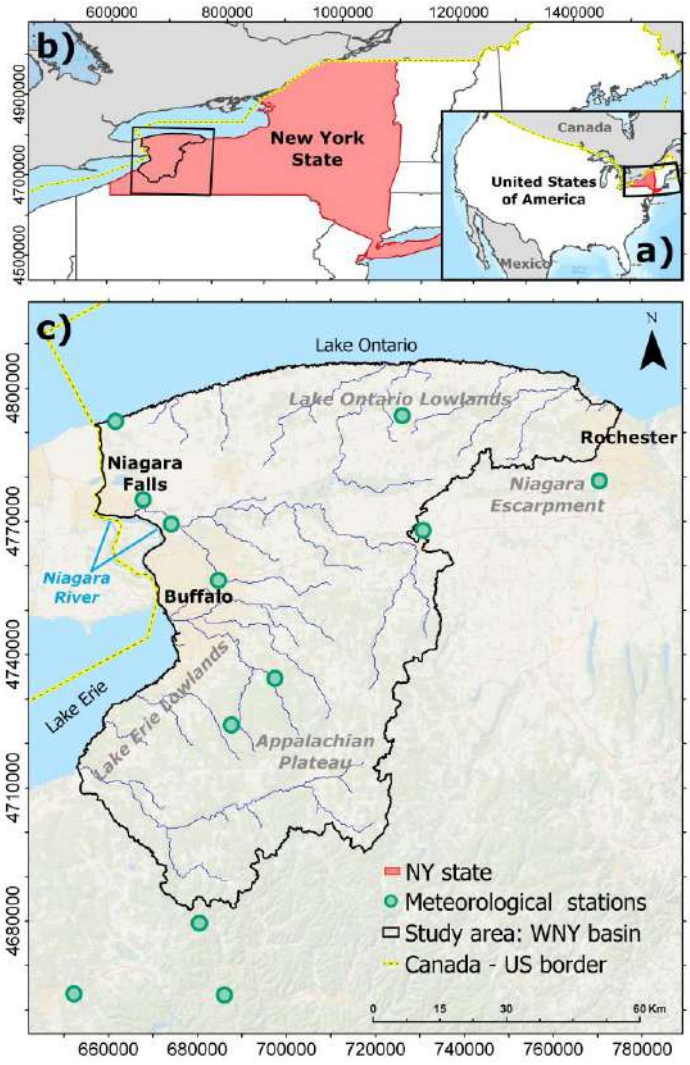

Figure A 1: Study site location in a) North America and b) the State of New York (NY). Panel c) shows the WNY basin's boundaries and the location of the meteorological stations used in this research.

A 3. Methods

A.3.1. GSFLOW model of the WNY basin

The coupled surface – groundwater model of WNY used in this research was previously developed by Soonthornrangsan & Lowry (2021) using the USGS software GSFLOW (Markstrom et al., 2008) that couples the Precipitation-Runoff Modeling System (PRMS, Markstrom et al., 2015) model with MODFLOW (Harbaugh, 2005) to simulate the coupled surface water and groundwater resources. The model of WNY has a 7,900 km^2 domain, which was discretized in 1 layer of 105 m thickness below the topography, 418 rows and 413 columns that form 172,632 finite-difference MODFLOW cells of 300 m by 300 m. MODFLOW cells are at the same time the hydrological response units (HRUs) of PRMS, and thus, the same spatial discretization is used for the hydrological and hydrogeological models. The Great Lakes were represented in the WNY model by constant head boundary conditions (CHD package), where 173 m ASL and 75 m ASL heads were defined at Lake Erie and Lake Ontario, respectively. The Niagara River was also defined by CHD, with a specified head equal to the river elevation. The remaining edges of the model were represented by no-flow boundary conditions at the surface water divides to the east and south. Discharges towards the Great Lakes are therefore simulated as lateral groundwater discharges from the aquifer and stream discharges from surface runoff. Readers are referred to the work of Soonthornrangsan & Lowry (2021) for a more detailed description of the model's features. However, here we briefly describe the interaction between surface water and groundwater as simulated in GSFLOW.

PRMS is coupled to MODFLOW through two-way exchanges between surface water and groundwater. This exchange at streams and lakes is simulated in MODFLOW by the SFR (Niswonger & Prudic, 2005) and LAK (Merritt & Konikow, 2000) packages, respectively, which allow these systems to recharge groundwater or receive groundwater discharge.

Within the soil zone, water can transfer to the unsaturated or saturated zone through UZF package in MODFLOW (Niswonger et al., 2006), depending on the volume of water stored in the unsaturated zone and the groundwater heads (Markstrom et al., 2008). Inputs to PRMS are daily precipitation, maximum and minimum temperature, and solar radiation, from which potential evapotranspiration, sublimation, and snowmelt are computed, which were acquired at each of the 12 stations used in the present research. The GSFLOW model then incorporates surface processes, including precipitation partitioning, infiltration, actual evapotranspiration (Actual ET), interflow, and recharge, as well as surface routing flow processes, unsaturated flow, and groundwater discharge (readers are referred to Markstrom et al. (2008) for details on the methodologies employed in GSFLOW).

For analyzing potential changes in the basin by the end of the century, future simulations were compared to a reference period simulation, which was driven with observed data from 2009 to 2019. Bias-adjusted data from ensembles SSP2 4.5 and SSP5 8.5 were used to drive the GSFLOW model of WNY between 2081 – 2100 were used to simulate the future period. The water table results of Soonthornrangsan & Lowry (2021) by the end of mid-century (December 2050) were used as the initial heads of the aquifer in the far future. Consequently, 20-year simulations for the future period were designed so that the first ten years of the simulations served as a warm-up period. The projected changes in the WNY system were thus assessed by comparing the results of the last decade of the future period (i.e., 2091 – 2100), henceforward far-future period, and the reference period (2009 – 2019).

A.3.2. Climate records

Temperature and precipitation data at 12 meteorological stations within the WNY aquifer domain (Figure 1c) were retrieved from the National Centers for Environmental Information of the National Oceanic and Atmospheric Administration (NOAA)

(https://www.ncei.noaa.gov/) for the period between January 1996 and December 2015. This period was defined to match the 20-year length of the future GSFLOW simulations, and it is limited at the end by the last year accounted as the past in CMIP6 models. To extend the records of three stations (Colden, Niagara Buffalo International Airport, and Youngstown) back to 1996, we used multiple linear regressions with the two stations that showed the highest correlation with the available records to estimate the regression coefficients for the corresponding multiple linear regression.

Given that future changes in hydrological processes are based on a relatively short reference period (2009-2019), it is important to analyze the climatic conditions that characterize this period to better understand the projected changes. One commonly used index for drought characterization and monitoring is the Standardized Precipitation Index (SPI) (McKee et al., 1993), which is based solely on precipitation data. The SPI normalizes the deviation from the mean of precipitation, allowing for comparisons of dry (water deficit) or wet (water surplus) conditions between different locations and time periods (Wang et al., 2022). By using the SPI at different time scales, it is possible to relate meteorological drought to hydrological processes, such as streamflow and groundwater recharge. In our study, we estimated the SPI for 3-month, 6-month, 12-month, and 48-month periods using the standard_precip Python library (https://github.com/e-baumer/standard_precip) to better assess the magnitude of the projected changes in hydrological processes compared to the reference period. To that end, data available from 1940 to 2019 at the meteorological stations shown in Figure 1c, were averaged to have SPI values representative of the basin.

A.3.3. Statistical downscaling of climate model outputs

A.3.3.1. Downscaling and bias adjustment of climate model outputs

Climate projections of temperature and precipitation were spatially downscaled to the meteorological stations' resolution using the bilinear interpolation approach. To adjust for biases in the future climate data, we implemented a statistical bias adjustment method at each meteorological station (Figure 1c) using the climQMBC MATLAB package (https://github.com/saedoquililongo/climQMBC). From the five quantile mapping-based methods available within the package, we selected the quantile delta mapping (QDM) method (Cannon et al., 2015) due to its ability to correct model biases based on observations while preserving model-projected relative changes in quantiles. By accounting for non-stationarity in climate data, the QDM method overcomes the stationarity assumption that limits the applicability of the classic quantile mapping (QM) method (Cannon et al., 2015; Chadwick et al., 2023).

The QDM method combines two steps in sequence: (1) future model outputs are detrended by quantile and bias corrected to observations by QM; (2) model-projected relative changes in quantiles are superimposed on the bias corrected model outputs (Cannon et al., 2015). Firstly, Firstly, the method applies the inverse cumulative distribution function (CDF) of the projected series, x_m, to estimate the non-exceedance probability associated with a precipitation event at a time *t*, within a projected period *p*, denoted as $x_{m,p}(t)$ in in Eq. (1):

$$Prob_{m,p}(t) = F_{m,p}^{(t)}\left[x_{m,p}(t)\right] \quad (0\text{-}1)$$

where $Prob_{m,p}(t)$ is the non-exceedance probability associated with $x_{m,p}(t)$, estimated considering a moving projected time window, and $F_{m,p}^{(t)}[\,]$ is the time-dependent CDF of the projected series x_m. Secondly, the relative change in model quantiles, $\Delta_m(t)$, is estimated as the ratio between the projected event $x_{m,p}(t)$ at a time t, and its corresponding quantile in the historical period, $F_{m,h}^{-1}[Prob_{m,p}(t)]$, as shown in:

$$\Delta_m(t) = \frac{x_{m,p}(t)}{F_{m,h}^{-1}\left[Prob_{m,p}(t)\right]} \tag{0-2}$$

In which $F_{m,h}^{-1}\left[Prob_{m,p}(t)\right]$ is obtained by applying the inverse CDF of x_m to $Prob_{m,p}(t)$ in the historical period, denoted as *h*. Therefore, $\Delta_m(t)$ is a factor between the projected modeled value at time *t* in the future and the value corresponding to the same modeled quantile in the historical period, or in other words, the climate model quantile change. Thirdly, $x_{m,p}(t)$ is bias-adjusted with the inverse CDF of observations in the historical period, $F_{o,h}^{-1}[\,]$, which is scaled by applying $\Delta_m(t)$ multiplicatively to obtain the corresponding bias-adjusted future projection at time t, $\hat{x}_{m,p}(t)$, according to:

$$\hat{x}_{m,p}(t) = F_{o,h}^{-1}\left[Prob_{m,p}(t)\right]\Delta_m(t) \tag{0-3}$$

For temperature, $\Delta_m(t)$ is calculated as the difference between $x_{m,p}(t)$ and $F_{m,h}^{-1}\left[\tau_{m,p}(t)\right]$, and it is incorporated additively rather than multiplicatively (for further detail the reader is referred to Cannon et al., 2015; Chadwick et al., 2023).

A.3.3.2. Temporal disaggregation

The bias-adjusted model projections of temperature and precipitation at monthly basis were temporarily disaggregated using a k-Nearest Neighbors (k-NN) approach to obtain daily values required to drive the hydrogeological model. The k-NN method originally applied for daily generation of climate (Lall & Sharma, 1996), has been adapted and used for disaggregating climate before (Barría et al., 2021; Greene et al., 2012). The method uses daily records of the variables over the historical period to generate future daily time series by applying the changes projected by the model in a certain month to observed daily data within that month. These data from the observed month used for the resampling is randomly selected from a window of k neighbors with similar behavior to the monthly data that is to be disaggregated. In this way, future daily time series are randomly generated while preserving the statistical properties of the historical data at the site (Rajagopalan & Lall, 1999). In this case, the model uses as input maximum and minimum daily temperatures for estimating recharge to the aquifer, however, since mean air temperature is the variable that is available in all GCMs we applied the changes projected by the models of this variable into daily observations of minimum and maximum temperatures.

A.3.4. CMIP6 scenarios and model ensembles

For the assessment of climate change impacts over the WNY aquifer, two Shared Socioeconomic Pathway (SSP) scenarios from CMIP6 were used: SSP2 4.5 and SSP5 8.5. The SSPs scenarios provide societal factors such as demographic, political orientation and economic growth, described as narratives focused on future challenges of adaptation and mitigation. The new framework of CMIP6 incorporates the greenhouse gas concentration of the Representative Concentration Pathways (RCP) (Moss et al., 2010) from CMIP5 to represent how society and climate may change by the end of the century, facilitating their application in integrated studies (O'Neill et al., 2020).

Scenarios SSP2 4.5 and SSP5 8.5 were chosen for the current research as they give continuity to previous studies in the area, which used RCPs 4.5 and 8.5 from CMIP5 (Soonthornrangsan & Lowry, 2021), and provide information on contrasting plausible future outcomes. SSP2 4.5 represents a future in which social, technological, and economic trends do not shift drastically from historical patterns, and therefore, moderate challenges to mitigation and adaptation will be required (O'Neill et al., 2017). On the other hand, SSP5 8.5 represents a future in which rapid economic growth results from the exploitation of abundant fossil fuel resources, leading to high challenges to mitigation (O'Neill et al., 2017). The warming predicted for these scenarios by the end of the century ranges between 2 – 2.9℃ (SSP2 4.5) and 4 – 4.3℃ (SSP5 8.5) (Nazarenko et al., 2022). Note that by generating small ensembles, the goal is to determine if models of the same climate change scenario can lead to different realizations as a result of the initial conditions and equations of physical processes employed in each GCM. However, analyzing the source of such difference is beyond our scope.

Datasets of the chosen scenarios were available from 27 climate models from the ScenarioMIP intercomparison project of CMIP6 at the CMIP6 Search Interface of the World Climate Research Program (WCRP) (https://esgf-node.llnl.gov/projects/cmip6/) for the historical and future periods. As some models had more than one run of the same scenario, the total number of datasets used in this research was 45 (i.e., climate projections), which can be found in Table A1.

Model ensembles were defined in both scenarios to take into account the uncertainty inherent in future projections. Because no method for building ensembles is universally

accepted (Crawford et al., 2019; Knutti et al., 2010), and considering the simulation time as a limiting factor (24 hours are required to run a 5-year simulation in the hydrogeological model), ensembles were generated using four climate models within each scenario. Climate models were chosen according to the climate change signal they project into the future precipitation, such that members of the ensembles project different magnitudes (percentiles) of changes (Chadwick et al., 2018). It is important to note that the change projected by a model in precipitation may not the same as the change it projects in temperature. Therefore, this selection criteria may result in higher temperatures being projected in some members of SSP2 compared to SSP5, despite the latter scenario projecting generally higher temperature changes. Preserving the climate change signal of the raw models is important to maintain physical scaling relationships between variables such as precipitation and temperature (Cannon et al., 2015). With that aim, a single climate change signal was calculated for each model as the average of the Δ_m of all the quantiles, calculated according to (Eq2, which represent the climate change signal reintroduced in the bias-corrected series according to the statistical downscaling method. Models selected for the ensembles of both scenarios are presented in Table 1.

Table 0-1: Ensemble members selected for the SSP2 4.5 and SSP5 8.5 scenarios. The first column indicates the range of precipitation delta percentile that each model projects within the ensemble. The name given to the models in the ensemble, as well as their original names, are presented in the two columns below each scenario ensemble.

Percentile range of Δ_m (%)	**Ensemble SSP2 4.5**		**Ensemble SSP5 8.5**	
	Name in ensemble	*Model name*	*Name in ensemble*	*Model name*
1 – 25	A	INM_CM5_0 (r1i1p1f)	E	ACCESS_CM2 (r1i1p1f1)
25 – 50	B	IPSL_CM6A_LR (r4i1p1f1)	F	MRI_ESM_2 (r1i1p1f1)
50 – 75	C	GDL_ESM4 (r1i1p1f1)	G	MPI_ESM1_2_LR (r4i1p1f1)

75 – 100	D	CESM2_WACCM (r2i1p1f1)	H	MPI_ESM1_2_LR (r5i1p1f1)

A 4. Results

A.4.1. Analysis of droughts and wet periods within the historical period

The resulting SPIs show fluctuating cycles of wet and dry periods according to the time-window used for their estimation (Figure 2). Particularly, lower time-windows lead to SPI with more alternating cycles (Figure 2a, b). However, longer time-windows, which are associated to groundwater-scale processes, result in positive values of SPI that can be clearly noticed during the period between 2009 and 2019 (Figure 2d) used for the reference period simulation in GSFLOW. Therefore, the projected changes in groundwater processes in the present work are calculated with respect to a relatively wet reference period.

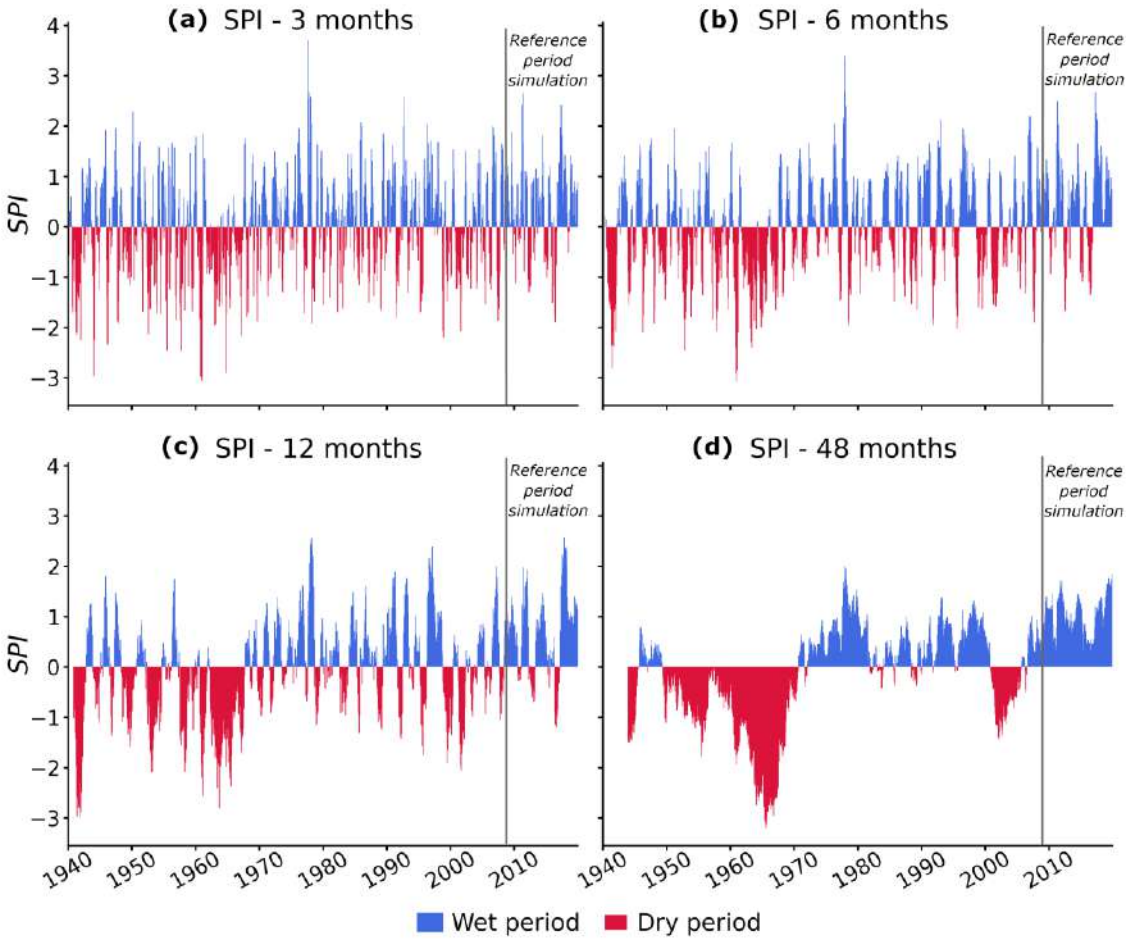

Figure 0-1: SPI values calculated between 1940 – 2019 using different time scales: a) 3 months, b) 6 months, c) 12 months and d) 48 months. The vertical lines mark the beginning of the reference period simulation in GSFLOW (2009 – 2019).

A.4.2. Bias-corrected temperature and precipitation projections in WNY

Monthly mean temperatures projected across all ensemble members are similar, regardless of the scenario, resulting thus in nearly identical projected mean ensembles (Figure 3a, b). Although slightly less variability between members is projected in temperature statistics in SSP5 8.5 (Table 2), in all models the mean, median, minimum, and maximum monthly

values are expected to increase by at least 2.4, 2.4, 1.6, and 2.3℃ , respectively, under both ensembles.

Unlike temperatures, noticeable differences are projected in the total monthly precipitation of both ensembles (Figure 3d, e). While such projections increase from the models representing the lowest to the highest percentiles of change of SSP2 4.5, in SSP5 8.5 a large difference of about 100 mm separates the lowest models (ensemble members E and F) with the highest (ensemble members G and H). Moreover, results in Table 2 demonstrate that the changes in precipitation are different from those in temperature projected by the same model, which results in this case in the SSP2 4.5 ensemble with higher projected temperatures than SSP5 8.5.

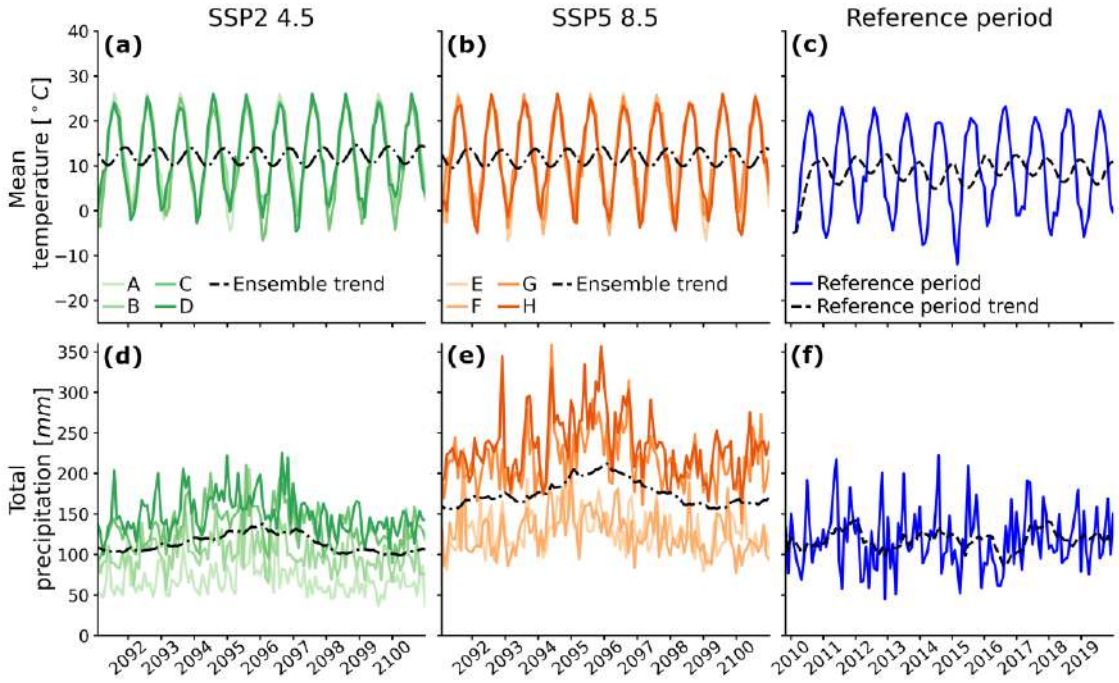

Figure 0-2: Comparison of projected monthly temperature (top row) and precipitation (bottom row) over the far-future (2091 – 2100), with respect to the reference period (2009 – 2019) (third column), averaged over the entire study area. The continuous lines graduated shades of green (for SSP2 4.5) and orange (for SSP5 8.5) depict the monthly values of the variables, with each shade representing a different model within the ensemble. The Ensemble trend (dashed black) line represents the average of all individual trends (estimated as 10-year moving means) projected by the members of the ensemble. The trends were estimated in the reference period as 5-year moving means given its length.

Table 0-2: Statistical properties of monthly temperature and precipitation observed in the period of 1996 – 2015 (defined as historical in the downscaling process) and projected in the future period (2081 – 2100) at monthly basis.

Scenario	Ensemble member	Temperature					Precipitation				
		Mean (°C)	Std (°C)	Min (°C)	Median (°C)	Max (°C)	Mean (mm)	Std (mm)	Min (mm)	Median (mm)	Max (mm)
Historical		8.9	9.2	-11.9	9.0	23.2	118.9	37.8	45.2	113.2	222.4

SSP2 4.5	A	12.8	8.9	-5.0	11.6	26.1	68.2	18.8	27.6	65.4	169.2
	B	12.4	8.4	-3.1	11.5	25.5	100.1	21.8	57.0	97.5	205.6
	C	11.3	9.0	-7.1	10.6	25.5	133.3	24.4	88.0	130.5	214.0
	D	12.1	8.5	-4.6	10.9	26.1	151.2	25.4	99.8	146.1	268.0
SSP5 8.5	E	11.7	8.9	-6.9	11.2	26.1	126.5	25.3	79.3	125.1	218.2
	F	11.7	9.0	-6.6	11.9	26.1	122.4	27.4	69.9	118.3	230.7
	G	12.2	8.9	-9.5	12.0	26.0	214.6	34.5	135.9	211.1	364.6
	H	11.4	9.3	-6.8	12.2	26.1	235.1	36.2	165.9	230.5	356.7

Differences in precipitations projected over the future period among ensemble members are also observed across the months of the year in both scenarios (Figure 4c, d). The driest month will likely shift from March, as observed in the reference period (Figure 4c, d), to February. Although the wettest month varies among ensemble members, both scenarios project wetter summers as higher precipitations are likely to occur earlier within the year. These changes, added to the consistent temperature increase, could lead to potential changes in the timings of groundwater recharge, and other processes dependent on climate.

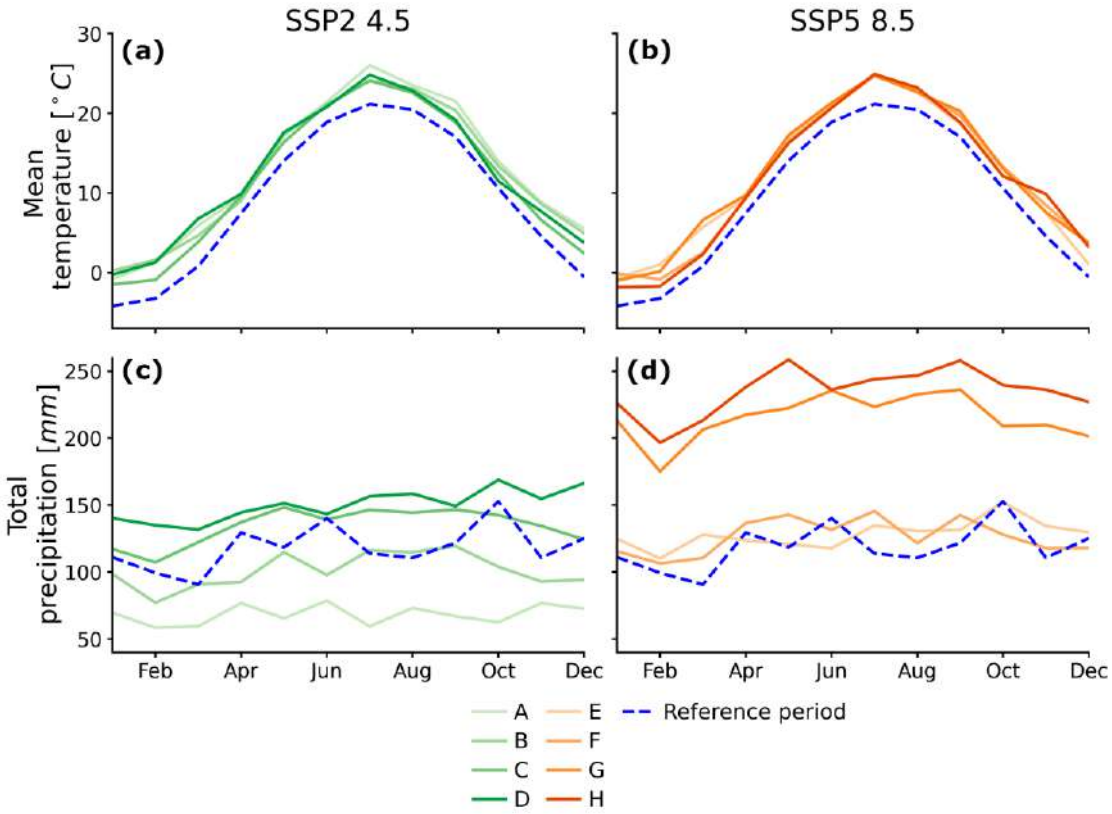

Figure 0-3: Average of monthly temperature (a and b) and precipitation(c and d) projected throughout the year under both scenarios for the far-future period (2091-2100), with each shade representing a different model within the ensemble, in comparison to the reference period (2009 – 2019), represented by the dashed blue line.

A.4.3. Changes projected in WNY's water balance and their associated impacts on the basin's discharges to the Great Lakes

A substantial difference between the projected and reference recharge–precipitation ratio is observed in March in both scenarios (Figure 5a, b). While historically very high (i.e., 90%) for the driest month of March, this ratio diminishes in the future as higher precipitations and temperatures in March are projected by most models (Figure 4a, b), which will likely

increase evaporation. Recharge will increase towards mid-summer until mid-winter, where temperatures are predicted to increase in average by 3 – 4.9℃ and 2.5 – 3.6℃ between July and September, in SSP2 4.5 and SSP5 8.5, respectively (Figure 4 a, c). As a result of warmer future conditions, larger evapotranspiration rates are projected (Figure 6d), which will likely result in decreasing mean recharge rates if the mean future precipitation were to increase below ~ 15% (Table 3). Therefore, both changes projected in temperature and precipitation will alter the timing of hydrological processes.

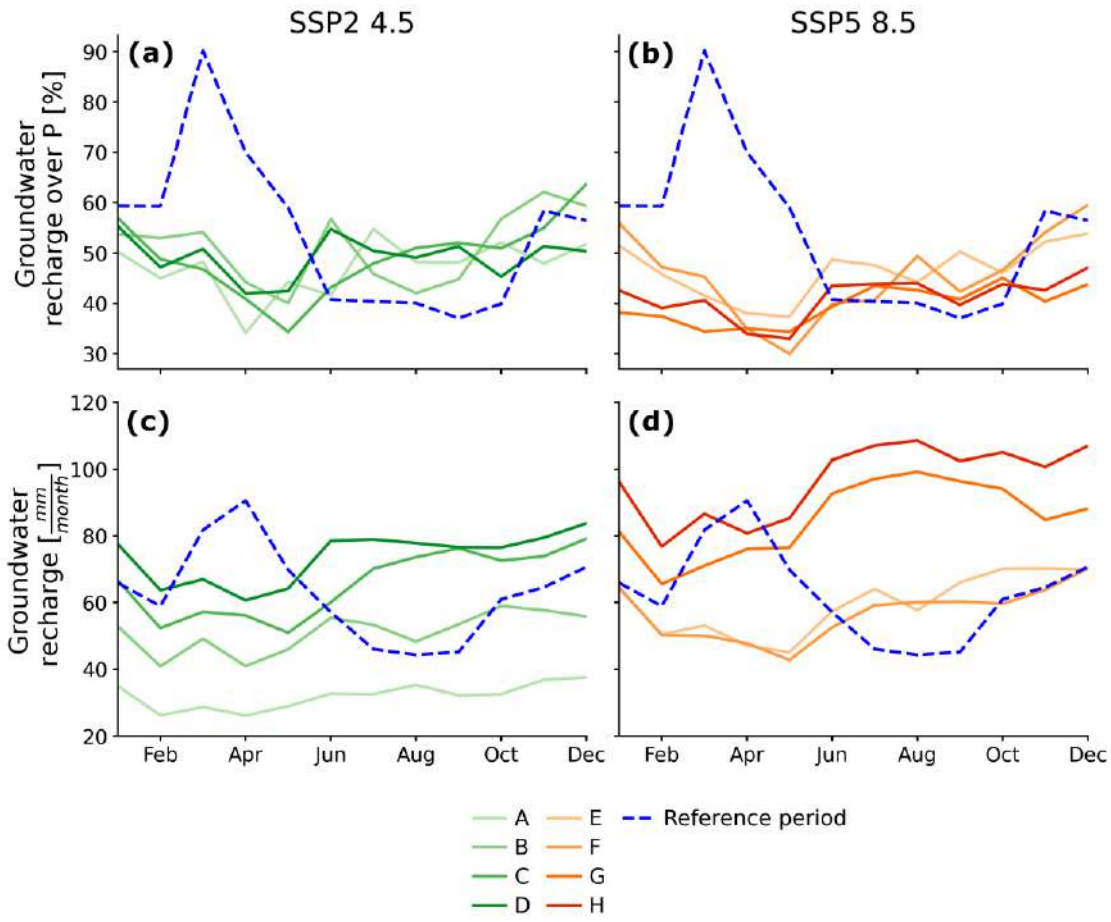

Figure 0-4: Comparison of the mean ratio of groundwater recharge over precipitation (P) (a and b), and mean groundwater recharge rate (c and d) projected throughout the year in the far-future period (2091-2100)

with respect to the reference period (2009-2019). The continuous lines in green and orange represent SSP2 4.5 and SSP5 8.5 projections, respectively, with shades representing a different model within the ensemble, while the dashed blue line represents the reference period.

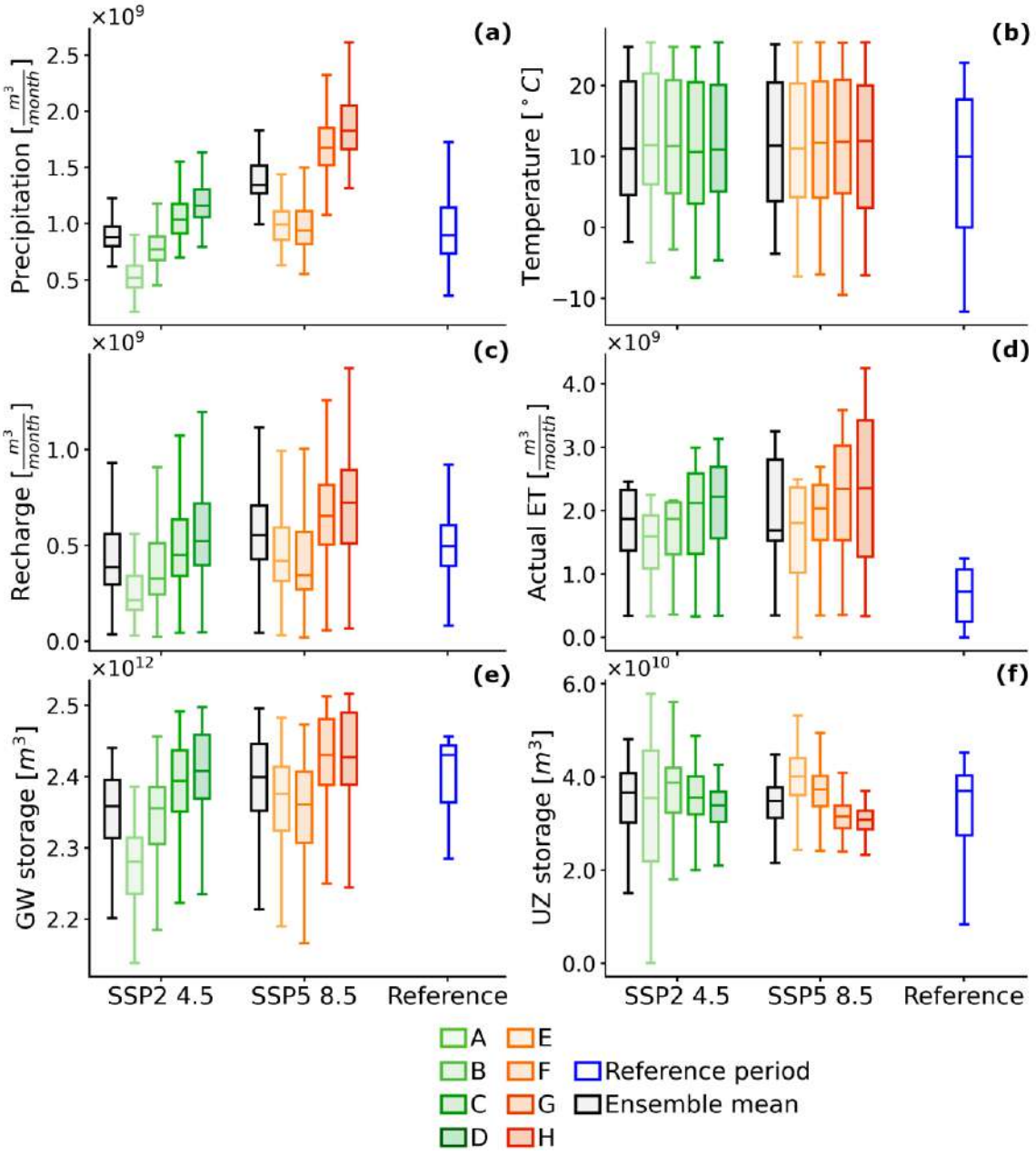

Figure 0-5: Box plots of monthly variables projected over the far-future period (2091-2100) compared to the reference period (2009 – 2019). Panels a and b present climatic variables driving the hydrological process, while panels below show the water budget response: c) recharge, d) actual evapotranspiration (Actual ET), e) groundwater (GW) storage, and f) unsaturated zone (UZ) storage. Graduated-colored boxes

represent the members of the ensembles, the black box depict the ensemble mean (first box of SSP2 4.5 and SSP5 8.5 groups), and the blue box represents the reference period. The whiskers of the boxplots depict 1.5 times the interquartile range (IQR).

GSFLOW simulates the behavior of the water table in response to changes in recharge rates. Accordingly, as recharge rates increase, the water table rises, and water stored in the unsaturated zone is added as recharge to the aquifer. As a result, the storage in the unsaturated zone decreases, while the storage in the saturated zone increases. Nevertheless, stream discharges to the Great Lakes do not decline to the same extent as unsaturated storage, as shown in Table 3, which suggests that groundwater storage would be able to sustain processes at the surface if the unsaturated storage diminishes. However, as higher Actual ET rates are expected in the basin, the average precipitation should increase somewhere about ~27.1% in SSP2 4.5 and ~ 80% in SSP5 8.5 (Table 3) so that the resulting groundwater recharge is enough to allow the aquifer to alleviate negative changes in the unsaturated zone without reducing its storage. The changes projected in the mean temperatures are lower in ensemble SSP5 8.5 than in SSP2 4.5, as the minimum and maximum temperatures are expected to be more extreme in the former than in the latter. However, the percentages of change in the median temperatures range around ~ 18– 28% and ~ 23 – 35% in SSP2 4.5 and SSP5 8.5, respectively.

The response of most of the water balance components varies greatly among ensemble members of the same scenario, which reinforces the importance of analyzing them individually. Therefore, while analyzing individual models contributes to understanding the sensitivity and response of the system under different stresses, the ensemble mean provides a range of changes projected in the system under a climate change scenario.

Table 0-3: Projected percentages of change in mean monthly variables with respect to their monthly means in the reference period. The table presents in columns 3 and 4 the changes projected in climatic variables, while the following columns present the changes in groundwater recharge and actual evaporation flows that

are projected as a consequence of the changes in climatic variables, as well as the changes in the saturated (groundwater) and unsaturated zones storages.

Ensemble		*Change in mean precipitation [%]*	*Change in mean temperature [℃]*	*Change in mean recharge [%]*	*Change in mean Actual ET [%]*	*Change in mean groundwater storage [%]*	*Change in mean unsaturated zone storage [%]*
SSP2 4.5	A	3.9	43.9	-48.9	25.3	-5.4	-0.7
	B	3.5	38.6	-21.1	80.3	-2.2	5.3
	C	2.4	26.6	2.3	87.6	-0.6	3.0
	D	3.2	36.3	14.9	95.0	0.2	-2.6
SSP5 8.5	E	2.8	31.7	-5.2	91.7	-1.4	15.5
	F	2.8	31.5	-13.2	83.9	-2.0	4.7
	G	3.3	36.5	34.3	105.9	0.9	-6.5
	H	2.5	28.2	44.1	98.2	1.1	-9.0

The relationship between the WNY basin and the Great Lakes depends on the effect that climatic changes will have on the water budget of the basin. There is a pronounced seasonal variability in future monthly stream discharges to the Great Lakes in comparison to the reference period (Figure 7a, b, c). While the seasonal variability of groundwater discharges is also expected to increase, it is two orders of magnitude lower than that of stream discharges. This suggests that streams would be more sensitive to climatic changes than groundwater. Despite this, the average ensemble trends of both flows discharging into the lakes are similar in shape to precipitation trends, represented in the opposite y-axis of all panels of Figure 7 by grey lines. This suggests that both flows are mainly driven by precipitation, although in different magnitudes. Furthermore, discharges from the streams are expected to respond earlier than those from groundwater, which can be observed in the

stream discharge response to the 2096 peak in precipitation. Accordingly, groundwater is likely expected to be less affected by climatic changes than streams.

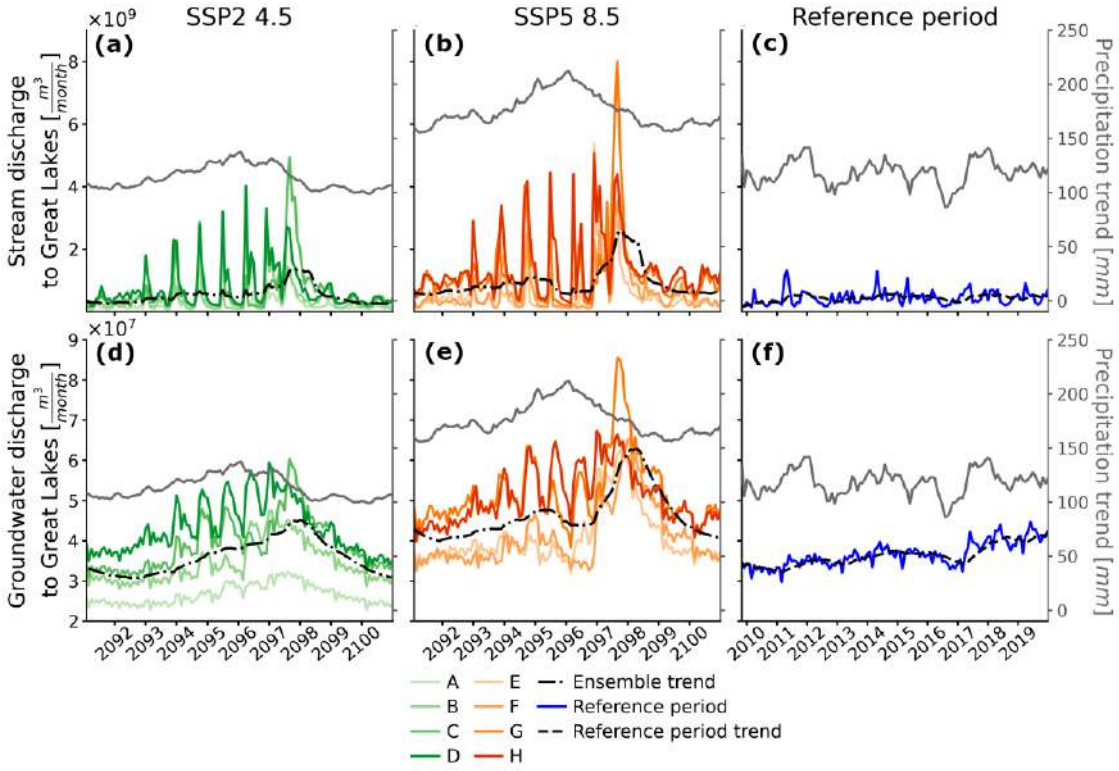

Figure 0-6: Stream (first row of plots) and groundwater (second row of plots) discharges towards the Great Lakes projected under SSP2 4.5 (a and d) and SSP5 8.5 (b and e) scenarios in comparison to the reference period (c and f). The average of all individual trends (estimated as 10-year moving means) projected by the members of each ensemble is presented as the Ensemble trend (dashed black) of the variable. The precipitation trend (mean of ensemble trends in SSP2 4.5 and SSP5 8.5) is plotted in the right y-axis of each panel in grey.

In models where the mean precipitation is expected to decrease (Table 3), both the stream and groundwater discharges to the Great Lakes will also decrease (Table 4), and therefore the WNY basin will likely continue to rely on the Great Lakes for water supply. However, the projected changes in the mean of discharge fluxes into the Great Lakes indicate that

discharges from streams will be more sensitive to precipitation changes than from groundwater. This is because streams discharging into the Great Lakes, as well as groundwater recharge, result from surface processes that directly depend on climatic variables. Nevertheless, groundwater discharges to the Great Lakes are not expected to be affected by climatic changes to the same extent as recharge, and therefore, stable head gradients between the Great Lakes and the water table are expected near the edges of the model.

Table 0-4: Projected percentages of change in the mean of monthly discharge flows into the Great Lakes (GL) in the far-future period (2091 – 2100) with respect to the reference period (2009 – 2019).

Scenario	*Ensemble members*	*Change in mean stream discharge to the GL [%]*	*Change in mean groundwater discharge to the GL [%]*
SSP2 4.5	A	-38.7	-26.0
	B	-10.6	-10.9
	C	38.9	1.2
	D	65.1	12.3
SSP5 8.5	E	23.0	5.4
	F	21.2	4.1
	G	160.8	35.4
	H	201.2	30.8

A.4.4. Projected groundwater response and spatial variation of water table changes

Under higher recharge rates, groundwater discharges to the Great Lakes, streams (as baseflow) and the soil zone are expected to increase (Figure 8b, c, d, respectively). As baseflow supports the storage of inland lakes, their increase could sustain water demand in agricultural lands. Meanwhile, enhanced surface runoff may support the stream discharge

to the Great Lakes when more groundwater discharges into the soil zone. Model H exemplifies this scenario, as it projects the highest recharge of the SSP5 8.5 ensemble, and consequently, the highest groundwater discharges into the soil and streams are expected. While the groundwater discharge to the Great Lakes projected by model H is not the largest of the ensemble, it projects the highest groundwater evaporation (ET_{gw}), evidencing the influence of the spatial distribution of water table changes on groundwater discharge flows. Accordingly, while in model H the water table is not expected to rise near the edges of the model as much as in model G (Figure 9-Model H and Figure 9-Model G), the water table in model H is likely to increase more in areas where ET_{gw} occurs.

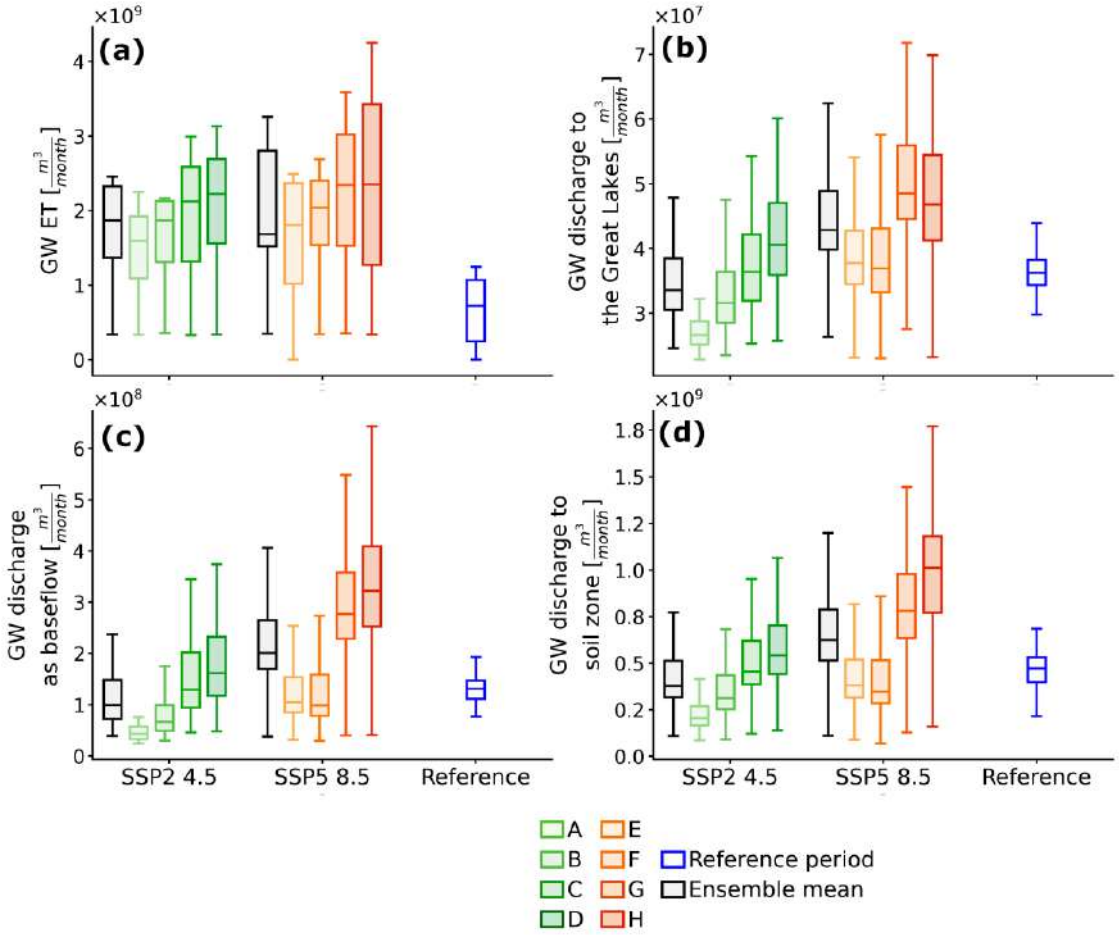

Figure 0-7: Boxplots of groundwater (GW) discharge flows as: a) groundwater evapotranspiration (GW ET), b) flow into the Great Lakes, c) baseflow, and d) flow towards the soil, estimated for the aquifer of WNY across models in both ensembles. Graduated-colored boxes represent the members of the ensembles, the black box depict the ensemble mean (first box of SSP2 4.5 and SSP5 8.5 groups), and the blue box represents the reference period. The whiskers of the boxplots depict 1.5 times the interquartile range (IQR).

Furthermore, impacts of different magnitudes are expected on the groundwater discharge to the Great Lakes given by the spatial variation of water table changes projected in 2100 with respect to 2019 (Figure 9). The Lake Ontario Lowlands area is likely to be the most sensitive to climate change within the WNY aquifer as different magnitudes (and directions) of head changes are projected across all models (Figure 9). These changes

could alter the head gradient between the Lake Ontario and the aquifer, thereby affecting the groundwater discharging into the lake. In fact, the mean groundwater discharge to the Great Lakes of models A and B is projected to be the lowest among all models (Table 4), which could be attributed to the substantial water table decreases projected by both models in the Lake Ontario Lowlands, as depicted in the corresponding model panels of Figure 9.

In addition, negligible changes in the water table are expected in the Appalachian Plateau area, making it the most resilient to climate change within the WNY aquifer. Conversely, the water table in urban areas, particularly in the city of Buffalo, is likely to decrease in the SSP2 4.5 scenario due to lower projected precipitations across all ensemble members. In the SSP5 8.5 scenario, however, the water table is projected to increase in all models except for model F, which is the only one projecting lower precipitation changes. It is worth noting that this research does not simulate future changes in impervious surfaces or groundwater abstractions in WNY. However, future studies focusing on groundwater management for future water availability and allocation should consider these factors, as they are likely to affect groundwater recharge and discharge processes.

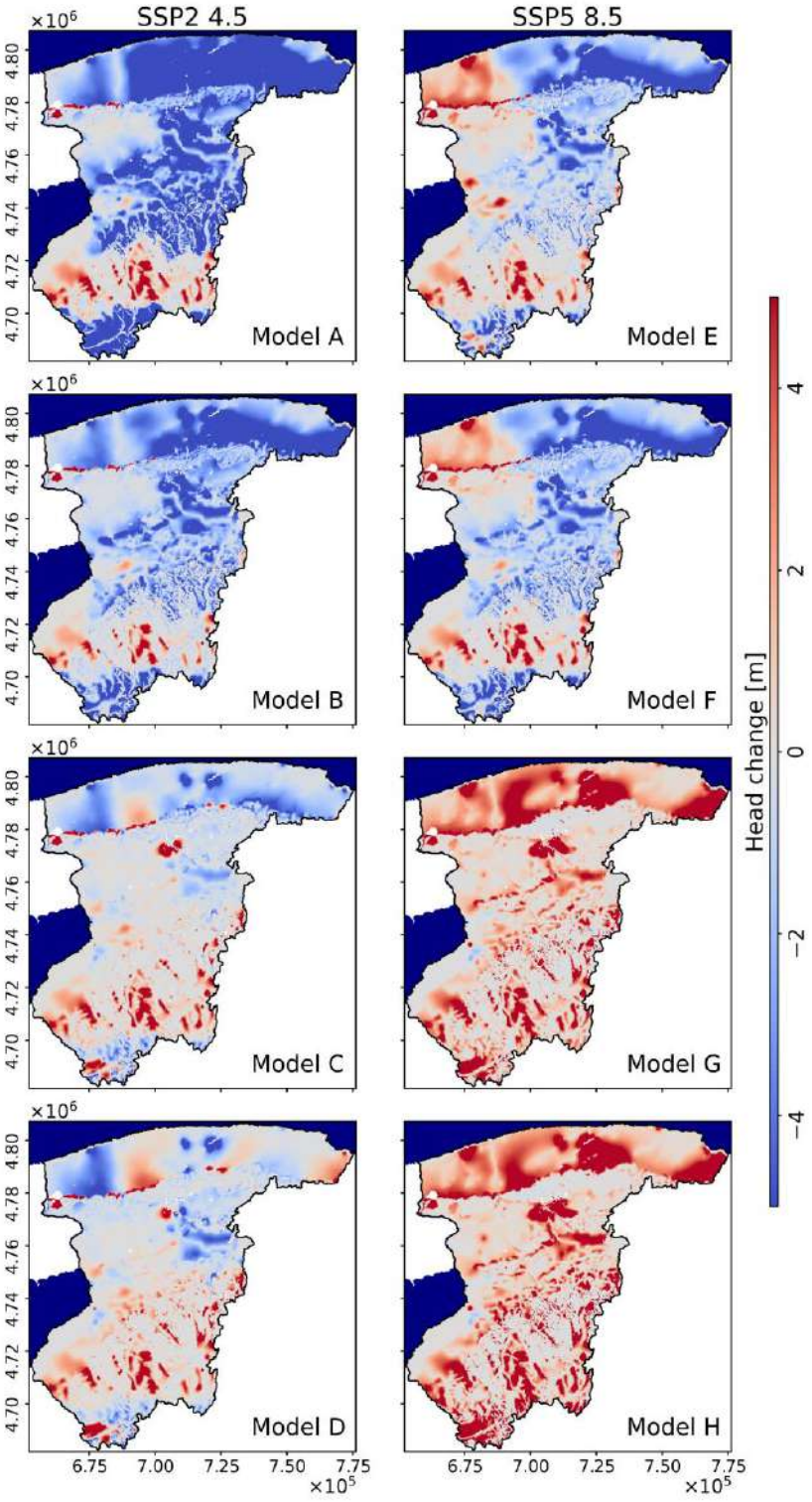
SSP2 4.5
SSP5 8.5
Model A
Model E
Model B
Model F
Model C
Model G
Model D
Model H
×10⁶
4.70
4.72
4.74
4.76
4.78
4.80
6.75
7.00
7.25
7.50
7.75
×10⁵
Head change [m]
4
2
0
−2
−4

Figure 0-8: Spatial variations of the changes projected in groundwater levels between December 2019 and December 2100 in WNY. Inactive cells are represented as white areas surrounding the watershed while constant head boundary conditions (Lake Erie, Ontario and the Niagara River) are represented in blue.

A 5. Discussion

A.5.1. The role of the groundwater system as a buffer of climate change impacts on surface waters

The response of groundwater presented in section 4.4 suggest that the aquifer would be able to buffer the impacts of climate change on surface water through its storage if future recharge increases. However, doing so will likely have negative impacts on groundwater storage unless the mean recharge increases by ~15% in SSP2 4.5 and somewhere between ~32 – 37% in SSP5 8.5 as a consequence of ~27.1% and ~ 80% increase of mean precipitation in the respective scenarios. This is consistent with previous studies performed in watersheds within the Great Lakes region, where it was found that future recharge rates and groundwater storage will likely increase as a result of increasing precipitations and warmer winters (Cherkauer & Sinha, 2010; Cochand et al., 2019; Dubois et al., 2022; Larocque et al., 2022).

Results on the potential buffering capacity of the groundwater system in WNY are also consistent with those of previous works (Costa et al., 2021; Erler et al., 2019; Kayastha et al., 2022; Niu et al., 2014; Persaud et al., 2020). Erler et al. (2019), for example, evaluated the impacts of climate change on groundwater resources in a watershed in the Great Lakes Basin, and found that regions characterized by a shallow water table may be able to rely on groundwater resources to supply moisture to soil under drier conditions. Costa et al. (2021) reviewed existing research on the potential effects of a changing climate on the quality and quantity of groundwater in the Great Lakes Basin. They observed that studies performed

on small/medium basins generally project groundwater systems to be resilient to climate change impacts, and those performed on larger basins predict an increase in groundwater storage. Niu et al. (2014) analyzed water budgets and storage changes in two of the largest watersheds in the State of Michigan (the Grand River and the Saginaw Bay watersheds) using remotely sensed data and a process-based hydrologic model (PAWS). They concluded that water storage was increasing in both watersheds and that subsurface components (mainly water in the vadose zone and the unconfined aquifer) are responsible for those changes in storage. Soonthornrangsan & Lowry (2021) concluded that surface water in the WNY basin will be more sensitive to changes in precipitation than groundwater. Unlike said research, we found that groundwater could alleviate changes in surface water under future water stress conditions but not vice versa. However, they predicted spatial changes in the water table and storage consistent with our findings, particularly the decreasing heads and storage in urban areas such as the city of Buffalo.

A.5.2. Sources of uncertainty in predicting climate change impacts in the WNY basin and future work

Our results indicate that groundwater discharge to the Great Lakes would be severely altered under future conditions similar to those projected by models A and B in the WNY basin, which could have negative impacts on the water balance of the lakes. In the current research, the Great Lakes are represented in the GSFLOW model with a constant head boundary condition throughout the entire simulation period (past and future), which means that changes in the lakes' water budget are not being simulated. This modeling assumption adds uncertainty to the interpretation of future impacts on WNY, as previous studies have shown that factors such as subsurface (unsaturated and saturated zones) contribution to lakes, surface runoff and open lake evaporation, among others, are key factors in driving changes in levels and storage in the Great Lakes (Kayastha et al., 2022; Niu et al., 2014; Seglenieks & Temgoua, 2022; Xu et al., 2021). Moreover, future fluctuations in lake levels

are expected to vary over time in the Great Lakes e (Gronewold et al., 2016b; Kayastha et al., 2022; Seglenieks & Temgoua, 2022; Xu et al., 2021), which could bring negative impacts on their surrounding watersheds, such as flooding, contamination of water quality, jeopardize crop production, habitat destruction, among other effects (Cherkauer & Sinha, 2010).

In our research, we aimed to represent the uncertainty of future projections in the WNY basin by generating ensembles of future scenarios SSP2 4.5 and SSP5 8.5, each with four models. While the number of ensemble members in our research was limited by the simulation time of the GSFLOW model, previous studies have shown that increasing the number of ensemble members can reduce the uncertainty associated with future projections (Deser et al., 2012; Lehner et al., 2020). Therefore, we recommend for future work on climate change assessment to increase the number of ensemble members to reduce the uncertainty in their projections. To that aim, we suggest considering the simulation time as an important factor in the construction of their models to achieve a balance between the adequate representation of the systems' processes and the simulation times.

A 6. Conclusions

A previously developed integrated surface – groundwater model of the WNY basin (within the Lower Great Lakes) was forced under two climate change scenarios from CMIP6 to assess the hydrological response of the system and the potential impacts on discharge flows to the Great Lakes (Erie and Ontario). To that end, small ensembles of both scenarios were generated from four selected models to represent a span of potential outcomes and reduce uncertainty of future projections. The models were selected based on the precipitation change projected by the raw GCMs. The QDM approach was applied to statistically adjust model biases to the WNY area using the climQMBC MATLAB package.

The bias-adjusted projections of climatic variables show less uncertainty across models of ensemble SSP2 4.5 than those of SSP5 8.5. Unlike temperatures, precipitation projections are uncertain in both ensembles as their members differ in the magnitudes and changes projected throughout the year, particularly in SSP5 8.5. The selection criteria for ensemble members based solely on precipitation, which is the main driver of the hydrological system, resulted in SSP2 4.5 projecting higher temperatures (~36% mean increase) than SSP5 8.5 (~32% mean increase).

It was found that the soil and unsaturated zones will be highly sensitive to climatic changes, while groundwater will be less sensitive to such changes. Furthermore, the WNY aquifer would be able to buffer negative impacts of climate change on surface water processes if groundwater recharge increases by ~15% and between ~32 – 37% in SSP2 4.5 and SSP5 8.5, respectively. Consequently, groundwater could sustain discharges to the Great Lakes. Yet, if precipitation increases below ~27% and ~ 80% in the respective scenarios, the generated recharge will not sustain groundwater storage, and the aquifer will lose its buffering capacity.

These results highlight the importance of evaluating further the response of groundwater to climate change to gain more certainty regarding the ability of groundwater to mitigate potential impacts on surface water. To that end, incorporating more detailed modeling of lake dynamics and levels is crucial in future research, as well as accounting for anthropogenic factors, such as projected changes in impervious surfaces and groundwater abstractions, which may affect groundwater recharge and discharge processes. Finally, increasing members of multi – model ensembles is encouraged to better represent the inherent uncertainty of climatic projections, allowing a more comprehensive understanding

of the potential impacts of climate change on the WNY aquifer and designing sustainable management strategies for the region's water resources.

A 7. Acknowledgments

…

A 8. References

Amanambu, A. C., Obarein, O. A., Mossa, J., Li, L., Ayeni, S. S., Balogun, O., … Ochege, F. U. (2020). Groundwater system and climate change: Present status and future considerations. https://doi.org/10.1016/j.jhydrol.2020.125163

Aygün, O., Kinnard, C., & Campeau, S. (2019). Impacts of climate change on the hydrology of northern midlatitude cold regions: Https://Doi.Org/10.1177/0309133319878123, 44(3), 338–375. https://doi.org/10.1177/0309133319878123

Barría, P., Chadwick, C., Ocampo-Melgar, A., Galleguillos, M., Garreaud, R., Díaz-Vasconcellos, R., … Poblete-Caballero, D. (2021). Water management or megadrought: what caused the Chilean Aculeo Lake drying? Regional Environmental Change, 21(1), 19. https://doi.org/10.1007/s10113-021-01750-w

Brunner, P., & Simmons, C. T. (2012). HydroGeoSphere: A Fully Integrated, Physically Based Hydrological Model. Groundwater, 50(2), 170–176. https://doi.org/https://doi.org/10.1111/j.1745-6584.2011.00882.x

Cannon, A. J., Sobie, S. R., & Murdock, T. Q. (2015). Bias Correction of GCM Precipitation by Quantile Mapping: How Well Do Methods Preserve Changes in

Quantiles and Extremes? Journal of Climate, 28(17), 6938–6959. https://doi.org/10.1175/JCLI-D-14-00754.1

Chadwick, Cristian, Gironás, J., González-Leiva, F., & Aedo, S. (n.d.). Bias-Adjustment to Preserve the Changes in Variability: The Unbiased Mapping of GCM Changes. Hydrological Science Journal.

Chadwick, Cristián, Gironás, J., Vicuña, S., Meza, F., & Mcphee, J. (2018). Using a Statistical Preanalysis Approach as an Ensemble Technique for the Unbiased Mapping of GCM Changes to Local Stations. Journal of Hydrometeorology, 19(9), 1447–1465. https://doi.org/10.1175/JHM-D-17-0198.1

Cherkauer, K. A., & Sinha, T. (2010). Hydrologic impacts of projected future climate change in the Lake Michigan region. Journal of Great Lakes Research, 36(SUPPL. 2), 33–50. https://doi.org/10.1016/J.JGLR.2009.11.012

Cochand, F., Therrien, R., & Lemieux, J. M. (2019). Integrated Hydrological Modeling of Climate Change Impacts in a Snow-Influenced Catchment. Groundwater, 57(1), 3–20. https://doi.org/10.1111/GWAT.12848

Condon, L. E., Atchley, A. L., & Maxwell, R. M. (2020). Evapotranspiration depletes groundwater under warming over the contiguous United States. Nature Communications 2020 11:1, 11(1), 1–8. https://doi.org/10.1038/s41467-020-14688-0

Costa, D., Zhang, H., & Levison, J. (2021). Impacts of climate change on groundwater in the Great Lakes Basin: A review. Journal of Great Lakes Research, 47(6), 1613–1625. https://doi.org/10.1016/J.JGLR.2021.10.011

Crawford, J., Venkataraman, K., & Booth, J. (2019). Developing climate model ensembles: A comparative case study. Journal of Hydrology, 568, 160–173. https://doi.org/10.1016/J.JHYDROL.2018.10.054

Deser, C., Phillips, A., Bourdette, V., & Teng, H. (2012). Uncertainty in climate change projections: the role of internal variability. Climate Dynamics, 38(3), 527–546. https://doi.org/10.1007/s00382-010-0977-x

Dubois, E., Larocque, M., Gagné, S., & Braun, M. (2022). Climate Change Impacts on Groundwater Recharge in Cold and Humid Climates: Controlling Processes and Thresholds. https://doi.org/10.3390/cli10010006

Eckhardt, D., Reddy, J. E., & Tamulonis, K. (2008). Ground-Water Quality in Western New York, 2006. In undefined. https://doi.org/10.3133/OFR20081140

Erler, A. R., Frey, S. K., Khader, O., d'Orgeville, M., Park, Y. J., Hwang, H. T., … Sudicky, E. A. (2019). Evaluating Climate Change Impacts on Soil Moisture and Groundwater Resources Within a Lake-Affected Region. Water Resources Research, 55(10), 8142–8163. https://doi.org/10.1029/2018WR023822

Eyring, V., Bony, S., Meehl, G. A., Senior, C. A., Stevens, B., Stouffer, R. J., & Taylor, K. E. (2016). Overview of the Coupled Model Intercomparison Project Phase 6 (CMIP6) experimental design and organization. Geoscientific Model Development, 9(5), 1937–1958. https://doi.org/10.5194/gmd-9-1937-2016

Farhadzadeh, A. (2017). A study of Lake Erie seiche and low frequency water level fluctuations in the presence of surface ice. Ocean Engineering, 135, 117–136. https://doi.org/https://doi.org/10.1016/j.oceaneng.2017.02.027

Grannemann, N. G. (2000). The importance of ground water in the Great Lakes region. US Department of the Interior, US Geological Survey.

Greene, A. M., Hellmuth, M., & Lumsden, T. (2012). Stochastic decadal climate simulations for the Berg and Breede Water Management Areas, Western Cape province, South Africa. Water Resources Research, 48(6). https://doi.org/https://doi.org/10.1029/2011WR011152

Gronewold, A. D., Bruxer, J., Durnford, D., Smith, J. P., Clites, A. H., Seglenieks, F., … Fortin, V. (2016a). Hydrological drivers of record-setting water level rise on Earth's largest lake system. https://doi.org/10.1002/2015WR018209

Gronewold, A. D., Bruxer, J., Durnford, D., Smith, J. P., Clites, A. H., Seglenieks, F., … Fortin, V. (2016b). Hydrological drivers of record-setting water level rise on

Earth's largest lake system. Water Resources Research, 52(5), 4026–4042. https://doi.org/10.1002/2015WR018209

Harbaugh, A. (2005). MODFLOW-2005, the US Geological Survey modular ground-water model: the ground-water flow process. Retrieved from https://md.water.usgs.gov/gw/modflow/MODFLOW_Docs/TM6-A16-MODFLOW-2005.pdf

Kayastha, M. B., Ye, X., Huang, C., & Xue, P. (2022). Future rise of the Great Lakes water levels under climate change. Journal of Hydrology, 612, 22–1694. https://doi.org/10.1016/j.jhydrol.2022.128205

Knutti, R., Furrer, R., Tebaldi, C., Cermak, J., & Meehl, G. A. (2010). Challenges in combining projections from multiple climate models. Journal of Climate, 23(10), 2739–2758. https://doi.org/10.1175/2009JCLI3361.1

Lall, U., & Sharma, A. (1996). A Nearest Neighbor Bootstrap For Resampling Hydrologic Time Series. Water Resources Research, 32(3), 679–693. https://doi.org/10.1029/95WR02966

Larocque, M., Levison, J., Gagné, S., & Saleem, S. (2019). Groundwater use for agricultural production–current water budget and expected trends under climate change. Final report submitted to MAPAQ and OMAFRA.

Lehner, F., Deser, C., Maher, N., Marotzke, J., Fischer, E. M., Brunner, L., … Hawkins, E. (2020). Partitioning climate projection uncertainty with multiple large ensembles and CMIP5/6. Earth System Dynamics, 11(2), 491–508. https://doi.org/10.5194/esd-11-491-2020

Markstrom, S. L., Niswonger, R. G., Regan, R. S., Prudic, D. E., & Barlow, P. M. (2008). GSFLOW—Coupled Ground-Water and Surface-Water Flow Model Based on the Integration of the Precipitation-Runoff Modeling System (PRMS) and the Modular Ground-Water Flow Model (MODFLOW-2005). Retrieved from U.S. Geological Survey Techniques and Methods 6-D1, 240 p. website: https://pubs.usgs.gov/tm/tm6d1/

Markstrom, S. L., Regan, R. S., Hay, L. E., Viger, R. J., Webb, R. M., Payn, R. A., & LaFontaine, J. H. (2015). PRMS-IV, the precipitation-runoff modeling system, version 4. In Techniques and Methods. https://doi.org/10.3133/tm6B7

McKee, T. B., Doesken, N. J., & Kleist, J. (1993). The relationship of drought frequency and duration to time scales. Proceedings of the 8th Conference on Applied Climatology, 17(22), 179–183. Boston.

Meixner, T., Manning, A. H., Stonestrom, D. A., Allen, D. M., Ajami, H., Blasch, K. W., … Walvoord, M. A. (2016). Meixner). Journal of Hydrology, 534, 124–138. https://doi.org/10.1016/j.jhydrol.2015.12.027

Merritt, M. L., & Konikow, L. F. (2000). Documentation of a computer program to simulate lake-aquifer interaction using the MODFLOW ground water flow model and the MOC3D solute-transport model. In Water-Resources Investigations Report. https://doi.org/10.3133/wri004167

Moss, R. H., Edmonds, J. A., Hibbard, K. A., Manning, M. R., Rose, S. K., Van Vuuren, D. P., … Wilbanks, T. J. (2010). The next generation of scenarios for climate change research and assessment. Nature 2010 463:7282, 463(7282), 747–756. https://doi.org/10.1038/NATURE08823

Nazarenko, L. S., Tausnev, N., Russell, G. L., Rind, D., Miller, R. L., Schmidt, G. A., … Yao, M. S. (2022). Future Climate Change Under SSP Emission Scenarios With GISS-E2.1. Journal of Advances in Modeling Earth Systems, 14(7), e2021MS002871. https://doi.org/10.1029/2021MS002871

Niswonger, R. G., & Prudic, D. E. (2005). Documentation of the Streamflow-Routing (SFR2) Package to Include Unsaturated Flow Beneath Streams-A Modification to SFR1. In U.S. Geological Survey (Ed.), Modeling Techniques 6-A13. Retrieved from http://www.usgs.gov/

Niswonger, R. G., Prudic, D. E., & Regan, R. S. (2006). Documentation of the Unsaturated-Zone Flow (UZF1) Package for Modeling Unsaturated Flow Between the Land Surface and the Water Table with MODFLOW-2005. In U.S. Geological

Survay (Ed.), Book 6, Modeling Techniques. Retrieved from https://pubs.usgs.gov/tm/2006/tm6a19/

Niu, J., Shen, C., Li, S. G., & Phanikumar, M. S. (2014). Quantifying storage changes in regional Great Lakes watersheds using a coupled subsurface-land surface process model and GRACE, MODIS products. Water Resources Research, 50(9), 7359–7377. https://doi.org/10.1002/2014WR015589

Notaro, M., Bennington, V., & Lofgren, B. (2015). Dynamical Downscaling–Based Projections of Great Lakes Water Levels. Journal of Climate, 28(24), 9721–9745. https://doi.org/10.1175/JCLI-D-14-00847.1

O'Neill, B. C., Carter, T. R., Ebi, K., Harrison, P. A., Kemp-Benedict, E., Kok, K., … Pichs-Madruga, R. (2020). Achievements and needs for the climate change scenario framework. Nature Climate Change, 10(12), 1074–1084. https://doi.org/10.1038/s41558-020-00952-0

O'Neill, B. C., Kriegler, E., Ebi, K. L., Kemp-Benedict, E., Riahi, K., Rothman, D. S., … Solecki, W. (2017). The roads ahead: Narratives for shared socioeconomic pathways describing world futures in the 21st century. Global Environmental Change, 42, 169–180. https://doi.org/10.1016/J.GLOENVCHA.2015.01.004

Persaud, E., Levison, J., MacRitchie, S., Berg, S. J., Erler, A. R., Parker, B., & Sudicky, E. (2020). Integrated modelling to assess climate change impacts on groundwater and surface water in the Great Lakes Basin using diverse climate forcing. Journal of Hydrology, 584, 124682. Retrieved from https://linkinghub.elsevier.com/retrieve/pii/S0022169420301426

Portmann, F. T., Döll, P., Eisner, S., & Flörke, M. (2013). Impact of climate change on renewable groundwater resources: assessing the benefits of avoided greenhouse gas emissions using selected CMIP5 climate projections. Environmental Research Letters, 8(2), 24023. https://doi.org/10.1088/1748-9326/8/2/024023

Rajagopalan, B., & Lall, U. (1999). A k-nearest-neighbor simulator for daily precipitation and other weather variables. Water Resources Research, 35(10), 3089–3101. https://doi.org/10.1029/1999WR900028

Seglenieks, F., & Temgoua, A. (2022). Future water levels of the Great Lakes under 1.5 °C to 3 °C warmer climates. Journal of Great Lakes Research, 48(4), 865–875. https://doi.org/https://doi.org/10.1016/j.jglr.2022.05.012

Soonthornrangsan, J., & Lowry, C. (2021). Analyzing future climate change and anthropogenic effects on water resources in Western New York. Hydrological Processes, Under revi.

Soonthornrangsan, J. T., & Lowry, C. S. (2021). Vulnerability of water resources under a changing climate and human activity in the lower Great Lakes region. Hydrological Processes, 35(12), e14440. https://doi.org/10.1002/HYP.14440

Sutton, C., Kumar, S., Lee, M.-K., & Davis, E. (2021). Human imprint of water withdrawals in the wet environment: A case study of declining groundwater in Georgia, USA. Journal of Hydrology: Regional Studies, 35, 100813. https://doi.org/10.1016/j.ejrh.2021.100813

Sweet, S. K., Wolfe, D. W., Degaetano, A., & Benner, R. (2017). Anatomy of the 2016 drought in the Northeastern United States: Implications for agriculture and water resources in humid climates. https://doi.org/10.1016/j.agrformet.2017.08.024

Tabari, H. (2020). Climate change impact on flood and extreme precipitation increases with water availability. https://doi.org/10.1038/s41598-020-70816-2

Tague, C., Grant, G., Farrell, M., Choate, J., & Jefferson, A. (2008). Deep groundwater mediates streamflow response to climate warming in the Oregon Cascades. Climatic Change, 86(1–2), 189–210. https://doi.org/10.1007/S10584-007-9294-8/METRICS

Wang, Q., Zhang, R., Qi, J., Zeng, J., Wu, J., Shui, W., … Li, J. (2022). An improved daily standardized precipitation index dataset for mainland China from 1961 to 2018. Scientific Data 2022 9:1, 9(1), 1–12. https://doi.org/10.1038/s41597-022-01201-z

Xu, S., Frey, S. K., Erler, A. R., Khader, O., Berg, S. J., Hwang, H. T., … Sudicky, E. A. (2021). Investigating groundwater-lake interactions in the Laurentian Great Lakes with a fully-integrated surface water-groundwater model. Journal of Hydrology, 594, 125911. https://doi.org/10.1016/j.jhydrol.2020.125911.